学位論文

Detection and statistical analysis of earthquake swarms at subduction zones globally: Implications to slow slip activity

（全世界沈み込み帯における群発地震活動解析と
スロースリップ活動への示唆）

平成２９年１２月博士（理学）申請

東京大学大学院理学系研究科
地球惑星科学専攻
西川　友章

Abstract

Slow earthquakes, which are slip phenomena with longer time scales than ordinary earthquakes, occur in the vicinity of locked regions in subduction zones and are speculated to be related with occurrence of large earthquakes. Furthermore, slow slip events (SSEs), which are slip phenomena with a time scale of days to years, were reported to have preceded some large earthquakes. Therefore, revealing SSE activity in subduction zones globally is indispensable to understand large earthquake activity worldwide. However, currently, there are many areas where geodetic observation networks have not been well developed, such as offshore ocean areas, and it is difficult to elucidate SSE activity in subduction zones globally only from current geodetic observation networks. On the other hand, two kinds of ordinary earthquakes are known to closely related to SSE activity in subduction zones. One is an earthquake swarm. An earthquake swarm is a seismic sequence without a distinguished mainshock, and swarms triggered by SSEs have been observed in subduction zones such as Boso-Oki, Japan and the Hikurangi trench, New Zealand. The other one is a repeating earthquake. Repeating earthquakes are repetitive rupture of almost the same area on the plate interface and can be used as a creep meter on the plate interface. By using these two kinds of ordinary earthquakes as potential indicators of SSEs, we can infer the occurrence of SSEs even in areas where geodetic observation networks have not been well developed. In this study, by investigating earthquake swarms and repeating earthquake, we aim to obtain implications for global SSE activity and the mechanism of large earthquake occurrences.

We make a global catalog of earthquake swarms in subduction zones. We present a

method for detecting earthquake swarms using the space-time epidemic-type aftershock-sequence (ETAS) model. We applied this method to seismicity ($M \geq 4.5$) in the Advanced National Seismic System catalog at subduction zones during the period of 1995–2009. As a result, we detected 453 swarm sequences. Subduction zones such as Kermadec and Vanuatu are characterized by especially high swarm activity. Moreover, in some subduction zones such as Ibaraki-Oki, Japan, foreshock sequences of large earthquakes are also detected as earthquake swarms. In these regions, the large earthquakes may have been preceded by SSEs. We then compare the swarm activity and tectonic properties of subduction zones, finding that the swarm activity is positively correlated with curvature of the incoming plate before subduction. This correlation implies that swarm activity is controlled by hydration of the incoming plate and/or by heterogeneity on the plate interface due to fracturing related to slab bending.

We then further explore the possibility of occurrence of SSEs in Ibaraki-Oki, Japan by examining the space-time distribution of earthquake swarms and foreshocks of large earthquakes. We use the space-time ETAS model, the matched filter technique, and the repeating earthquake analysis to reveal a more detailed history of swarm activity, restore small events missing from the earthquake catalog, and estimate the amount of interplate fault slip in Ibaraki-Oki. We found that 19 swarm sequences repeatedly occur during 1982–2009 at almost the same location as foreshock sequences preceding the 1982 and 2008 *M* 7 Ibaraki-Oki earthquakes. Both the foreshock and swarm sequences contain repeating earthquakes and have anomalously high seismicity rates inexplicable by the ETAS model, suggesting recurrence of SSEs in the source of the 1982 and 2008 *M* 7 Ibaraki-Oki earthquakes. The foreshock sequences in 1982 and 2008 have a larger

number of events inexplicable by the ETAS model than the swarm sequences. The amount of slip of repeating earthquakes in the foreshock sequence in 2008 is also larger than those of the swarm sequences, and the slip rate increased 12 hours before the 2008 *M* 7 event. These results imply that the SSEs that preceded the 1982 and 2008 *M* 7 Ibaraki-Oki earthquakes have larger seismic moments than the other SSEs that triggered the swarm sequences. These large SSEs might be related to the nucleation phase of the *M* 7 Ibaraki-Oki earthquakes.

Our study reveals earthquake swarm activity in subduction zones worldwide, tectonic controls on earthquake swarm activity, and the relationship between the *M* 7 Ibaraki-Oki earthquakes and recurring SSEs in their source region. Our results and insights may be useful for future investigations of global SSE activity and studies on the mechanism of large earthquake occurrence in subduction zones.

Contents

1. Overall Introduction

In subduction zones, where oceanic plates formed at oceanic ridges return to Earth's mantle [e.g., Hess, 1962], many megathrust earthquakes have occurred. In 2004, the M_w 9.1 Sumatra-Andaman earthquake generated a great tsunami and killed hundreds of thousands of people in Southeast Asia [e.g., Lay et al., 2005]. In 2011, the M_w 9.0 Tohoku-Oki earthquake ruptured the plate interface in the Japan Trench [e.g., Ide et al., 2011] and caused tens of thousands of deaths in Northeast Japan. Because of such devastating damage, revealing the mechanism of large earthquake occurrence in subduction zones is critically important not only for earthquake science but also for human society. In the past four decades, researchers have tried to elucidate the mechanism of large earthquake occurrence by using various models and taking various approaches, such as the asperity model, which assumes the plate interface consists of mechanically strong spots and weak surrounding areas [e.g., Kanamori, 1986], and comparative subductology, which explains variations in seismicity among subduction zones from the viewpoint of plate tectonics [e.g., Uyeda and Kanamori, 1979; Scholz and Campos, 2012]. Although these models and approaches succeeded in explaining some important aspects of the earthquake phenomenon, the mechanism of large earthquake occurrence still remains unclear, and it seems currently impossible to predict large earthquakes in subduction zones.

On the other hand, recently, slip phenomena called "slow earthquakes", which are characterized by longer time scales than ordinary earthquakes [Ide et al., 2007], have attracted much attention and been energetically studied. Various types of slow earthquakes have been discovered in subduction zones by previous studies in the past

two decades [e.g., Beroza and Ide, 2011; Obara and Kato, 2016]. For example, in the Nankai subduction zone, slow slip events (SSEs) [Hirose et al., 1999], deep tectonic tremors [Obara, 2002], and very low frequency earthquakes (VLFEs) [Ito et al., 2007] were discovered in the deeper transition zone, which is the deeper extension of the seismogenic zone. SSEs are episodic aseismic slips on the plate interface whose duration ranges from days (short-term SSE) to years (long-term SSE). Geodetics observation networks such as Global Navigation Satellite System (GNSS), tilt meters, and stain meters can observe SSEs. Deep tectonic tremors and VLFEs are seismic signals in the 1–10 Hz and 0.01–0.1 Hz frequency bands respectively. Deep tectonic tremors have very ambiguous P- and S-wave arrivals, and their duration is typically tens of minutes. Shelly et al. [2007] revealed that deep tectonic tremor is actually a swarm of low frequency earthquakes (LFEs) [Nishide et al., 2000]. Both LFEs and VLFEs are considered to be shear faulting on the plate interface with much longer characteristic duration than ordinary earthquakes with the same seismic moment [Shelly et al., 2007; Ito et al., 2007]. Furthermore, Ide et al. [2007] revealed that these slow earthquakes follow a simple scaling law, which states that the seismic moment of slow earthquakes is proportional to their characteristic duration, and suggested that slow earthquakes can be thought of as different manifestations of the same slip phenomena on the plate interface.

Similar to the deeper side of the seismogenic zone, various types of slow earthquakes also have been observed on the shallower side in subduction zones. Shallow SSEs, tectonic tremors, and VLFEs were found in the Nankai subduction zone [Obara and Ito, 2005; Araki et al., 2017]. Similar observations of deep and shallow slow earthquakes

have been reported in many of circum-Pacific subduction zones, such as the Peru–Chile Trench, the Middle America Trench, the Cascadia subdcution zone, the Aleutian Trench, the Japan Trench, the Ryukyu Trench, Taiwan, and the Hikurangi Trench as summarized by Saffer and Wallace [2015] and Obara and Kato [2016]. Therefore, slow earthquakes seem to be slip phenomena common to many subduction zones.

Importantly, these slow earthquakes are mainly located on the periphery of locked regions on the plate interface, and researchers are speculating the relationship between slow earthquakes and large earthquake [e.g., Dragert et al., 2004; Matsuzawa et al., 2010]. In recent years, SSEs preceding large earthquakes were actually observed in subduction zones such as the Japan Trench, northern Chile, and Mexico by geodetic observations [e.g., Ito et al., 2013; Ruiz et al., 2014; Radiguet et al., 2016]. The physical mechanism that relates the SSEs to the large earthquakes is controversial. Some interpreted the SSEs as the nucleation phase of the large earthquakes [Kato et al., 2012; Ruiz et al., 2014], similar to those observed in laboratory experiments [e.g., Ohnaka, 1992] and numerical simulations [e.g., Tse and Rice, 1986; Dieterich 1992, Shibazaki and Matsu'ura, 1992]. Others suggested that the SSEs induced stress perturbation on the plate interface and triggered the large earthquakes [Ando and Imanishi, 2011; Radiuget et al., 2016]. Although these controversies are still continuing, it is clear that SSEs are closely related to occurrence of large earthquakes in subduction zones. Therefore, revealing SSE activity in subduction zones globally is indispensable in order to understand large earthquake activity worldwide, which is one of the most important goals in earthquake science.

However, currently, there are many areas where geodetic observation networks have not been well developed, such as offshore sea areas. Even in Japan, which is one of the countries with the most developed geodetic observation network, SSEs occurring offshore have only recently been observed [Ito et al., 2013; Araki et al., 2017], and the whole picture of their activity is still unclear. Therefore, it seems difficult to elucidate SSE activity in subduction zones globally only from geodetic observation networks, currently and even in near future.

On the other hand, two kinds of ordinary earthquakes are known to be closely related to SSE activity in subduction zones. One is an earthquake swarm, which is a seismic sequence without a distinguished mainshock. For example, in Boso-Oki, Japan, earthquake swarms accompanied by SSEs occur every 5 to 7 years [e.g., Ozawa et al., 2003; Hirose et al., 2012]. Likewise, swarms of small earthquakes (from M 2 to M 3) accompanied by SSEs have been observed in the Hikurangi Trench, New Zealand [Delahaye et al., 2009]. Similar observations also have been reported in Ecuador and Mexico [Liu et al., 2007; Vallée et al., 2013]. Furthermore, several studies have tried to detect SSEs using earthquake swarms as potential indicators of SSEs in subduction zones such as the Sagami Trough and the Aleutian Trench [e.g., Okutani and Ide, 2011; Kato et al., 2014; Reverso et al., 2015].

The other ordinary earthquake that is closely related to SSE activity is a repeating earthquake, which is sometimes called “repeater”. Repeating earthquakes are earthquakes with almost identical waveforms and considered to be repetitive rupture of the same area on the plate interface [e.g., Ellsworth, 1995]. Recurrence intervals of

repeating earthquakes are known to reflect a rate of aseismic-slip on the plate interface [e.g., Nadeau and Johnson, 1998; Igarashi et al., 2003], and thus repeating earthquakes can be used as a creep meter on the plate interface. For example, in the Parkfield segment of the San Andreas Fault, detailed slip rate distribution on the plate interface was estimated from recurrence intervals of repeating earthquakes [Nadeau and McEvilly, 1999]. In offshore Sanriku, the Japan Trench, periodic SSEs with a recurrence interval of about 3 years were discovered by repeating earthquake analyses [Uchida et al., 2016]. These periodic SSEs are speculated to induce stress perturbation on the plate interface and modulate occurrence time of large earthquakes in the Japan Trench.

Given these previous studies, by using earthquake swarms and repeating earthquakes as potential indicators of SSEs, we can detect SSEs in subdcution zones worldwide including areas where geodetic observation networks have not been well developed. In this study, we aim to obtain implications for global SSE activity and the mechanism of large earthquake occurrence through detection of earthquake swarms at subduction zones worldwide and repeating earthquake analyses.

In Chapter 2, we make a global earthquake swarm catalog and specify possible locations of unknown SSEs in subduction zones worldwide. We then investigate tectonic controls on swarm activity in subduction zones. In Chapter 3, we further explore the possibility of recurrence of SSEs in Ibaraki-Oki, Japan, where results in Chapter 2 strongly suggest occurrence of SSEs. We then discuss the relationship between the SSEs and the 1982 and 2008 *M* 7 Ibaraki-Oki earthquakes. In Chapter 4,

we discuss the structure of the seismogenic zone at subduction zones implied by results and insights in Chapter 2 and Chapter 3. In Chapter 5, we summarized our conclusions.

2. Detection of earthquake swarms at subduction zones globally: Insights into tectonic controls on swarm activity

This chapter is modified from Nishikawa and Ide [2017], which was published in Journal of Geophysical Research.

2.1. Summary

Earthquake swarms are characterized by an increase in seismicity rate that lacks a distinguished mainshock and does not obey Omori's law. At subduction zones, they are thought to be related to slow slip events (SSEs) on the plate interface. Earthquake swarms in subduction zones can therefore be used as potential indicators of slow slip events. However, the global distribution of earthquake swarms at subduction zones remains unclear. Here, we present a method for detecting such earthquake sequences using the space–time epidemic-type aftershock-sequence (ETAS) model. We applied this method to seismicity ($M \geq 4.5$) recorded in the ANSS catalog at subduction zones during the period 1995–2009. We detected 453 swarms, which is about 6.7 times the number observed in a previous catalog. Foreshocks of some large earthquakes are also detected as earthquake swarms. In some subduction zones, such as at Ibaraki-Oki, Japan, swarm-like foreshocks and ordinary swarms repeatedly occur at the same location. Given that both foreshocks and swarms are related to SSEs on the plate interface, these regions may have experienced recurring SSEs. We then compare the swarm activity and tectonic properties of subduction zones, finding that swarm activity is positively correlated with curvature of the incoming plate before subduction. This result implies that swarm activity is controlled either by hydration of the incoming plate and/or by

heterogeneity on the plate interface due to fracturing related to slab bending.

2.2. Introduction

A seismic sequence usually consists of one large mainshock and many small aftershocks. The seismicity rate of this mainshock–aftershock sequence follows Omori's law, which states that the rate of aftershock decay follows a power law [Utsu, 1961]. On the other hand, some seismic sequences have neither a clear mainshock nor decay according to Omori's law; such sequences are called earthquake swarms [e.g., Richter, 1958; Llenos et al., 2009].

Earthquake swarms are observed in various tectonic settings and are thought to be triggered by phenomena other than earthquake-to-earthquake triggering. For example, swarms observed near volcanoes are considered to be related to magmatic intrusion and fluid migration [e.g., Aoyama et al., 2002; Toda et al., 2002; Waite and Smith, 2002]. Magma and fluids can reduce the strength of faults and thus cause earthquakes. Injection of water into the subsurface has induced earthquake swarms in historically quiet regions of North America [Ellsworth, 2013]. Swarms are also observed along transform plate boundaries and are explained as earthquakes triggered by aseismic-creep events [Forsyth et al., 2003; Roland and McGuire, 2009].

Earthquake swarms in subduction zones are thought to be related to the heterogeneous locking of, and fluids on, the plate interface. Holtkamp and Brudzinski [2014] compared the spatial distribution of swarms and plate locking along the Chile Trench, revealing that earthquake swarms are most likely to occur in regions with intermediate amounts of

plate locking, and that regions with active swarms act as barriers to the propagation of large earthquake ruptures. Consequently, they suggested that regions with active swarms might be indicative of heterogeneous locking. Poli et al. [2017] found that earthquake swarms in the central Chile Trench are clustered spatially and have orientations similar to those of local fracture zones, suggesting that fluids expelled from hydrated fracture zones facilitate the occurrence of earthquake swarms.

On the other hand, recent observations suggest that earthquake swarms in subduction zones are triggered by slow slip events (SSEs). For example, recurrent SSEs that accompany earthquake swarms are observed at Boso-Oki, Japan [Ozawa et al., 2003; Sagiya, 2004]. These SSEs have a recurrence interval of 5 to 7 years, and earthquake swarms are observed to occur in the periphery of the SSE areas [Hirose et al., 2012]. SSEs accompanying earthquake swarms are also observed at other subduction zones, including the Hikurangi Trench and Ecuador [Delahaye et al., 2009; Vallée et al. 2013].

It is also possible to use earthquake swarms as potential indicators of SSEs. Kato et al. [2014] detected SSEs at Boso-Oki, Japan, by identifying swarm activity that included repeating earthquakes [e.g., Ellsworth 1995; Nadeau and Johnson, 1998]. Reverso et al. [2016] found a linear relationship between the seismic moment released by SSEs and changes in background seismicity rate during earthquake-swarm periods. Therefore, the systematic detection and analysis of swarm activity at subduction zones is useful for understanding SSE activity globally, which is thought to be related to large earthquakes on the plate interface [e.g., Matsuzawa et al., 2010]. Holtkamp and Brudzinski [2011] compiled an earthquake swarm catalog of circum-Pacific subduction zones for the

period 1973–2010; however, they used a visual search to detect swarms and their criteria for detection were not objective. Zaliapin and Ben-zion [2016] classified and characterized global seismicity using the Nearest Neighbor earthquake Distance method (NND) and found "swarm-like" clusters globally. However, "swarm-like" clusters detected by NND are not necessarily anomalous in terms of Omori's law as pointed out by Reverso et al. [2015].

Reverso et al. [2015] proposed a method to detect earthquake swarms using the space–time epidemic-type aftershock-sequence (ETAS) model [Zhuang et al., 2002], which expresses the seismicity rate as the sum of a stationary background seismicity rate and a superposition of Omori's law, and detected earthquake swarms in the Aleutian arc. They estimated temporal changes in background seismicity rates and classified seismic sequences with increased background seismicity rates as earthquake swarms. To find the increased background seismicity, the method of Reverso et al. [2015] needs to consider an additional parameter that represents durations of earthquake swarms, and they fixed it (e.g., 1 day). However, this is not suitable for global detection of earthquake swarms because durations of earthquake swarms in subduction zones can have large variations (e.g., from a few hours to several months) [Holtkamp and Brudzinski, 2011]. Here, we present another method to objectively detect earthquake swarms using the space–time ETAS model, by which we can detect earthquake swarms with various durations, and we apply this method to detect swarms at subduction zones globally.

2.3. Methods

2.3.1. Space–time ETAS model

The ETAS model [Ogata, 1988] expresses the seismicity rate as the sum of a stationary background seismicity rate and a superposition of Omori's law. Swarms have much higher seismicity rates than predicted by the ETAS model because they occur due to phenomena other than earthquake-to-earthquake triggering and do not decay according to Omori's law [e.g., Llenos et al., 2009; Okutani and Ide, 2011]. In fact, we can use this characteristic to detect seismic swarms within seismic sequences.

In this study, we use the space–time ETAS model of Zhuang et al. [2002]. The model expresses the seismicity rate as

$$\lambda(t,x,y) = \mu(x,y) + \sum_{t_i<t} \kappa(M_i)\, g(t-t_i) f(x-x_i, y-y_i; M_i) \quad (2.1)$$

$$\kappa(M) = Ae^{\alpha(M-M_c)} \quad (2.2)$$

$$g(t) = \frac{p-1}{c}\left(1 + \frac{t}{c}\right)^{-p} \quad (2.3)$$

$$f(x,y;M) = \frac{q-1}{\pi D^2 e^{\gamma(M-M_c)}}\left(1 + \frac{x^2+y^2}{D^2 e^{\gamma(M-M_c)}}\right)^{-q} \quad (2.4)$$

where $\mu(x,y)$ is the background seismicity rate. The second term in (2.1) is the contribution from preceding earthquakes of magnitude M_i located at $(x_i,\ y_i)$ and time t_i, where $M_i \geq M_c$ and $t_i < t$. The dependence on preceding earthquakes is controlled by the seven parameters A, c, α, p, D, q, and γ. M_c denotes the minimum earthquake magnitude in the catalog being used. $\kappa(M)$ defines the expected number of aftershocks, $g(t)$ is the probability density of aftershock lag times, and $f(x,y;M)$ is the probability density of aftershock locations. The seven parameters can be estimated by the maximum likelihood method. The log likelihood is given by

$$\log L = \sum_k \log\lambda(t_k,x_k,y_k) - \int_0^T \iint_A \lambda(t',x,y)\,dxdydt' \quad (2.5)$$

where k runs over all events in the study region A and the time period [0, T] [e.g., Zhuang et al., 2002]. According to Zhuang et al. [2002], the probability that an event at x_i, y_i, and time t_i is a background event is given by

$$P_b = \frac{\mu(x_i,y_i)}{\lambda(t_i,x_i,y_i)} \quad (2.6).$$

Thus, the probability of an event at time t being a triggered event is

$$P_t = 1 - P_b \quad (2.7).$$

Using the above equations, we can calculate the number of events expected from the ETAS model $\Lambda(t)$ in an area S from time 0 to t as

$$\Lambda(t) = \int_0^t \iint_S \lambda(t', x, y) dx dy dt' \quad (2.8).$$

We can then transform the occurrence time t_i of event i in the area S into a transformed time $\tau_i \equiv \Lambda(t_i)$ [Ogata, 1988]. If the seismicity in area S is well described by the ETAS model, the transformed time τ_i will follow a standard Poisson process, and a plot of the cumulative number of observed events against transformed time (i.e., the number of events expected from the ETAS model) will be linear with a slope of unity (Figure 2.1). Slopes greater than unity imply that the observed seismicity rate is greater than that expected from the ETAS model.

The number of events expected by the ETAS model between two successive events (event i and $i+1$) in an area S is calculated as

$$\tau_{i+1} - \tau_i = \int_{t_i}^{t_{i+1}} \iint_S \lambda(t,x,y) dx dy dt \quad (2.9).$$

If the transformed time τ_i follows a standard Poisson process, the standard deviation of the number of events between τ_i and τ_{i+1} will be

$$\sigma = \sqrt{\tau_{i+1} - \tau_i} \quad (2.10).$$

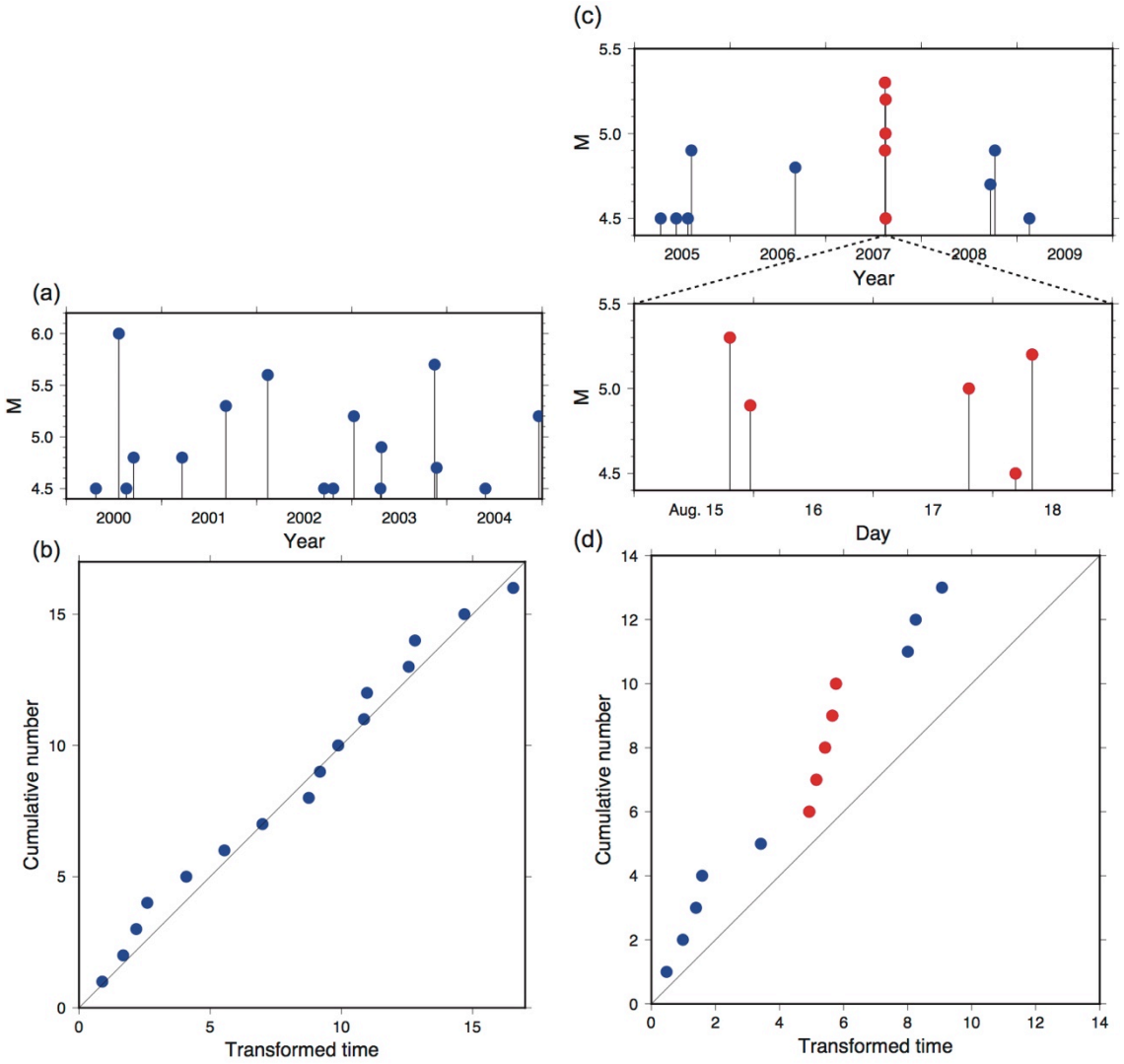

Figure 2.1 | Example calculations of transformed time for the southern Japan Trench. (a) Magnitude versus time diagram for seismicity in the southern Japan Trench. Blue circles denote non-swarm events. (b) Calculated transformed time for the seismicity shown in (a); a line with a slope of unity is also plotted. (c) Magnitude versus time diagram for the 2007 Boso-Oki swarm. Earthquake swarms detected by our analysis are shown as red circles; blue circles denote non-swarm events. (d) Transformed time of the 2007 Boso-Oki swarm; this earthquake swarm has a slope much larger than unity.

2.3.2. Study regions and estimation of the ETAS parameters

We first divided the world's subduction zones into 146 half-overlapping study regions, following Ide [2013]. Each region is bordered by a trench section that is about 500 km long and extends 200 km in the direction of relative plate motion (Figure 2.2). The locations of the trench sections and relative plate motions are based on the plate model PB2002 [Bird, 2003].

We extracted seismic events for the period 1995–2009 from the Advanced National Seismic System (ANSS) catalog and estimated M_c for the 146 study regions using the MAXC method [Wiemer and Wyss, 2000; Woessner and Wiemer, 2005]. The average M_c of the 146 study regions is 4.5, with a standard deviation of 0.2. If we use the largest M_c among 146 study regions for our analysis, we miss many small events in study regions with better magnitude completeness. This is wasteful for statistical analysis of seismicity. Ogata [2005] pointed out that the ETAS model can be used to detect anomalies in seismicity even if the M_c used in the analysis is slightly lower than the actual M_c of the catalog. For these reasons, we used the averaged M_c (= 4.5) of the 146 study regions in the following analyses. However, when comparing seismicity globally, the spatial variations in the M_c can bias results. Therefore, we repeated our analysis using a sufficiently high M_c (= 4.8) in Section 2.5.6. It should also be noted that we neglected the temporal changes in the M_c during intensive earthquake swarms in the following analysis, so we may have missed some small events during intensive earthquake swarms.

We then estimated the seven ETAS parameters for each five-year period 1995–1999,

2000–2004, and 2005–2009 using the maximum likelihood method [Zhuang et al., 2002]. When estimating the ETAS parameters, the background seismicity rate $\mu(x, y)$ was also simultaneously estimated. For the details, see Zhuang et al. [2002]. Considering calculation time needed for the estimation of the ETAS parameters, we divided the ANSS catalog into the three five-year periods. The seismicity in the two years preceding each of these periods was also used to calculate the increase in seismicity rate that is caused by events that occur before each of the time intervals under analysis. According to Maeda [1996], *M* 8 or larger events in subduction zones can have aftershock durations, which are time intervals needed for an increased seismicity rate to return to a background seismicity rate, longer than two years. Therefore, we visually checked seismicity in study regions where *M* 8 or larger events had occurred during 1990–2002 and confirmed that these great earthquakes did not bias our swarm detection. In addition, great earthquakes can rupture across multiple study regions. Therefore, in each study region, we removed aftershock sequences of large earthquakes ($\geq$ *M* 6.5) that had occurred in adjacent study regions from our swarm detection, based on the definition of aftershocks in Maeda [1996].

We did not estimate ETAS parameters for regions in which fewer than 50 events occurred in a seven-year period (i.e., the five-year analysis interval plus the preceding two years) because a lack of events can result in large errors in the derived ETAS parameters. Of the 146 study regions, 36 have fewer than 50 events for all three time intervals; in the following, we exclude these regions from analysis and consider only the remaining 110 regions. It should also be noted that the calculation of ETAS parameters did not converge in some regions; these regions are also not used to detect earthquake

swarms for use in our analysis. We used a code of the space-time ETAS model written by Zhuang et al. [2002] in our analysis. The code tends to not converge when the number of events in the catalog is small or has an increasing trend of the seismicity rate. We attempted to estimate ETAS parameters for 82, 95, and 105 regions for the periods 1995–1999, 2000–2004, and 2005–2009 respectively, with each of these regions having more than 50 events in the relevant seven-year period. The calculation of ETAS parameters converged for 66, 72, and 71 regions for the three respective time periods. In 10 of the 110 study regions, the calculation of ETAS parameters did not converge for all three time periods. In the following analysis, we use only the remaining 100 regions for which the ETAS parameter calculation converged. The estimated ETAS parameters are shown in Appendix A1.1.

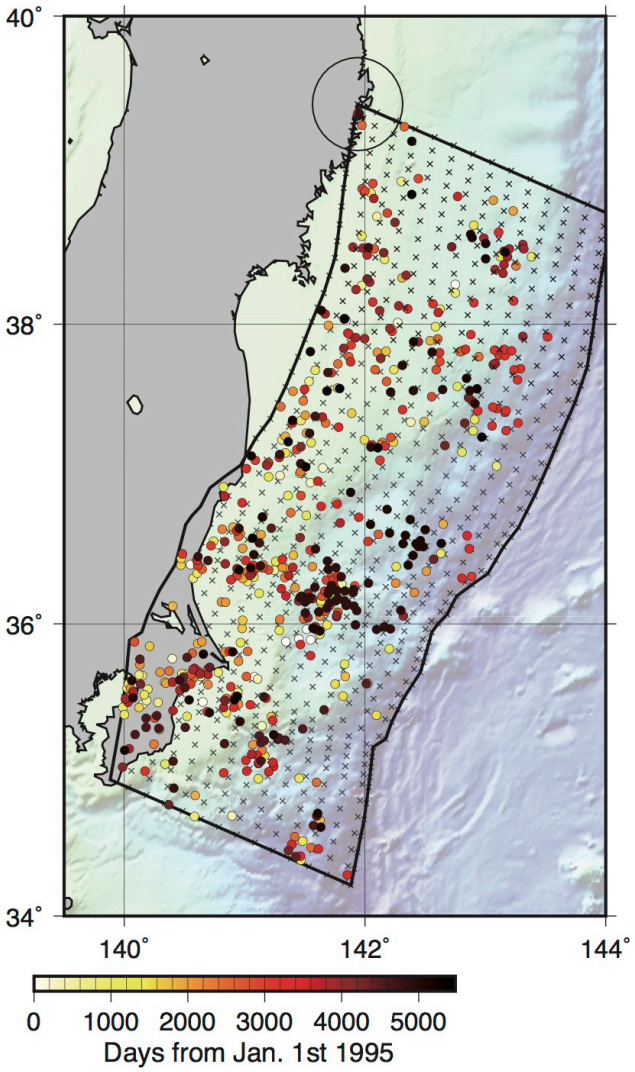

Figure 2.2 | Study region in the southern Japan Trench. Seismic events with $M \geq 4.5$ from the ANSS catalog for the period 1995–2009 are shown by small circles, colored according to their occurrence time. The large circle is an example of a "detection circle" of radius 30 km; small crosses indicate the centers of detection circles used in the analysis of this region (see Section 2.3.3).

2.3.3. Swarm detection and its criterion

We then used (2.8) to calculate the number of events expected by the ETAS model in circles of radius 30 km in each study region (Figure 2.2). The centers of the circles are

distributed at intervals of less than 15 km along strike and dip of the plate interface. Hereafter, we call these circles "detection circles". We used 30-km-radius detection circles because the 2007 Boso-Oki swarm area had a radius of about 30 km [Hirose et al., 2012]. We repeated our analysis using detection circles of radius 60 km, which confirmed that the size of detection circles does not significantly affect our results.

We classify a seismic sequence as a "potential earthquake swarm" when the condition $\tau_{i+1} - \tau_i + \sigma < 1$ continuously holds true four times or more. In other words, the expected number of events between two successive events $\tau_{i+1} - \tau_i$ (2.9) in each detection circle should not exceed unity, even when considering the 1σ error (2.10), for at least four successive events. This criterion enables us to detect seismic sequences with seismicity rates that are higher than those expected by the ETAS model, and requires at least five events for a sequence to be classified as a potential earthquake swarm (see Figure 2.1c and 2.1d). Here, the probability $P_{5,1\sigma}$ that five events obeying the ETAS model have such a high seismicity rate can be calculated as follows. First we rearrange (2.10) to obtain $\tau_{i+1} - \tau_i + \sigma < 1$. Then, we have

$$\tau_{i+1} - \tau_i + \sqrt{\tau_{i+1} - \tau_i} < 1 \quad (2.11),$$

$$\tau_{i+1} - \tau_i < \left(\frac{\sqrt{5}-1}{2}\right)^2 \approx 0.382 \quad (2.12).$$

Since the transformed times of the five events follow the standard Poisson process, we then have

$$P_{5,1\sigma} = (1 - e^{-0.382})^4 \approx 1.02 \times 10^{-2} \quad (2.13).$$

We also investigated cases of 1.5σ and 2σ errors; i.e., $\tau_{i+1} - \tau_i + 1.5\sigma < 1$ and $\tau_{i+1} - \tau_i + 2\sigma < 1$. In both cases, however, we could not detect the 2007 Boso-Oki

swarm, which is quite likely to be triggered by a SSE [Hirose et al., 2012], because the criteria were too strict. Therefore, we use a 1σ error criterion in the following.

In addition, we require the first event of each potential swarm to be a background event (i.e., $P_b \geq 0.5$ (2.6)) because we do not want to classify aftershock sequences with anomalously high seismicity rates as earthquake swarms. Although aftershock sequences with anomalously high seismicity rates might be related to large afterslip events [Marsan et al., 2014], here we focus on earthquake swarms that are potentially related to SSEs rather than afterslip events. However, this requirement ($P_b \geq 0.5$ (2.6)) can result in detection failures of some swarm sequences. This is discussed in Section 2.5.3.

After applying the above detection criterion, we grouped any potential swarms that have common events into a single cluster. Finally, we identified clusters for which the magnitude difference between the largest (M_1) and second largest event (M_2) is less than unity, as Båth's Law implies that $M_1 - M_2 \geq 1$ for typical mainshock–aftershock sequences [Båth, 1965], and we defined these as earthquake swarms. The parameters used for our earthquake-swarm detection analysis are summarized in Table 2.1.

Note that our detection scheme does not assume that earthquake swarms is clustered in a short duration. Therefore, seismic sequences with higher seismicity rates than the prediction of the ETAS model for a long duration can also be classified as earthquake swarms. Thus some earthquake swarms have very long durations (e.g., longer than several months) and are unlike typical earthquake swarms. However, such long-term

increases in background seismicity rates inexplicable by the ETAS model may also suggest some background phenomena. In fact, SSEs can trigger not only typical swarms but also long-term increases in background seismicity rates. For example, an increase in the background seismicity rate that lasted 6 months associated with an SSE from October 2001 and April 2002 was observed in Guerrero, Mexico [Liu et al., 2007; Radiguet et al., 2016].

Table 2.1 | Parameters used for our earthquake-swarm detection analysis.

Parameter for detection	Value
Radius of detection circle	30 km
Required anomaly	$\tau_{i+1} - \tau_i + \sigma < 1$[a]
Minimum number of events in one swarm	5
P_b of the first event of a swarm[b]	≥0.5
$M_1 - M_2$[c]	<1

[a] τ_i is the transformed time for the i-th event in a detection circle, and σ is the standard deviation of the number of events between τ_i and τ_{i+1} (2.10).

[b] P_b is the probability that an event is a background event (2.6).

[c] M_1 and M_2 are magnitudes of the largest and second largest events in a cluster, respectively.

2.3.4. False swarm detections

Even if the transformed times of seismic sequences completely follow a standard Poisson process (i.e., the seismic sequences completely follow the ETAS model), some sequences are falsely classified as swarms by our method. In this section, we estimate

the proportion of events in our catalog that are false positives.

Let us consider a study region with 650 detection circles, and assume that each detection circle contains 7 events. These choices are reasonable since they respectively correspond to the average number of detection circles in all study regions and the average number of events in all detection circles in this study. For simplicity, we assume that these detection circles do not overlap; i.e., we have $650 \times 7 = 4550$ distinct events. We determined the transformed times of events in each detection circle using a Monte Carlo method, assuming that the transformed times in each detection circle follow a standard Poisson process. Then, we applied the criterion described in the previous section to detect potential earthquake swarms. We repeated this procedure 1000 times. In these simulations, on average 1.8% of the 4550 events were classified as potential swarms, with a standard deviation of 0.5%. This result suggests that on average our method falsely classifies 1.8% of all events in the catalog as potential swarms even if seismic sequences completely follow the ETAS model. False detections tend to increase with the number of events per detection circle. A study region in Philippines during 1995–1999 has the largest average number of events per detection circle (29 events per detection circle). We repeated our Monte Carlo simulation assuming that each detection circle contains 29 events. As a result, we detected 3.4 % of the all events as potential swarms on average. This suggests that our method classify 3.4 % of all events in catalog as potential swarms at the most.

2.4. Results

2.4.1. Example swarm detections

2.4.1.1. Southern Japan Trench

Figure 2.3 shows an example of swarms detected in the southern Japan Trench. We detected nine earthquake swarms during the interval 1995–2009. At Boso-Oki, three swarms are known to have been accompanied by SSEs in this period [Hirose et al., 2012]. Of these, we detected only the 2007 swarm in our analysis because the magnitude of all events in the other two swarms is below the magnitude of completeness $M_c = 4.5$ for our catalog. The cumulative number of events during 2005–2009 is plotted against transformed time (i.e., the number of events expected from the ETAS model) in Figure 2.1c and 2.1d. The slope during the 2007 Boso-Oki swarm period is much greater than unity, which implies that this swarm had much higher seismicity rates than those expected by the ETAS model.

Figure 2.3b shows the ratio between the number of background events in detected swarms and the number of all background events in each detection circle; we call this ratio the "swarm ratio". This figure shows that Boso-Oki and offshore Boso-Oki have high swarm ratios. Only two colored detection circles on the southwest edge of the study region detected the 2007 Boso-Oki swarm. This is because the 2007 Boso-Oki swarm contains only five events, which are the minimum requirement in our detection criterion, although its seismicity rate is about 5 times higher than the prediction of the ETAS model. On the other hand, two swarms in offshore Boso-Oki in 2004 (nine events with a seismicity rate 14 times higher than the prediction) and 2007 (eight events with a seismicity rate 10 times higher than the prediction) have more anomalous seismicity and

were detected by many detection circles. They are not related to the Boso-Oki SSEs and newly detected by our analysis. Ibaraki-Oki also shows very high swarm activity. This region experienced four swarms during the period 1995–2009 (Figure 2.4). One of these swarms is actually a foreshock sequence of the M 6.9 2008 Ibaraki-Oki earthquake (see Figures 2.3, 2.4c, and 2.4d). Here, we define foreshocks as seismic sequences that are followed by an event with $M \geq 6.5$ that occurs within five days and 50 km of the each foreshock events.

An $M \geq 6.5$ event can also be triggered by an event larger than itself, which is assumed to have occurred when the probability that the $M \geq 6.5$ event was triggered by a larger event calculated by the ETAS model exceeds 0.5. In this case, we do not treat seismic sequences preceding the $M \geq 6.5$ event as foreshocks, because they actually represent early aftershocks of the larger event. Hereafter, we refer to a foreshock sequence with high seismicity rates that cannot be explained by the ETAS model as a "swarm-like foreshock sequence".

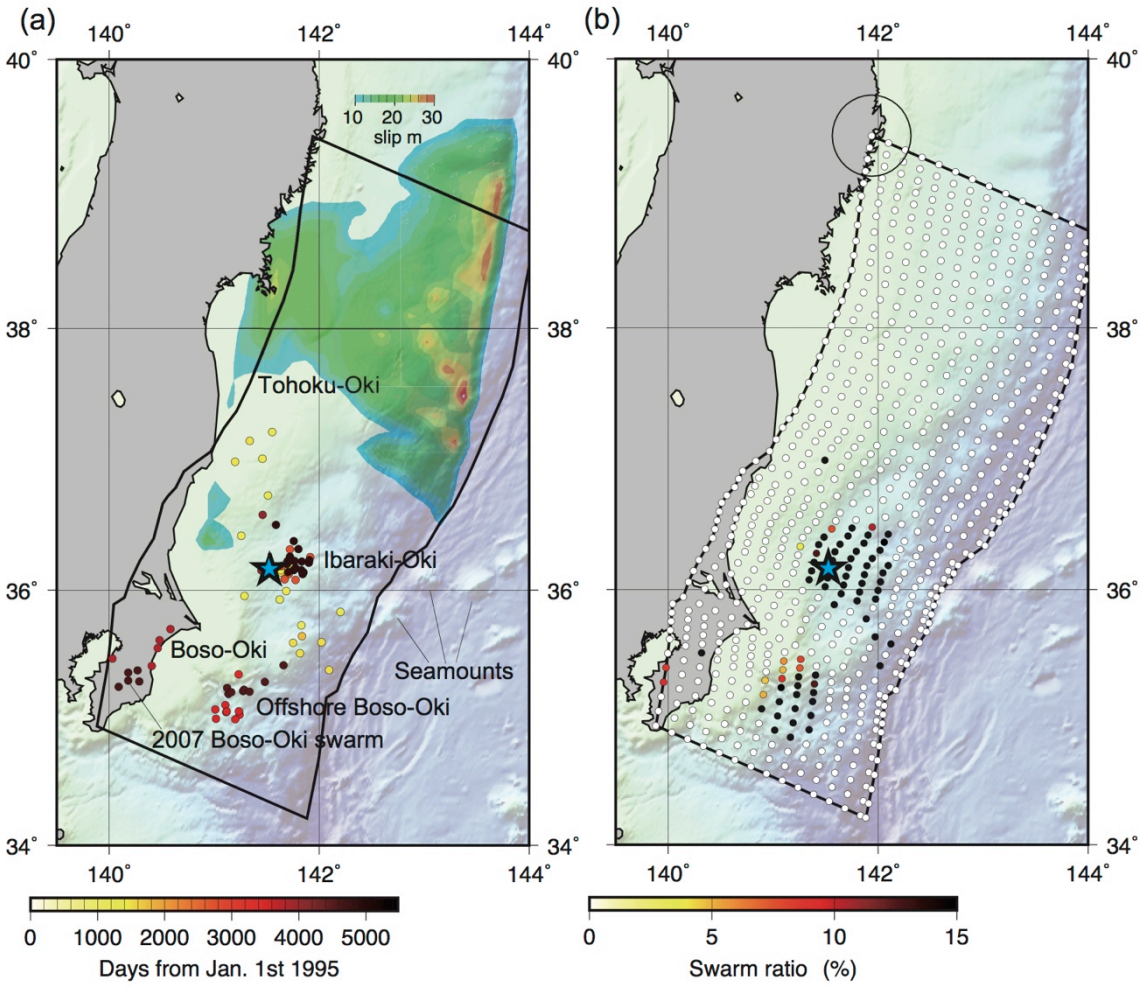

Figure 2.3 | Detected swarms and swarm ratios in the southern Japan Trench. (a) Hypocenters of swarms detected by our analysis. Hypocenters of detected swarms are shown as small circles and colored according to their occurrence time. The hypocenter of the 2008 *M* 6.9 Ibaraki-Oki earthquake is indicated by the blue star. The color shading denotes areas where more than 10 m of slip occurred during the 2011 Tohoku earthquake [Ide et al., 2011]. (b) Swarm ratios calculated for each detection circle. The large circle is an example of a detection circle of radius 30 km; small circles indicate the center of each detection circle and are colored according to the computed swarm ratio.

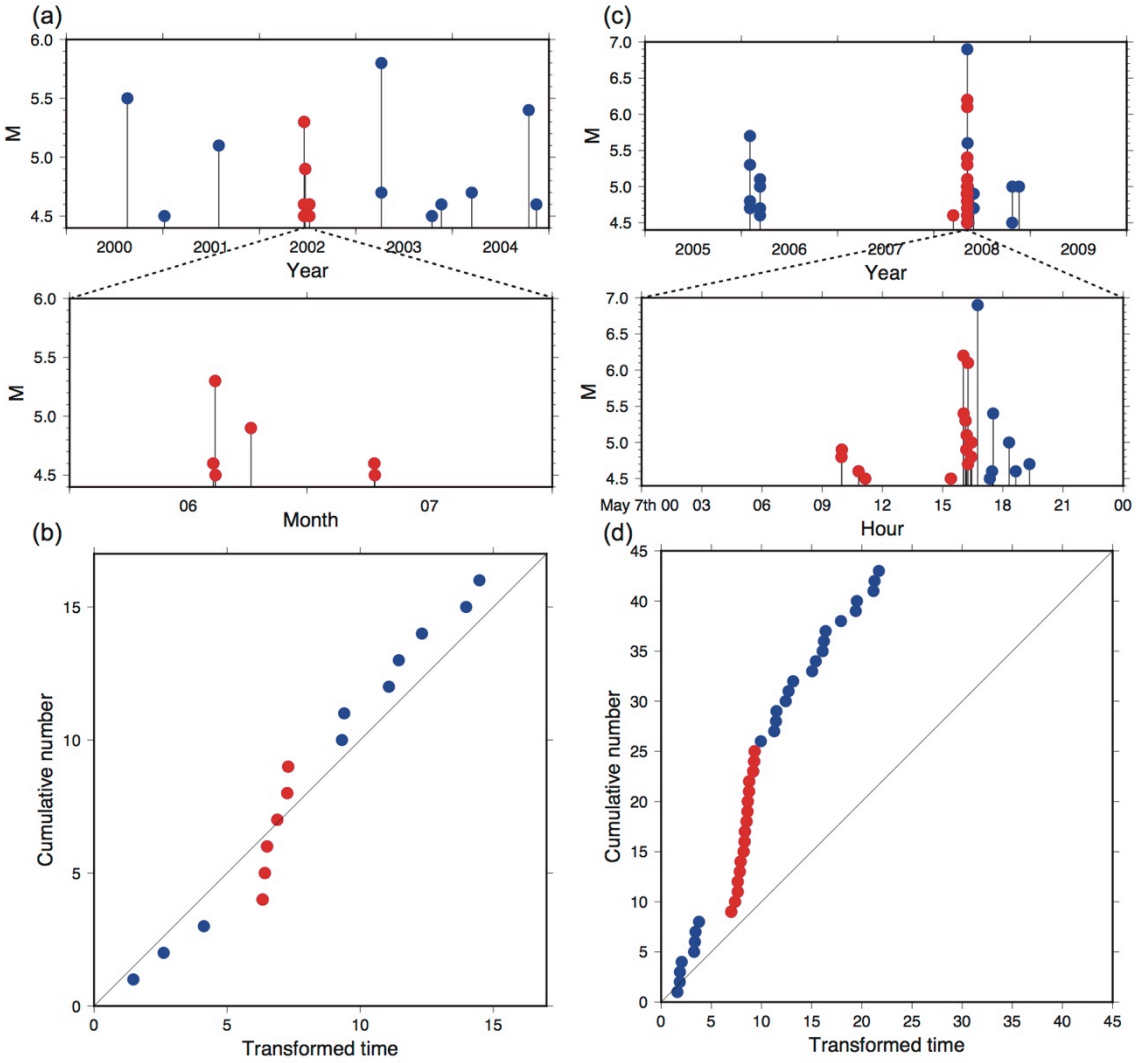

Figure 2.4 | Transformed times of earthquake swarms in Ibaraki-Oki, Japan. (a) Magnitude versus time diagram of an earthquake swarm in 2002 in Ibaraki-Oki. Red circles denote earthquake swarms detected by our analysis; blue circles represent non-swarm events. (b) Calculated transformed time for the seismicity shown in (a). (c) Magnitude versus time diagram for a swarm-like foreshock sequence preceding the 2008 *M* 6.9 Ibaraki-Oki earthquake. (d) Transformed time of the swarm-like foreshock sequence preceding the 2008 *M* 6.9 Ibaraki-Oki earthquake.

2.4.1.2. Kurile

We detected 10 earthquake swarms during the period 1995–2009 in the Kurile study region (Figure 2.5). The 1995 Iturup swarm [The Headquarters for Earthquake Research Promotion, 1995], which was not reported in the catalog of Holtkamp and Brudzinski [2011], is successfully detected by our method (see Figures 2.5, 2.6a, and 2.6b). Another swarm is detected in 2003 in the same detection circle as the 1995 Iturup swarm, and areas around the 1995 Iturup earthquake swarm have relatively high swarm ratios (Figure 2.5b).

Large amounts of swarm activity are also observed offshore of Simushir Island, with two swarms occurring during 1995–2009 (Figure 2.5a). The first swarm, in 1997, was an ordinary swarm; the second was a swarm-like foreshock sequence preceding an M 6.6 event that occurred in September 2006 (Figure 2.6c and 2.6d). Relatively high seismicity rates continued in this region until November 2006 (Figure 2.6c), leading to the occurrence of the 2006 M 8.3 Kurile Islands earthquake [Ammon et al., 2008], although we did not detect these sequences as earthquake swarms (see Section 2.5.3).

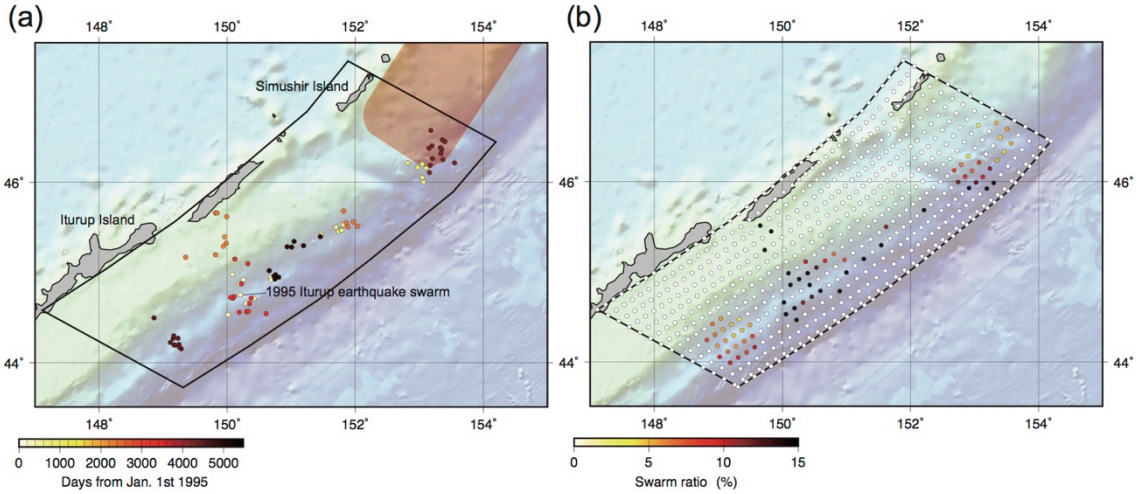

Figure 2.5 | Detected swarms and swarm ratios in the Kurile region. (a) Hypocenters of swarms detected by our analysis. Hypocenters of detected swarms are shown as small circles and colored according to their occurrence time. The orange shading denotes the area where more than 1 m of slip occurred during the 2006 *M* 8.3 Kurile Islands earthquake [Ammon et al., 2008]. (b) Swarm ratios calculated for each detection circle; small circles indicate the center of each detection circle and are colored according to the computed swarm ratio.

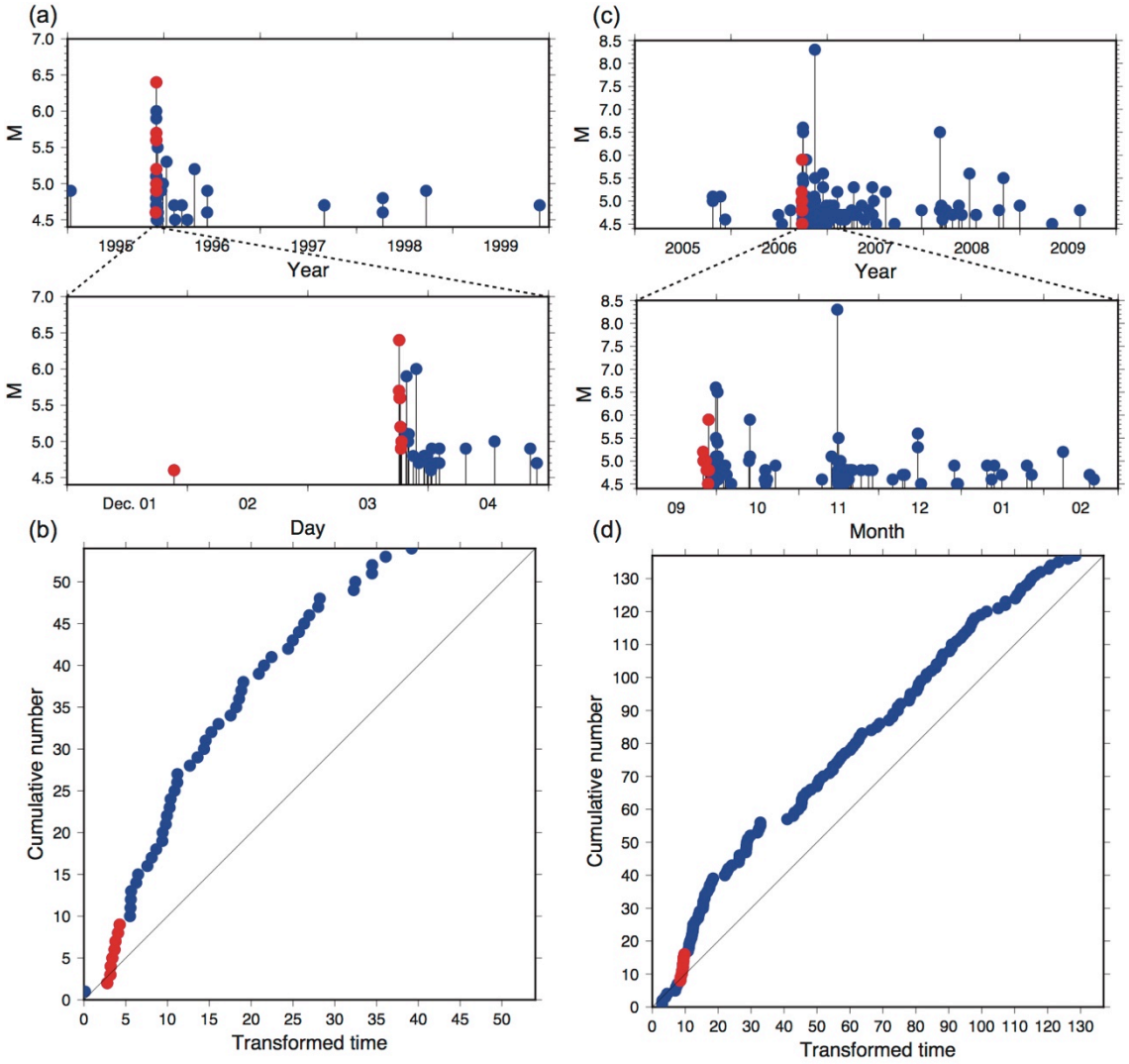

Figure 2.6 | Transformed times of earthquake swarms in Kurile. (a) Magnitude versus time diagram of the 1995 Iturup swarm. Red circles denote earthquake swarms detected by our analysis; blue circles represent non-swarm events. (b) Calculated transformed time of the 1995 Iturup swarm. (c) Magnitude versus time diagram of a swarm-like foreshock sequence for a *M* 6.6 event that preceded the 2006 Kurile Islands earthquake. (d) Transformed time of the swarm-like foreshock sequence of a *M* 6.6 event that preceded the 2006 Kurile Islands earthquake.

2.4.1.3. Kermadec

The Kermadec study region is characterized by intense swarm activity. We detected 28 earthquake swarms in the region during the period 1995–2009 (Figure 2.7), with swarms repeatedly being observed at the same locations. For example, four swarms are detected over this time interval within a detection circle centered at (33.2°S, 178.2°W); three of the four recurring swarms in this detection circle are visible in Figure 2.8.

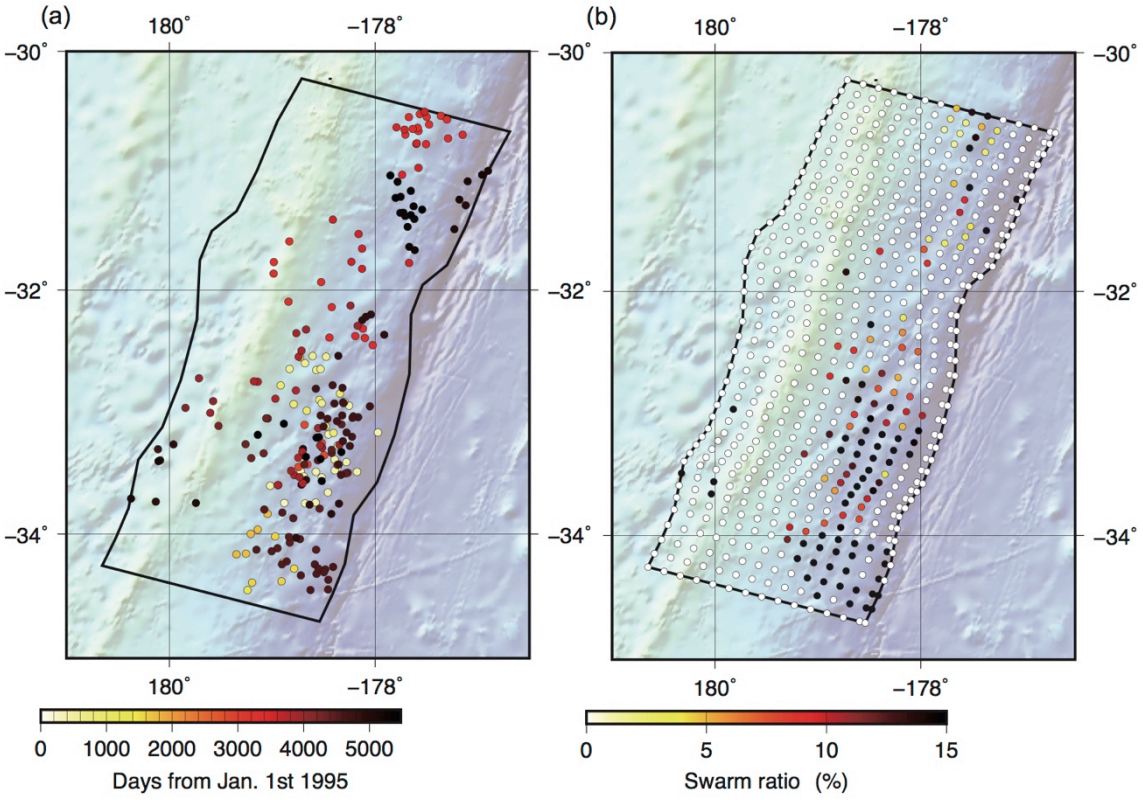

Figure 2.7 | Detected swarms and swarm ratios in Kermadec. (a) Hypocenters of swarms detected by our analysis. Hypocenters of detected swarms are shown as small circles and colored according to their occurrence time. (b) Swarm ratios calculated for each detection circle; small circles indicate the center of each detection circle and are colored according to the computed swarm ratio.

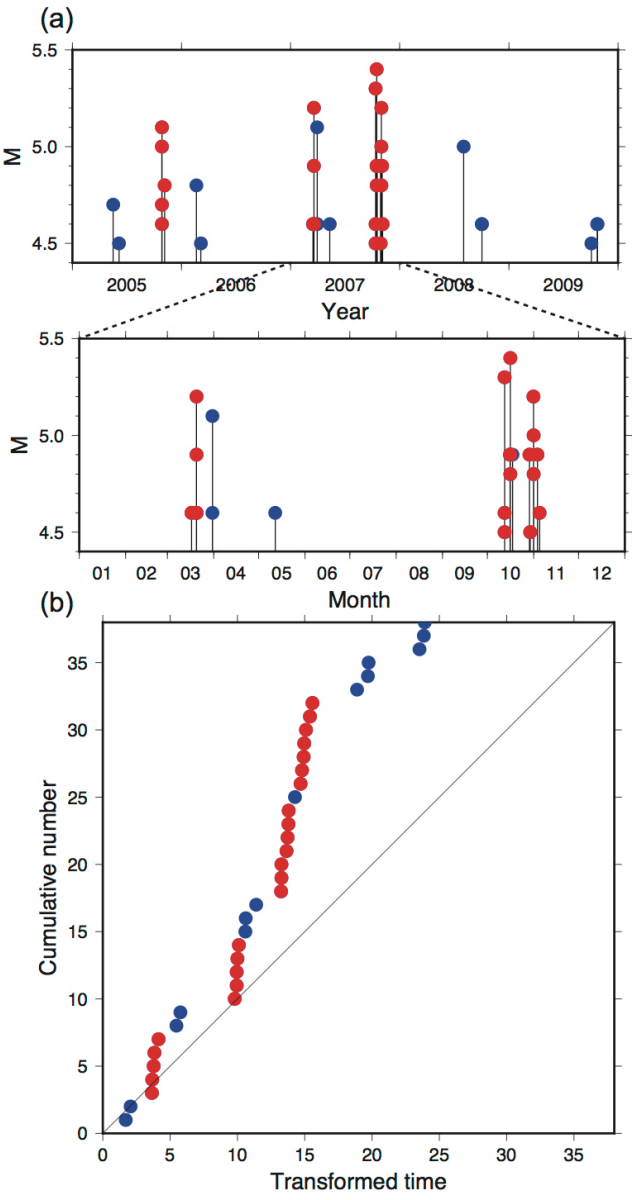

Figure 2.8 | Transformed times of earthquake swarms in Kermadec. (a) Magnitude versus time diagrams for three swarms detected in Kermadec. Red circles denote earthquake swarms detected by our analysis; blue circles represent non-swarm events. (b) Calculated transformed times for the three swarms. The third swarm, which occurred in October 2007, has been separated into two swarms in these figures. However, clustering of the detected swarms meant that it was originally detected as a single swarm (see Section 2.3.3).

2.4.2. Swarms detected at subduction zones globally

2.4.2.1. Characteristics of detected swarms

We detected 453 swarms during the period 1995–2009 at subduction zones globally. Of the 453 swarms, 14 are actually swarm-like foreshocks. The number of events in each detected swarm sequence varies from five events to twenty-six events. Its average and standard deviation are 7.5 events and 3.6 events. The swarm sequence that contains the largest number of events (twenty six events) is a swarm in Kermadec from February 1997 to June 1997. Durations of detected swarms vary from a few tens of minutes to two years. Median inter-event time for each swarm sequence is useful for quantifying the degree of clustering in time of detected swarm sequence. The median inter-event time of 332 of the 453 detected swarm sequences (i.e., 73 %) are from 0 to 10 days. The remaining 121 sequences (i.e., 27 %) have longer median inter-event time. These sequences are not like typical earthquake swarms clustered in space and time, and rather classified as long-term increases in background seismicity rates.

Next, we characterize detected swarms following the method of Vidale and Shearer (2006). Figure 2.9 shows the relationship between the number of events and magnitude of the largest event in each swarm sequence, together with those of randomly sampled mainshock-aftershock sequences. The number of aftershocks is calculated as the summation of probabilities of being triggered by a mainshock for each event following the mainshock using the ETAS model. According to Zhuang [2002], the probability $\rho_{i,j}$ that the *j*th event is an aftershock of the *i*th event is

$$\rho_{i,j} = \frac{\kappa(M_i)g(t_j-t_i)f(x_j-x_i,y_j-y_i;M_i)}{\lambda(x_j,y_j)} \quad (2.14).$$

The summation also includes probabilities of being triggered by aftershocks (i.e.,

secondary aftershocks). For example, the probability that the *k*th event is an aftershock of the *j*th event and the *j*th event is an aftershock of the *i*th event, i.e., the *k*th event is a secondary aftershock of the *i*th event via the *j*th event, is given by $\rho_{j,k}\rho_{i,j}$. In Figure 2.9, we also showed the number of aftershocks expected from the ETAS model in the southern Japan Trench in the period 2005–2009 for reference (a green dashed line). This line only considers aftershocks directly triggered by a mainshock. In this figure, the number of events in detected swarm sequences, unlike mainshock-aftershock sequences, is not a function of the magnitude of the largest event in the sequence. Furthermore, swarms with the maximum magnitude smaller than M6.5 are well differentiated from mainshock-aftershock sequences. These results confirm that our method certainly detects swarm-like sequences defined by Vidale and Shearer (2006). On the other hand, swarms with the maximum magnitude larger M6.5 are not differentiated from mainshock-aftershock sequences. This may be due to a limitation of our method. Our method tends to underestimate the number of events in each swarm sequence when a swarm sequence has a small time-gap in the middle as discussed in Section 2.5.3.

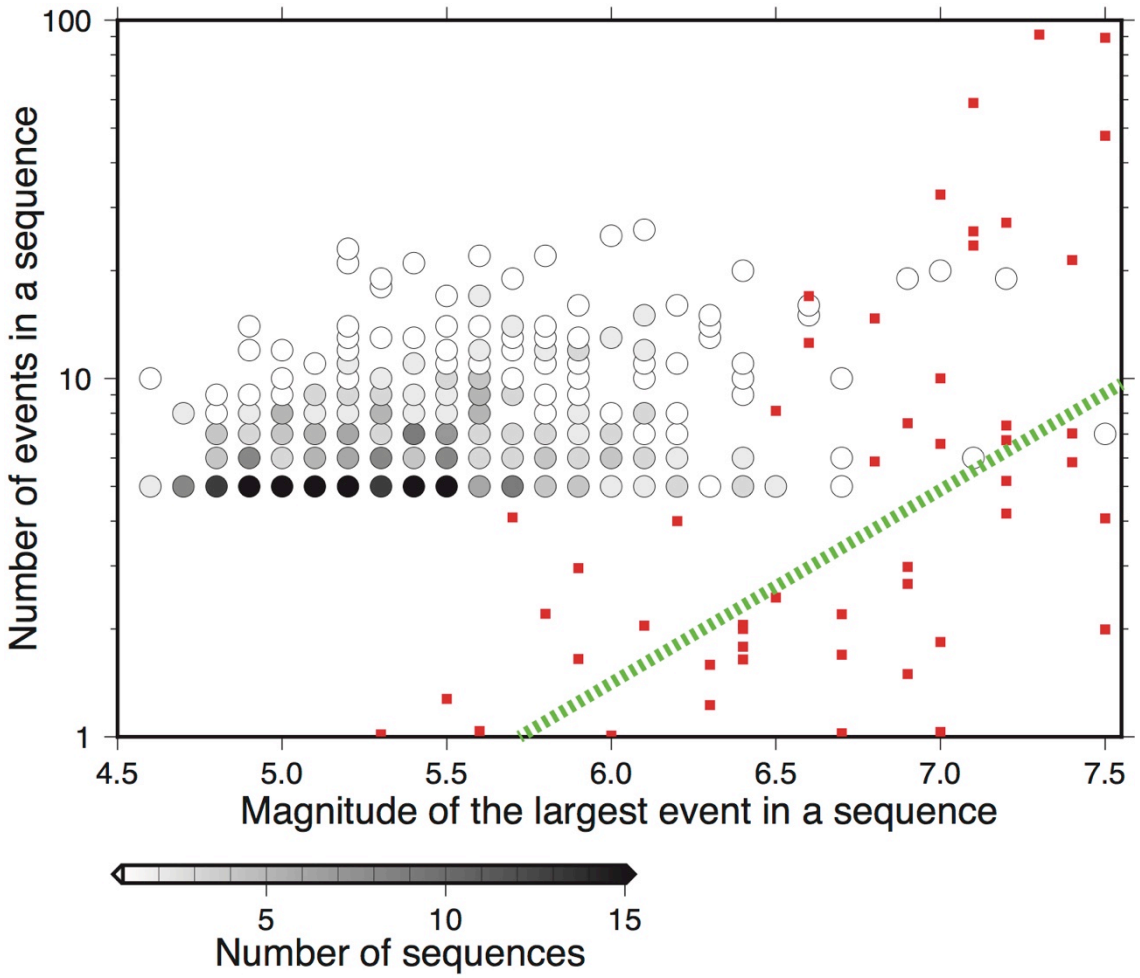

Figure 2.9 | Relationship between the number of events and magnitude of the largest event in an earthquake sequence. Gray-scaled circles are swarm sequences. The circles are colored according to the number of sequences with the same number of events and magnitude of the largest event. Red points are randomly sampled mainshock-aftershock sequences. The green dashed line indicates the number of aftershocks expected from the ETAS model in the southern Japan Trench in the period 2005–2009.

2.4.2.2. Spatial distribution of detected swarms

The hypocenters of the 453 detected swarms are shown in Figure 2.10a. Almost all

subduction zones globally experienced earthquake swarms during the period 1995–2009. However, no swarms were detected in the Andaman subduction zone. The absence of swarms there is partly a consequence of an extremely high aftershock rate caused by the M_w 9.3 Sumatra–Andaman earthquake of December 26th, 2004, which prevents us from detecting swarms in this region between 2005 and 2009. The number of swarm events and the swarm ratio in each study region are shown in Figure 2.10b and 2.10c, respectively. The number of swarm events and the swarm ratio are averaged over the three time periods 1995–1999, 2000–2004, and 2005–2009. Subduction zones such as those at Vanuatu, Tonga, Kermadec, the Philippines, and South Sandwich are characterized by very high swarm activity. In these regions, earthquake swarms repeatedly occur at the same location (Figure 2.10a).

In addition, swarm activity exhibits large along-strike variation at each subduction zone. For example, along the Japan Trench, Ibaraki–Boso-Oki has experienced recurring swarm activity. However, Figures 2.3a and 2.10a show that no swarms were observed in the rupture area of the 2011 M 9 Tohoku earthquake, which lies just north of Ibaraki–Boso-Oki [Ide et al., 2011], in agreement with Holtkamp and Brudzinski [2014]. On the other hand, in offshore Sanriku-Oki, which is further north of the rupture area, some earthquakes swarm sequences were observed (Figure 2.10a). Similarly, in the Kermadec region a large change in the swarm ratio from 11% to 3% is seen between (34.6°S, 181.5°E) and the area just to the south at (36.8°S, 180.3°E), as is apparent from Figure 2.10c.

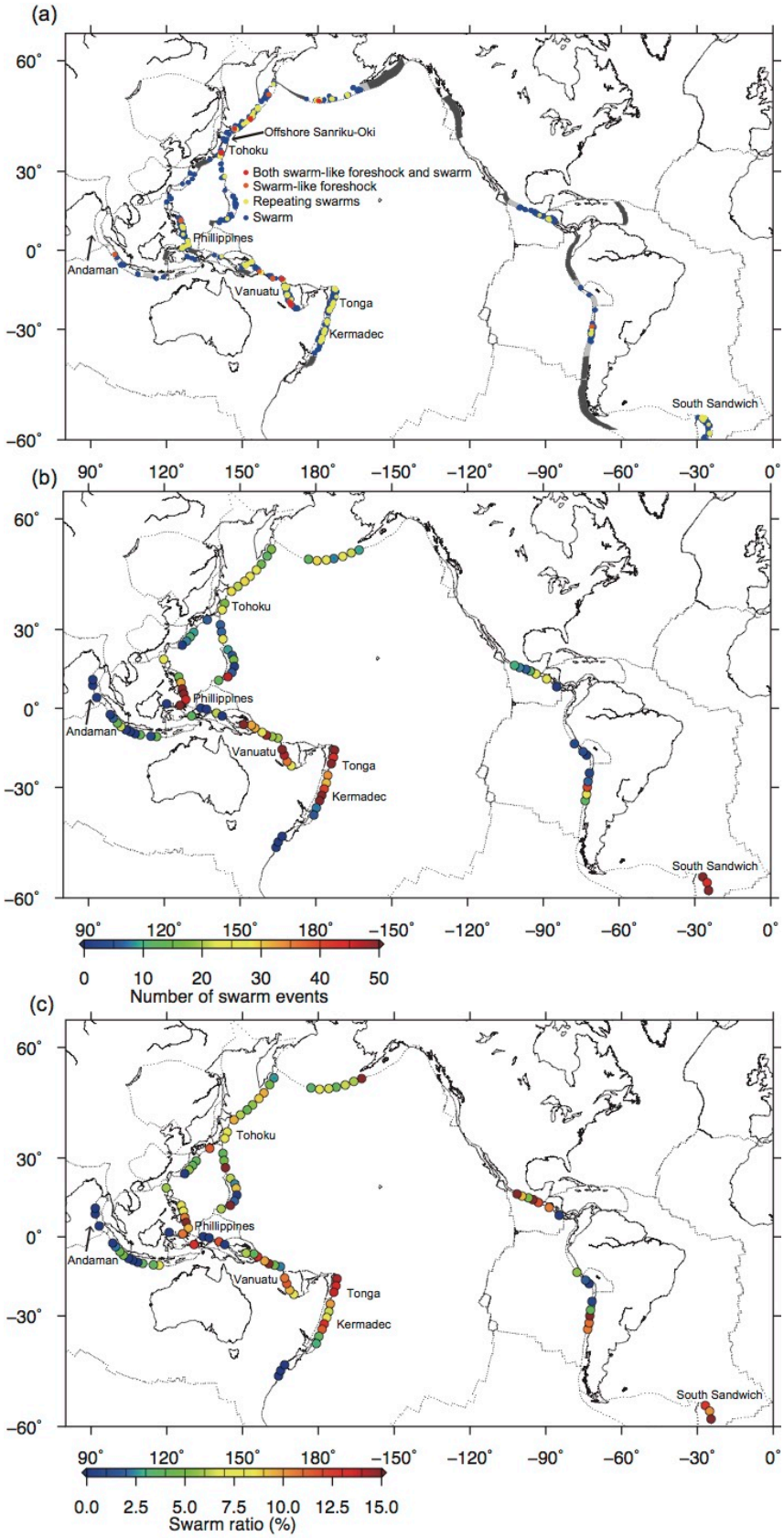

Figure 2.10 | Swarm activity at subduction zones globally. (a) Map showing the

hypocenters of swarms detected by our analysis, plotted as blue dots. Detection circles where two or more earthquake swarms were found (i.e., repeating swarms) are shown by yellow dots. Swarm-like foreshocks are plotted as orange dots; detection circles where we observed both swarm-like foreshocks and swarms are plotted as red dots. Areas shaded dark gray indicate study regions where we did not estimate the seven ETAS parameters because fewer than 50 events were observed in all three time periods under consideration. Areas shaded light gray represent the 10 regions where the calculation of ETAS parameters did not converge for all of the time periods. (b) Map showing the number of swarm events in the 100 study regions. (c) Map showing swarm ratios in the 100 study regions. The number of swarm events and the swarm ratios plotted are averaged over the three time periods 1995–1999, 2000–2004, and 2005–2009.

2.5. Discussion

2.5.1. Comparison with a previous swarm catalog

Holtkamp and Brudzinski [2011] detected 68 megathrust swarms by visual search in our 110 study regions during the period 1995–2009, which is about one-seventh of the number detected in this study. Of these 68 swarms, 44 (i.e., 65%) were also detected in our analysis; 16 of the 68 swarms (i.e., 24%) were not detected because their seismicity rates were not high enough compared with the values predicted by the ETAS model. A further three swarms were not detected in this study because they were not classified as earthquake swarms but rather as aftershock sequences with anomalously high seismicity rates. Two swarms were not detected because the magnitude difference between the largest two events is not less than unity. The remaining three swarms were not detected

in our analysis because the calculation of ETAS parameters did not converge or because the number of events was too small to estimate the ETAS parameters in the study region.

Comparing the spatial distribution of earthquake swarms in the two catalogs, we see that Holtkamp and Brudzinski [2011] also detected many swarms in Vanuatu and the Kermadec region, which is consistent with our analysis. However, they did not detect any swarms in northern Tonga, whereas Tonga is characterized by large amounts of swarm activity in our analysis (Figure 2.10). This difference might be explained by the very high rate of background seismicity in northern Tonga [Ide, 2013], which makes it difficult to detect swarms by a visual search.

2.5.2. Choice of detection threshold

The events in our earthquake-swarm catalog depend on the choice of parameters used for our analysis (Table 2.1), and especially on the anomaly required for detection, chosen here as 1σ. We adopted this value based on a preliminary analysis performed for the 2007 Boso-Oki swarm (Section 2.3.3), which is thought to have been triggered by an SSE [Hirose et al., 2012]. This value is appropriate because the focus in this study is earthquake swarms that are potentially related to SSEs and thus similar to the 2007 Boso-Oki swarm. Using a more strict detection threshold means that our scheme identifies only those seismic sequences with more anomalous seismicity rates, and so the number of earthquake swarms detected decreases. For example, from (2.11)–(2.13) and using 1.5σ and 2σ errors as the anomalies required for swarm detection, the probabilities $P_{5,1.5\sigma}$ and $P_{5,2\sigma}$ that five events that follow the ETAS model have such

high seismicity rates decrease to 2.39×10^{-3} and 6.18×10^{-4}, respectively. Therefore, when compared with the 1σ case, a seismic sequence must be 4.3 times or 16.5 times more anomalous for classification as a swarm when using a 1.5σ or 2σ criterion, respectively, since $P_{5,1\sigma} / P_{5,1.5\sigma} \approx 4.3$ and $P_{5,1\sigma} / P_{5,2\sigma} \approx 16.5$ (13). As a result, the number of earthquake swarms detected decreases from 453 (1σ) to 206 (1.5σ) to 94 (2σ); use of a stricter criterion also means that many earthquake swarms that are potentially related to SSEs, such as the 2007 Boso-Oki swarm, are excluded. We could also have used a less strict detection threshold, such as 0.5σ. In this case, the minimum number of events required to define a swarm should be increased to avoid false-positive swarm detections (see Section. 2.3.4).

2.5.3. Limitations of our method

Though our method is simple and useful to detect anomalous seismicity that does not follow the ETAS model, there are some limitations to be noted.

Because of the requirement that the first event of each potential swarm to be a background event (i.e., $P_b \geq 0.5$ (2.6)), we miss earthquake swarms in following two scenarios. The first scenario is that one swarm sequence with a small time-gap in the middle occurred. In this scenario, we can detect the beginning part of the swarm sequence, but often miss its succeeding part. This is because a probability that the first event in the succeeding part is an aftershock of the beginning part is high (i.e., $P_t > 0.5$ (2.7)). The second scenario is that an earthquake swarm was preceded by a foreshock sequence following the ETAS model. In this case, the swarm sequence cannot be differentiated from aftershock sequences with anomalously high seismicity rates in our

study. Examples of these detection failures in the southern Japan Trench and the Kurile trench are shown in Appendix A1.2. These examples show that our method may underestimate the number of events in each swarm sequence because we sometimes miss a succeeding part of each swarm sequence as in the first scenario. However, the number of swarm sequences is not strongly affected by the requirement of $P_b \geq 0.5$ because detection failures as in the second scenario are relatively rare.

The requirement that $\tau_{i+1} - \tau_i + \sigma < 1$ continuously holds true four times or more also can result in detection failures. This requirement is rather strict. If this requirement is broken once due to a small time gap in a swarm sequence, we can no longer detect events following the time gap. However, if we relax these requirements, we will have more false-positive swarm detections. Therefore, in this study, we used this simple and strict detection criterion.

The size of study regions (about 500 km along strike and 200 km in the direction of relative plate motion) also can affect our swarm detection. If there are small sub-regions where aftershock productivity is about three times larger than that of the entire study region, our method cannot differentiate between swarm sequences and aftershock sequences. To investigate how the size of study regions affects our swarm detection, we made a half-sized study region (about 250 km along strike) in the southern Japan Trench (Ibaraki-Boso-Oki), where swarm activities were especially high in our analysis (Figure 2.3a), and detected earthquake swarms again. Figure 2.11 shows detected earthquake swarms in the half-sized study region. The detected swarms are the same as those detected using the larger study region (about 500 km along strike). Therefore, the

influence of the size of the study region is small at least in the southern Japan Trench.

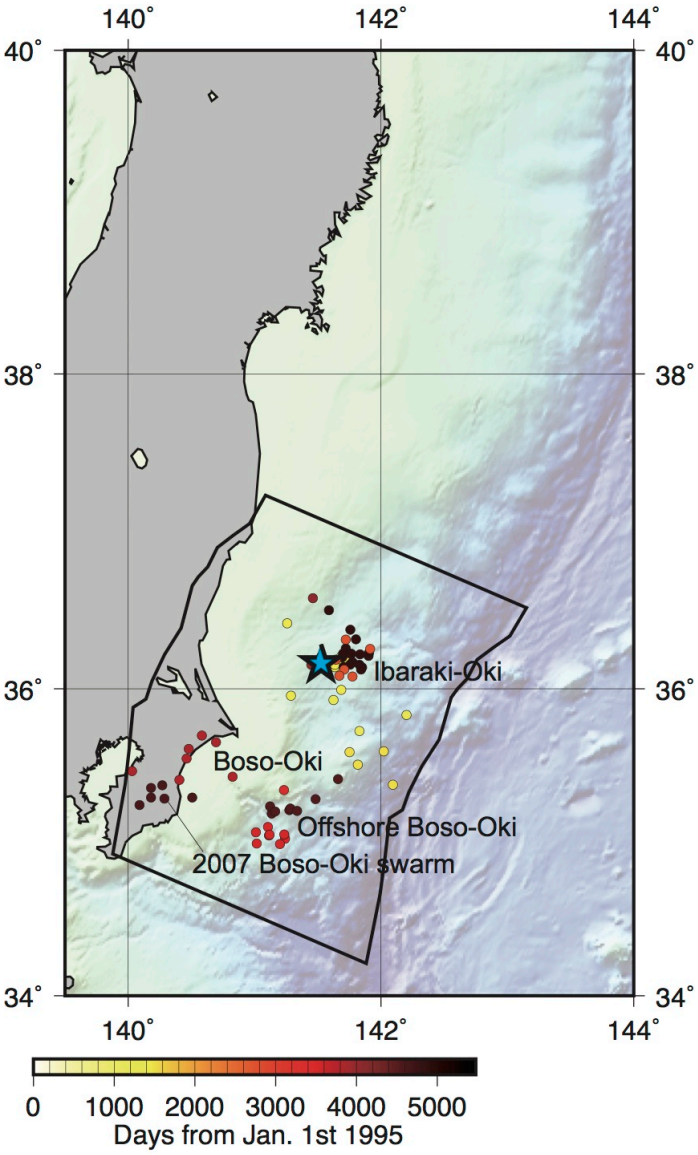

Figure 2.11 | Swarms detected in a half-sized study region in the southern Japan Trench. Hypocenters of detected swarms are shown as small circles and colored according to their occurrence time. The hypocenter of the 2008 *M* 6.9 Ibaraki-Oki earthquake is indicated by a blue star.

2.5.4. Earthquake swarms associated with SSEs

In some subduction zones, earthquake swarms accompanied by SSEs have been observed. As already mentioned in Section 2.2 and Section 2.4.1.1, recurring swarm activity and SSEs with a recurrence interval 5 to 7 years are observed in Boso-Oki, Japan. In addition to Boso-Oki, earthquake swarms associated with SSEs were also observed in Hikurangi (New Zealand), Ecuador, and Guerrero (Mexico). A complex history of SSEs in Hikurangi was revealed by Wallace and Beavan [2010]. These SSEs trigger swarm activities of small earthquakes [Delahaye et al., 2009]. However, we could not detect these swarms because their magnitude (from M 2 to M 3) is smaller than our M_c (= 4.5). In Ecuador, an SSE accompanying earthquake swarms were observed in 2010 [Vallée et al., 2013]. In addition to the 2010 SSE, Vallée et al. [2013] inferred occurrences of SSEs in 1977, 1998, 2002, and 2005 from occurrences of intense earthquake swarms. However, we also missed these swarms. This is because the background seismicity rate in Ecuador is very low, and we did not have enough events (more than 50 events in a seven-year period) to estimate ETAS parameters there. In contrast to Hikurangi and Ecuador, we successfully detected an increased seismicity rate associated with an SSE from October 2001 to April 2002 in Guerrero, Mexico [Liu et al., 2007; Radiguet et al., 2016] as a swarm sequence (Figures 2.12 and 2.13). The beginning of this increased seismicity coincided with that of the SSE and lasted for more than six months.

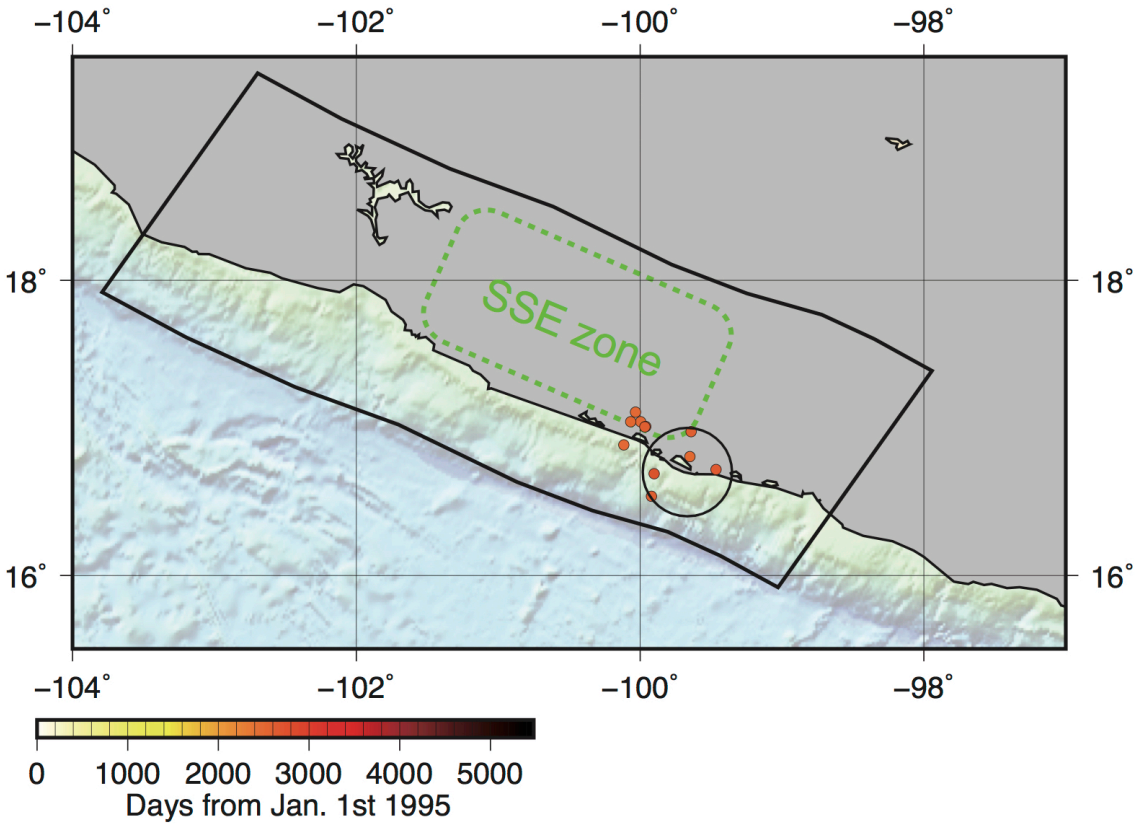

Figure 2.12 | Hypocenters of earthquake swarms associated with an SSE from October 2001 to April 2002 in Guerrero, Mexico. Hypocenters of the swarms are shown as small circles and colored according to their occurrence time. The black circle is one of the detection circles in which we detected this swarm sequence. Seismicity in this detection circle is shown in Figure 2.13. The green dashed rectangle indicates the SSE zone [Radiguet et al., 2016].

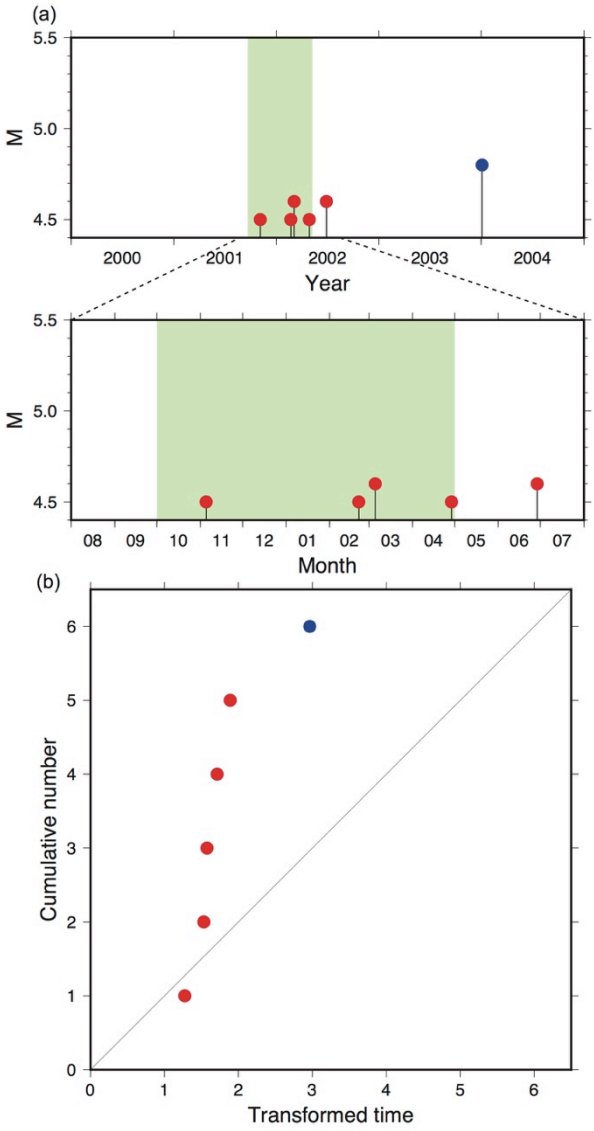

Figure 2.13 | Transformed time of an earthquake swarm in Guerrero, Mexico. (a) Magnitude versus time diagram of a swarm sequence associated with an SSE from October 2001 to April 2002 in Guerrero. Red circles denote earthquake swarms detected by our analysis; blue circles represent non-swarm events. The green shaded time period indicates the duration of the SSE. (b) Calculated transformed time for the seismicity shown in (a).

2.5.5. Swarm-like foreshocks and recurring swarm activity

In our study regions, 227 large earthquakes ($M \geq 6.5$) occurred during the period 1995–2009. Here we excluded $M \geq 6.5$ events that were triggered by a larger event (See Section 2.4.1.1). 57 events of the 227 events (25%) were preceded by foreshock sequences. 14 events of the 227 events (6%) were preceded by swarm-like foreshock sequences (Figure 2.10a). Some of the 14 swarm-like foreshock sequences were particularly vigorous and included more than 10 events. Examples include the sequences preceding the 2008 M 6.9 Ibaraki-Oki earthquake (Figure 2.4c and 2.4d), a M 6.6 event preceding the M 8.3 2006 Kurile Island earthquake (Figure 2.6c and 2.6d), and a M 6.5 event in 2007 in Vanuatu. From (2.11)–(2.13), we see that the probability $P_{10,1\sigma}$ that 10 events obeying the ETAS model have such high seismicity rates is less than 3×10^{-5}. Therefore, these anomalously high seismicity rates imply the existence of a hidden mechanism, other than earthquake-to-earthquake triggering, that triggered these events.

Recent studies have also reported foreshock sequences in subduction zones that do not follow the stationary ETAS model. For example, Kato et al. [2016] observed an increase in background seismicity rate in the week preceding the 2014 M_w 8.2 Iquique earthquake. Analyses using repeating earthquakes and Global Positioning System (GPS) measurements suggest that an SSE preceding the M_w 8.2 event caused this increased rate of background seismicity [Ruiz et al., 2014; Kato et al., 2016]. Bouchon et al. [2013] investigated seismicity preceding large interplate earthquakes (i.e., $M \geq 6.5$) in circum-Pacific subduction zones. They found that seismicity preceding this type of event exhibits increasing rates that cannot be explained by the ETAS model. They

suggested that the occurrence of SSEs before large interplate earthquakes causes this increase in seismicity rates. Although the physical mechanism that relates SSEs to large interplate earthquakes is controversial [Ohnaka 1992; Ando and Imanishi, 2011; Dixon et al., 2014], other recent observations also support the idea that SSEs precede large interplate earthquakes [Bouchon et al., 2011; Ito et al., 2013]. The swarm-like foreshocks detected in our study are similar to these earlier observations, as the sequences we observe do not follow the ETAS model. It is possible that these swarm-like foreshocks were also triggered by SSEs, although further investigation using repeating earthquakes or GPS measurements is needed to confirm this hypothesis.

In addition, it is worth noting that we also detected ordinary earthquake-swarms in the three regions that experienced the vigorous swarm-like foreshock sequences mentioned above (Figure 2.10a). In Ibaraki-Oki, we detected three ordinary swarms in addition to the 2008 swarm-like foreshock sequence (Figure 2.4a and 2.4b). In Kurile, an ordinary earthquake-swarm occurred in 1997 in the same detection circle as the 2006 vigorous swarm-like foreshock sequence (Figure 2.5a). Likewise, in Vanuatu an ordinary swarm occurred in 2004 in the same detection circle as the 2007 vigorous swarm-like foreshock sequence. If these ordinary swarms are also related to SSEs then these regions may have experienced repeated SSEs.

2.5.6. Relationship between swarm activity and tectonic properties

Recent studies have shown that seismicity in subduction zones is controlled by the tectonic properties of the subduction zone. For example, Ide [2013] demonstrated that proportionality exists between plate velocity and seismicity rate. Given that plate

velocity represents the strain rate on the plate interface, this proportionality appears to be intuitive. Nishikawa and Ide [2014] found a positive correlation between plate age and the *b*-value of earthquake magnitude–frequency distributions [Gutenberg and Richter, 1944], and inferred that differences in slab buoyancy cause differences in stress state and hence control *b*-values at subduction zones. Nishikawa and Ide [2015] and Shillington et al. [2015] found that the degree of bending or curvature of the incoming plate prior to subduction is positively correlated with seismicity rates in subduction zones. They suggested that hydration of the incoming plate before subduction [Ranero et al., 2003; Faccenda et al., 2009] and/or a rough (i.e., heterogeneous) plate surface [Uyeda, 1983; Tanioka et al., 1997] caused by fracturing related to slab bending result in high seismicity rates in subduction zones with large amounts of plate bending. Furthermore, curvature of the incoming plate may also be related to the maximum possible earthquake magnitude for a particular subduction zone, because bending of the incoming plate produces heterogeneity in its shear strength, which makes it difficult for earthquake ruptures to propagate over large areas [Bletery et al., 2016]. With regard to earthquake swarms, Poli et al. [2017] reported that regions with large amounts of swarm activity in the central Chile Trench correspond to areas that have hydrated fractures related to slab bending. Holtkamp and Brudzinski [2011] note that swarms are pervasive in Marianas-type subduction zones [Uyeda and Kanamori, 1979], where old, dense slabs are subducting slowly, resulting in an extensional stress-field.

In this section, we investigate the relationship between earthquake swarm activity and the tectonic properties of subduction zones globally using our earthquake swarm catalog. In subsequent analysis, we compare swarm activity with plate velocity, curvature of the

incoming plate before subduction, and plate age. Plate motions and ages are based on Bird [2003] and Müller et al. [2008], respectively. We calculated plate curvature before subduction using the global bathymetry dataset of Smith and Sandwell [1997] (see Appendix A1.3 for details of the curvature calculations).

The relationship between swarm activity and various tectonic properties is shown in Figure 2.14. In Figure 2.14a, the number of swarm events is positively correlated with plate velocity though data points in the correlation appear to be vertically distributed (R = 0.60). This is due to two outliers (two study regions in Tonga) with plate velocity faster than 150 mm/yr. We excluded these two outliers, calculated the correlation coefficient again, and confirmed that the positive correlation between the number of swarm events and plate velocity still could be observed (R = 0.61). Given that plate velocity represents the strain rate on the plate interface, and thus determines the recurrence intervals of repeating events in subduction zones [Ide 2013], this correlation appears intuitive. On the other hand, the positive correlation between the number of swarm events and plate curvature shown in Figure 2.14b is more intriguing. Plate curvature is also correlated with the number of swarm events per meter of plate motion (i.e., the number of swarm events divided by plate velocity), as can be seen from Figure 2.14e, and these variables show a stronger correlation (R = 0.42) than that between plate velocity and the number of swarm events per meter of plate motion (R = 0.30; see Figure 2.14d). Therefore, plate curvature seems to correlate with swarm activity independently of plate velocity. There is also a positive correlation between the number of background events in regular earthquakes and plate curvature (R = 0.54) (see Figure 2.15), which is consistent with Nishikawa and Ide [2015]. However, there is a slight

difference between the correlation of regular earthquakes and that of swarm activity. The ratio between the number of background events in swarms and the number of background events in regular earthquakes increases with plate curvature as shown in Figure 2.14h. Seismicity in regions with large curvature tends to be more swarm-like than regions with small curvature. In contrast, no correlation is observed between plate age and swarm activity (see Figure 2.14c, 2.14f, and 2.14i). We repeated our analysis using a sufficiently high M_c (= 4.8) and confirmed that the correlations observed in Figure 2.14 still could be observed (see Figure 2.16) although some of the correlations become slightly week. When we used M_c = 4.8, the number of events available for our analysis decreased by about half compared with the analysis with M_c = 4.5.

Essentially, the amount of swarm activity is proportional to plate velocity. However, the positive correlations shown in Figure 2.14d and 2.14g cannot be explained by this proportionality. If swarm activity is completely proportional to plate velocity, no correlation should be observed between the number of swarm events per meter of plate motion, swarm ratio, and plate velocity. Given that earthquake swarms are thought to be related to both fluids and heterogeneity on the plate interface [e.g., Matsuzawa et al., 2004; Poli et al., 2017], plate velocity may be related to fluids and heterogeneity on the plate interface in a non-linear way. Bird et al. [2009] also found a non-linear relationship between plate velocity and seismicity. More earthquakes per unit plate motion occur in subduction zones with fast plate motion. They suggested a model called "velocity-dependent pore pressures", in which fluid pressure on the plate interface increases with plate velocity in non-linear way, and this non-linear dependence of fluid pressure on plate velocity cause the non-linear relationship between plate velocity and

seismicity. It is possible that this non-linear relationship between plate velocity and fluid pressure on the plate interface also influences the intensity of swarm activitiy in subduction zones.

Given that plate curvature is related to both hydration of the incoming plate prior to subduction and heterogeneity on the plate interface [e.g., Ranero et al., 2003; Shillington et al., 2015; Bletery et al., 2016], the observed positive correlation between plate curvature and swarm activity implies that earthquake swarms are more likely to occur in fluid-rich subduction zones with marked heterogeneity on the plate interface. This interpretation is consistent with the fact that many swarms occur in regions containing hydrated fractures related to slab bending and where plate locking is heterogeneous [Holtkamp and Brudzinski, 2014; Poli et al., 2017]. Furthermore, SSEs often trigger earthquake swarms in subduction zones and are known to occur in regions where fluids are abundant [e.g., Kodaira et al., 2004; Saffer and Tobin, 2011], which is consistent with the observed positive correlation between plate curvature and swarm activity. Therefore, it is possible that plate curvature is also related to SSE activity at seismogenic depths. In fact, fluid expelled from hydrated fractures related to slab bending could facilitate the decoupling of, and aseismic slip on, the plate interface [e.g., Moreno et al., 2014; Poli et al., 2017].

Plate age is considered to control the tectonic stress state and thermal structure of subduction zones [e.g., Peacock 1996; Nishikawa and Ide, 2014]. A very weak correlation between plate age and swarm activity therefore implies that the intensity of swarm activity is not sensitive to the tectonic stress state or thermal structure of the

subduction zone though stress heterogeneity can influence the intensity of swarm activity [Holtkamp and Brudzinski, 2014].

The observed correlations appear to explain the global distribution of swarms at subduction zones reasonably well (Figure 2.10). For example, Vanuatu, Tonga, Kermadec, the Philippines, and South Sandwich, which are characterized by intense swarm activity, have large plate curvatures exceeding 1×10^{-3} km^{-1} (see Appendix A1.3). However, an explanation is still sought for the more localized along-strike variations in swarm activity, such as those seen between the Ibaraki-Oki region and the neighboring rupture area of the 2011 M 9 Tohoku earthquake (Figure 2.3a). The plate velocity and curvature at Ibaraki-Oki are 92.5 ± 0.4 mm/yr and $7.0 \times 10^{-4} \pm 0.6 \times 10^{-4}$ km^{-1}, respectively, which are not significantly different from the values at Tohoku (91.8 ± 0.5 mm/yr and $5.3 \times 10^{-4} \pm 0.9 \times 10^{-4}$ km^{-1}). Therefore, these localized variations in swarm activity may be controlled by more local factors such as subduction of seamounts like those shown in Figure 2.3a [e.g., Mochizuki et al., 2008], rather than by large-scale tectonic properties. Fluid expelled from sediment entrained with subducted seamounts might facilitate earthquake swarms.

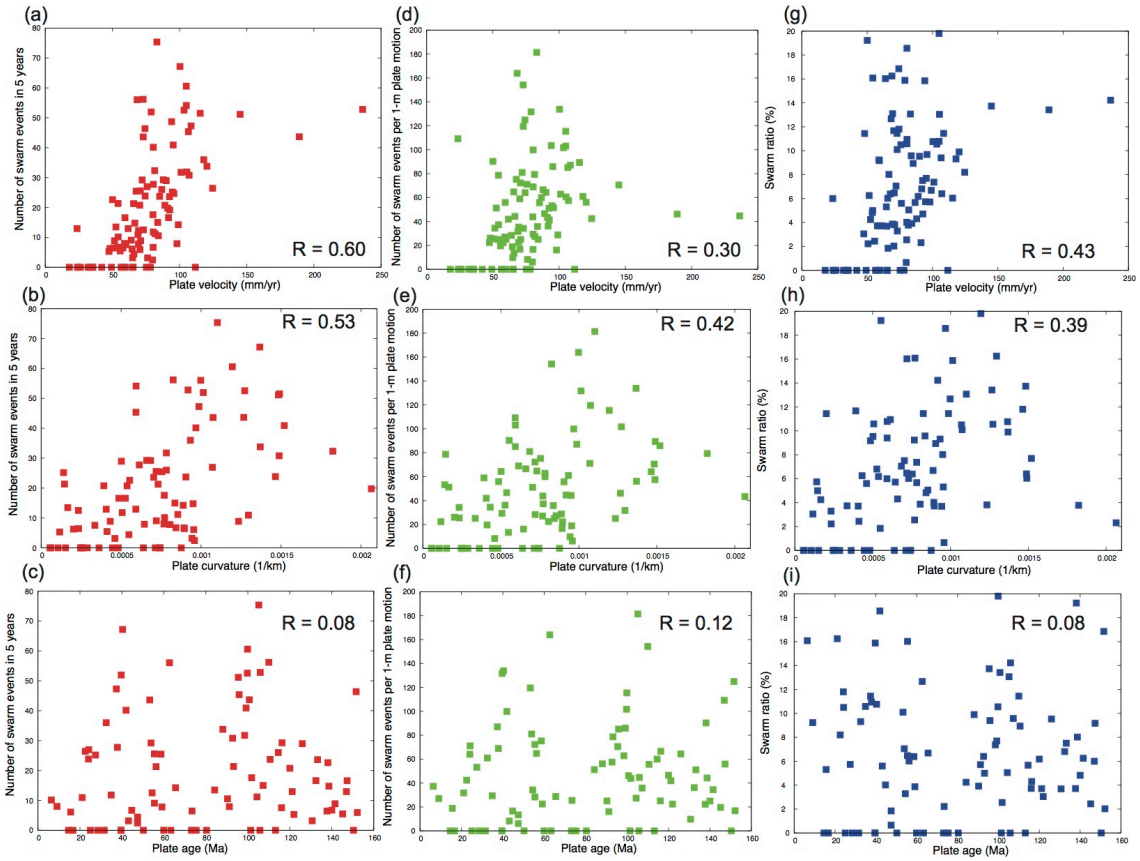

Figure 2.14 | Relationship between swarm activity and tectonic properties. (a)–(c) Relationship between the number of swarm events and plate velocity, plate curvature, and plate age, respectively. (d)–(f) Relationship between the number of swarm events per meter of plate motion and plate velocity, plate curvature, and plate age, respectively. (g)–(i) Relationship between swarm ratio and plate velocity, plate curvature, and plate age, respectively.

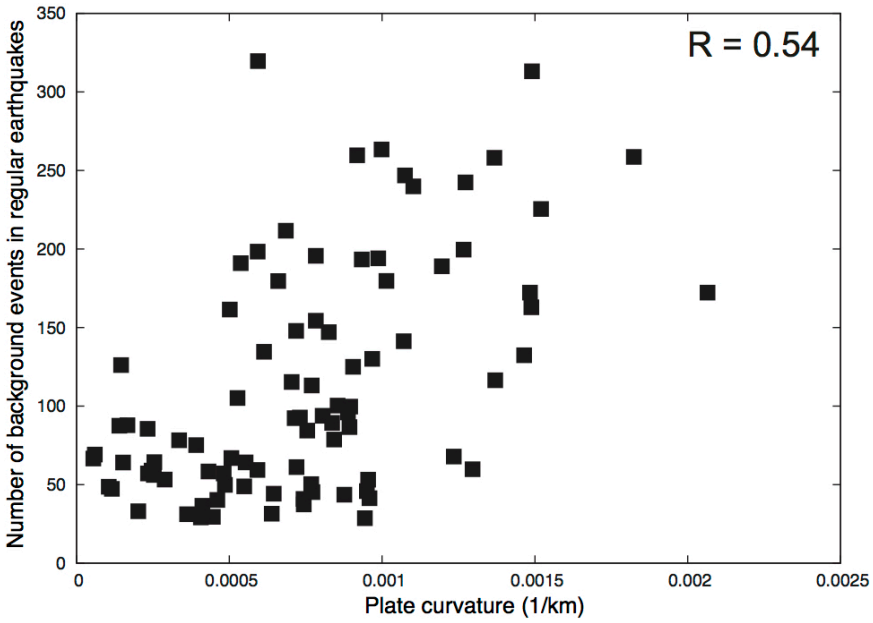

Figure 2.15 | Relationship between the number of background events in regular earthquakes and plate curvature.

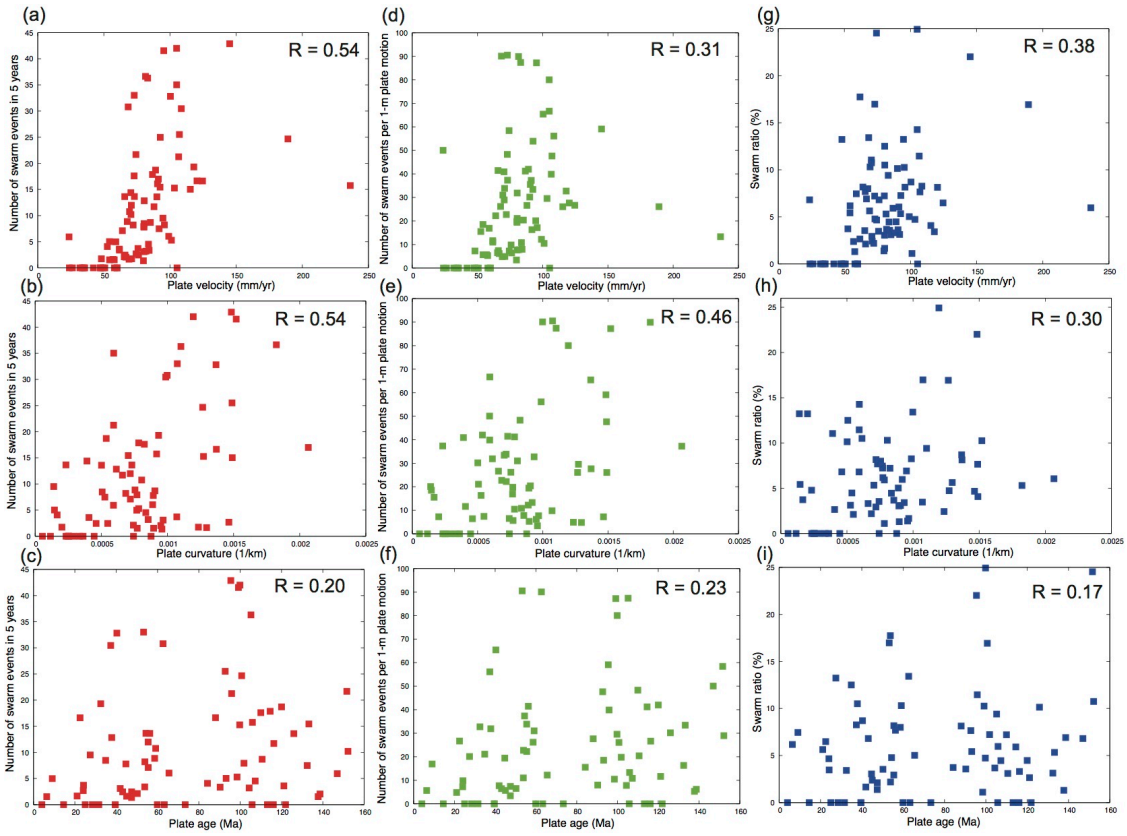

Figure 2.16 | Relationship between swarm activity and tectonic properties in the

analysis with Mc = 4.8. (a)–(c) Relationship between the number of swarm events and plate velocity, plate curvature, and plate age, respectively. (d)–(f) Relationship between the number of swarm events per meter of plate motion and plate velocity, plate curvature, and plate age, respectively. (g)–(i) Relationship between swarm ratio and plate velocity, plate curvature, and plate age, respectively.

2.6. Conclusion

We devised a new method for detecting earthquake swarms using the space–time ETAS model [Zhuang et al., 2002]. We detected 453 swarms in the ANSS earthquake catalog during the period 1995–2009 at subduction zones globally, which is about 6.7 times the number of swarms found in a previous catalog [Holtkamp and Brudzinski, 2011]. The foreshocks of some large earthquakes were also detected as earthquake swarms. Given their anomalously high seismicity rates, these foreshock sequences may have been triggered by SSEs preceding large interplate earthquakes. In addition, we found a positive correlation between the curvature of the incoming plate prior to subduction and swarm activity. Given that plate curvature is related to both the hydration of the incoming plate before subduction and heterogeneity on the plate interface [e.g., Ranero et al., 2003; Shillington et al., 2015; Bletery et al., 2016], the positive correlation between plate curvature and swarm activity implies that earthquake swarms are more likely to occur in subduction zones with abundant fluids and marked heterogeneity on the plate interface. SSEs are also known to occur in regions where fluids are abundant [Kodaira et al., 2004; Saffer and Tobin, 2011], meaning that this correlation is also consistent with the idea that SSEs trigger earthquake swarms in subduction zones. Our study reinforces the importance of fractures related to slab bending for seismicity in

subduction zones, and our earthquake swarm catalog may be useful for future global investigations of SSE activity.

3. Recurring slow slip events and earthquake nucleation in the source region of the *M* 7 Ibaraki-Oki earthquakes revealed by earthquake swarm and foreshock activity

This chapter has not been published in any peer-reviewed journals.

3.1. Summary

Slow slip events (SSEs) on the plate interface are closely related with occurrences of earthquakes. SSEs often trigger earthquake swarms in subduction zones. Moreover, some SSEs, which were accompanied by intensive foreshocks, are known to have preceded large interplate earthquakes. Therefore, detecting and monitoring SSEs are important for assessing the imminence of future large earthquakes. However, there are also many SSEs that are not followed by large earthquakes, and it is unclear whether SSEs preceding large earthquakes can be differentiated from them. Here we use the epidemic-type aftershock-sequence (ETAS) model and the matched-filter technique to examine the space-time distributions of earthquake swarms and foreshocks in Ibaraki-Oki, Japan. We found that 19 swarm sequences repeatedly occur during 1982–2008 at the same location as foreshock sequences preceding the 1982 and 2008 *M* 7 Ibaraki-Oki earthquakes. Both the foreshock and swarm sequences contain repeating earthquakes and have anomalously high seismicity rates inexplicable by the ETAS model, suggesting recurrence of SSEs in the source region of the *M* 7 Ibaraki-Oki earthquakes. The foreshock sequences in 1982 and 2008 have a larger number of events inexplicable by the ETAS model than the swarm sequences. The fault slip of repeating earthquakes in the 2008 foreshock sequence is also larger than those of the swarm

sequences, and the slip rate abruptly increased 12 hours before the 2008 *M* 7 event. Our results imply that the SSEs that preceded the 1982 and 2008 *M* 7 Ibaraki-Oki earthquakes have larger seismic moments than the other SSEs that triggered the swarm sequences. These large SSEs might be related to the nucleation phase of the *M* 7 Ibaraki-Oki earthquakes.

3.2. Introduction

Recent studies have shown that slow slip events (SSEs), which are episodic aseismic slips on faults, are related to large interplate earthquakes in subduction zones [e.g., Dragert et al., 2004; Radiguet et al., 2016]. In some subduction zones, SSEs preceding large interplate earthquakes were observed. For example, in Tohoku-Oki, Japan, measurements of ocean-bottom pressure gauges suggest that an SSE started one month before the 2011 M_w 9.0 Tohoku-Oki earthquake and triggered its foreshock sequence [Ito et al., 2013]. Migration of the foreshocks to the rupture initiation point of the mainshock was also observed [Ando and Imanishi, 2011; Kato et al., 2012], which was interpreted as propagation of aseismic slip. In northern Chile, GPS measurements and an analysis using repeating earthquakes revealed occurrence of an SSE about two weeks before the 2014 M_w 8.2 Iquique earthquake in its rupture area [Ruiz et al., 2014; Kato et al., 2016], and this SSE was interpreted as a nucleation phase, similar to those observed in laboratory experiments [e.g., Ohnaka, 1992] and numerical simulations [e.g., Tse and Rice, 1986; Dieterich, 1992; Shibazaki and Matsu'ura, 1992].

On the other hand, many SSEs occur without large earthquakes [Obara and Kato, 2016]. For example, in Boso-Oki, Japan, SSEs occur every 5 to 7 years [e.g., Ozawa et al.,

2003; Hirose et al., 2012]. All these SSEs triggered earthquake swarms with medium magnitude (≈ M 4). However, large interplate earthquakes (≥ M 7) have never followed these SSEs. In the Nankai subduction zone, SSEs of M_w 6.6 have been repeated at about 5 year interval since 1997 at the down-dip extension of a wide locked plate interface [Hirose et al., 1999; Yoshioka et al., 2015], where the M_w 8.3 Nankai earthquake ruptured in 1946. However, all these repeated SSE did not trigger rupture in the wide locked region so far.

Then, one important question is whether we can differentiate SSEs preceding large earthquakes from the other SSEs. In recent years, earthquake cycle simulations using the rate-and-state dependent friction law [Dieterich, 1979] have suggested some difference in the behavior of SSEs before large earthquakes. For example, Matsuzawa et al. [2010] modeled short- and long-term SSEs in the seismic cycles of large interplate earthquakes, similar to the observations in the Nankai subduction zone. They suggested that the recurrence intervals of short- and long-term SSEs decrease in the later stages of interseismic periods, and that the final aseismic transients leading to the nucleation of large interplate earthquakes start not in the SSE region itself but between the locked region and the SSE region. Lapusta and Liu [2009] and Noda et al. [2013] found that SSEs spontaneously occur in a seismogenic patch as its locked region shrink due to plate loading and a creeping front propagates inward of the patch. When the locked region is sufficiently large, these spontaneous SSEs does not lead to an earthquake. However, when the creeping region in the seismogenic patch is larger than the critical nucleation size of the seismogenic patch [e.g., Rubin and Ampuero, 2005], one of the spontaneous SSEs grows and accelerates to the seismic slip rate, resulting in the rupture

of the entire patch.

Nevertheless, there is little observational evidence for the differences in the behavior of SSEs suggested by numerical simulations. For example, in Guerreo, Mexico, SSEs in the deeper transition zone occur approximately every 4 years, and they last more than several months [Radiguet et al., 2012]. The 2014 SSE is supposed to have triggered the M_w 7.3 Papanoa earthquake, which occurred about 80 days after the initiation of the SSE, due to increases in Coulomb failure stress [Radiguet et al., 2016]. However, the difference between the 2014 SSE and the other SSEs in Guerrero has not been clear. Neither shortening of recurrence intervals nor acceleration of a slip rate toward the occurrence time of the Papanoa earthquake has been reported. Thus, to verify or reject the hypothesis that there are differences between SSEs preceding large earthquakes and the others, much more case studies are required.

Ibaraki-Oki in the Japan Trench is one of the ideal regions to test this hypothesis. In Ibaraki-Oki, M7-class events have been repeatedly observed every 20 to 30 years since 1923 [e.g., Mochizuki, 2008; Matsumura, 2010] (Figure 3.1). Based on their aftershock and slip distribution, these earthquakes are considered to share the same rupture area on the plate interface [Earthquake Prediction Information Division, JMA, 2008]. In addition, Ibaraki-Oki is characterized by recurring earthquake swarm and foreshock activity as shown in Chapter 2 and previous studies [e.g., Maeda, 1996]. Earthquake swarms in 1999, 2002, and 2006 occurred at the same location as the foreshock sequences of the 1982 and 2008 M 7 Ibaraki-Oki earthquakes. Given that earthquake swarms and foreshocks in subduction zones are often triggered by SSEs [e.g., Ozawa et

al., 2003; Ruiz et al., 2014], Ibaraki-Oki may have experienced recurring SSEs. Furthermore, by examining differences between the swarms and foreshocks, it may be possible to differentiate SSEs preceding the *M* 7 events from the other SSEs.

In Chapter 3, we further explore the possibility of recurrence of SSEs in Ibaraki-Oki by examining the space-time distribution of the earthquake swarms and foreshocks. We use the epidemic type aftershock sequence (ETAS) model [Ogata, 1988; Zhuang et al., 2002], the matched filter technique [e.g., Shelly et al., 2007], and the repeating earthquake analysis [e.g., Nadeau and Johnson, 1998] to reveal a more detailed history of swarm activity, restore small events missing from the earthquake catalog, and estimate the amount of interplate fault slip. Finally, comparing the swarms with the foreshocks, we discuss the question whether we can differentiate SSEs preceding large earthquakes from the other SSEs in Ibaraki-Oki.

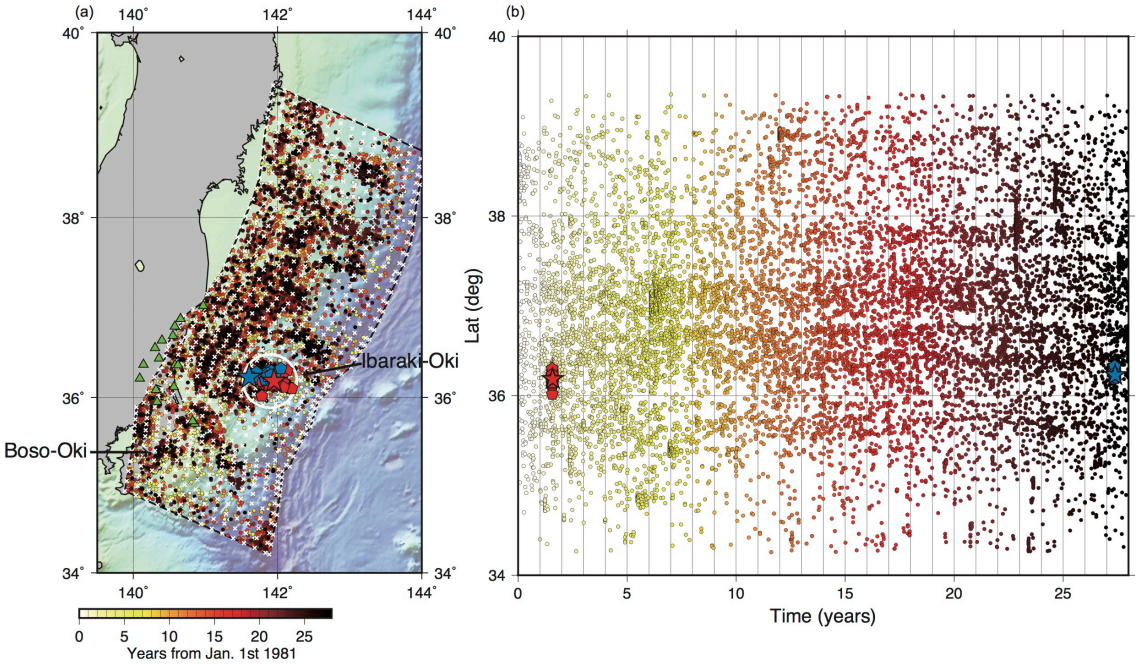

Figure 3.1 | Study region in the Japan Trench. (a) Earthquakes with $M \geq 3$ from the

JMA catalog during the period 1981–2008 are shown by small circles, colored according to their occurrence time. The large white circle is an example of a "detection circle" of radius 30 km, whose center is located at (36.2ºN, 141.9ºE) (See Section 3.3.1). Small white crosses indicate the centers of detection circles used in our analysis. The two stars are the hypocenters of the 1982 (red) and 2008 (blue) *M* 7 Ibaraki-Oki earthquakes, whose foreshocks are indicated by pentagons. We define foreshocks as earthquakes followed by large earthquakes that occur within 5 days. Green triangles are 16 stations of Hi-net used in this study (see Section 3.3.2 and 3.3.3). The bathymetry data is based on Smith and Sandwell [1997]. (b) Space-time distribution of seismicity in (a).

3.3. Methods

3.3.1. Detection of earthquake swarms using the ETAS model

Earthquake swarms do not obey Omori's law and thus the ETAS model, which expresses the seismicity rate as the sum of a stationary background seismicity rate and a superposition of Omori's law [e.g., Richter, 1958; Llenos et al., 2009]. This is because they are triggered by phenomena other than earthquake-to-earthquake triggering. In Chapter 2, we detected seismic sequences with higher seismicity rates than predicted by the ETAS model globally and classified them as earthquake swarms. In Chapter 3, we follow the methodology of Chapter 2 and detect earthquake swarms in the Japan Trench during the period 1981–2008. The period includes the 1982 and 2008 M7 Ibaraki-Oki earthquakes and is longer than that of Chapter 2.

Figure 3.1a shows a study region in the Japan Trench, which is bordered by a trench

section that is about 500 km long and extends 200 km in the direction of relative plate motion. The location of the trench section and relative plate motion are based on the plate model PB2002 [Bird, 2003]. We then extracted earthquakes during the period 1981–2008 from the Japan Meteorological Agency (JMA) catalog (Figure 3.1a and 3.1b), which is much more complete than a global catalog used in Chapter 2. We estimated the complete magnitude M_c for this region using the MAXC method [Wiemer and Wyss, 2000; Woessner and Wiemer, 2005]. In this estimation, we used all events in the study region regardless of their locations. Therefore, the estimated M_c should be regarded as a spatially averaged value. While the estimated M_c is below M 3 after January 1987, it was M 3.3 before January 1987. Nevertheless, we used M 3 or larger events for swarm detection, because it is known that the ETAS model can be used to detect anomalies in seismicity even if used events in the analysis is slightly smaller than the M_c of the catalog [Ogata, 2005; Chapter 2].

We estimated parameters of the space–time ETAS model [Zhuang et al., 2002] in the study region as in Chapter 2 (See Section 2.3.1 and (2.1) to (2.4)). Considering calculation time needed for the estimation of the parameters, we divided the period 1981–2008 into 14 two-year periods (i.e., 1981–1982, 1983–1984, 1985–1986, and so on) and estimated the ETAS parameters. The seismicity in the year preceding each of these periods was also used to calculate the increase in seismicity rate caused by events that occurred before each of these periods.

We then calculated the number of events expected by the ETAS model in circles of 30 km radius in the study region (Figure 3.1a, Figure 3.2a, and Figure 3.2b). The centers of

the circles are distributed at intervals less than 15 km along strike and dip of the plate interface (Figure 3.1a). We call these circles "detection circles". In the same way as (2.8), the number of events expected by the ETAS model $\Lambda(t)$ in a detection circle C from time 0 to t can be calculated as

$$\Lambda(t) = \int_0^t \iint_C \lambda(t', x, y) dx dy dt' \quad (3.1).$$

We executed this integration numerically in each detection circle. We can then transform the occurrence time t_i of event i in the detection circle C into a transformed time $\tau_i \equiv \Lambda(t_i)$ [Ogata, 1988]. If the seismicity in the detection circle C is well described by the ETAS model, the transformed time τ_i will follow a standard Poisson process, and a plot of the cumulative number of observed events against transformed time (i.e., the number of events predicted by the ETAS model) will be linear with a slope of unity. Slopes greater than unity mean that the observed seismicity rate is greater than that expected by the ETAS model (Figure 3.2b).

Using (3.1), the number of events expected by the ETAS model between two successive events (event i and $i+1$) in the detection circle C is calculated as

$$\tau_{i+1} - \tau_i = \int_{t_i}^{t_{i+1}} \iint_C \lambda(t, x, y) dx dy dt \quad (3.2).$$

In the same way as (2.10), the standard deviation of the number of events between τ_i and τ_{i+1} in the detection circle C will be

$$\sigma = \sqrt{\tau_{i+1} - \tau_i} \quad (3.3).$$

We classify a seismic sequence as "potential earthquake swarm" when the condition $\tau_{i+1} - \tau_i + 1.5\sigma < 1$ continuously holds true four times or more. In other words, the expected number of events between two successive events $\tau_{i+1} - \tau_i$ (3.2) in each detection circle should not exceed unity, even when considering the 1.5σ error (3.3),

for at least four successive events. Using this criterion, we can detect seismic sequences with higher seismicity rates than predicted by the ETAS model and require at least five events in a swarm sequence (Figure 3.2a and 3.2b). To suppress false positive swarm detections, we used the stricter criterion (1.5σ error) than Chapter 2, where we used 1σ error. The probability that five events obeying the ETAS model have such a high seismicity rate is 2.39×10^{-3}. Furthermore, we require that the probability that the first event of each potential earthquake swarm is a background event is 0.5 or larger to exclude aftershocks from our swarm detection. The probability that an event at x_i, y_i, and time t_i is a background event is given by (2.6).

After applying the above detection criterions to seismicity in all detection circles, we grouped any potential earthquake swarms that have common events into a single cluster. Finally, we identified clusters for which the magnitude difference between the largest (M_1) and second largest event (M_2) is less than unity because typical mainshock-aftershock sequences follow Båth's law ($M_1 - M_2 \geq 1$) [Båth, 1965], and defined them as earthquake swarms. The detail of characteristics and limitations of this method was discussed in Chapter 2.

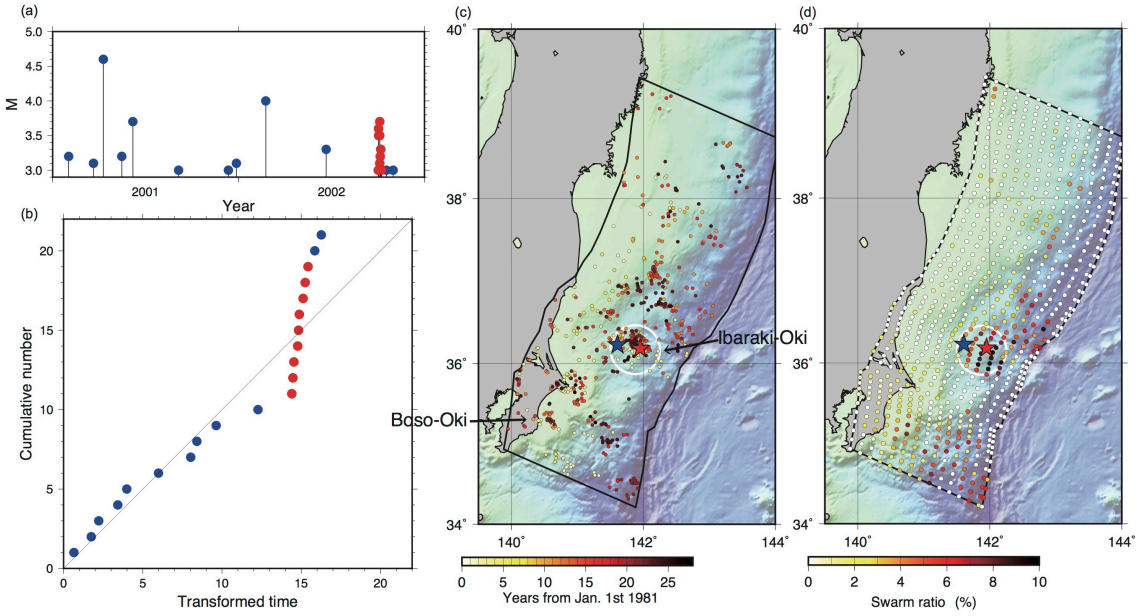

Figure 3.2 | Calculation of transformed time and detected swarms in the Japan Trench. (a) Magnitude versus time diagram in a detection circle in Boso-Oki, which includes the 2002 Boso-Oki swarm triggered by the 2002 Boso SSE [e.g., Hirose et al., 2012]. Earthquake swarms detected by our analysis are shown as red circles; blue circles denote non-swarm events. (b) Calculated transformed time of the 2002 Boso-Oki swarm. The swarm sequence has a slope much larger than unity while non-swarm events have a slope of close to unity. (c) Hypocenters of swarms detected by our analysis (See Section 3.4.1). The hypocenters are shown as small circles and colored according to their occurrence time. Red and blue stars indicate the hypocenters of the 1982 and 2008 M7 Ibaraki-Oki earthquakes respectively. The large white circle is the Ibaraki-Oki detection circle (See Section 3.3.2). (d) Swarm ratios calculated for each detection circle. Small circles indicate the center of each detection circle and are colored according to the computed swarm ratio.

3.3.2. Matched filter technique

During intensive earthquake swarms, some of small earthquakes can be missed out from the catalog. To restore missing small events, we applied the matched filter technique [e.g., Shelly et al., 2007; Peng and Zhao, 2009; Kato et al., 2013] to detected swarm sequences and the foreshock-aftershock sequence of the 2008 Ibaraki-Oki earthquake. Here we define foreshocks as earthquakes followed by large earthquakes that occur within 5 days. In this study, we basically followed the methodology of Kato et al. [2013].

We focused on swarm sequences whose centroid is located close to the foreshock sequences of the 1982 and 2008 Ibaraki-Oki earthquakes, i.e., inside a detection circle of radius 30 km centered at (36.2ºN, 141.9ºE) (See Figure 3.1a). Hereafter we call this detection circle "the Ibaraki-Oki detection circle". We used the continuous three-component velocity seismograms recorded at 16 stations of Hi-net in and around Ibaraki prefecture since 2004 (See Figure 3.1a). Hi-net is a high-sensitivity seismogram network operated by the National Research Institute for Earthquake Science and Disaster Resilience (NIED) of Japan.

We decimated the seismograms from 100 Hz to 50 Hz and applied a 4–12Hz Butterworth filter to them. We used this frequency band to suppress noise excited by low frequency waves of larger events. We used events in each swarm sequence and 123 foreshocks and 440 aftershocks of the 2008 Ibaraki-Oki earthquake as template events regardless of their magnitude. Each template event has a 10 s time window starting 5 s before the S-wave arrival time, which was calculated using the JMA2001 velocity

structure model [Ueno et al., 2002]. We calculated correlation coefficients between each template event and continuous seismograms as the time window is shifted with increments of 0.02 s. We decimated the time series of the correlation coefficients from 50 Hz and 5 Hz to downsize the data, keeping the maximum value of each 0.2 s. By this procedure, we accepted the uncertainty of 0.2 s in the S-wave arrival time of detected events and thus allow the hypocenter of detected events to be about 0.8 km (the S-wave velocity multiplied by 0.2 s) away from that of the template. Then the correlation coefficients were averaged over 3 components and 16 stations.

We calculated the normalized median absolute deviation of the averaged correlation coefficients for each template event and each day. We used 17-fold normalized median absolute deviation as a detection threshold. We decided this sufficiently high threshold visually to suppress false positive detections. We removed duplicate positive detections by keeping the highest correlation coefficient in each 10 s. Because the waveforms of template events and detected events are similar at multiple stations, their hypocenters are expected to be close. Therefore, the location of the template event is assigned to each detected event. We estimated the magnitude of each detected event by comparing the maximum amplitude of waveforms of the template event and the detected event at the station with the highest correlation coefficient. We assumed that a 10-fold increase in the maximum amplitude corresponds to one-unit increase in magnitude [Peng and Zhao, 2009; Kato et al., 2013].

3.3.3. Repeating earthquake analysis

Repeating earthquakes are earthquakes with almost identical waveforms and considered

to be repetitive ruptures of the same area on the plate interface [e.g., Ellsworth, 1995; Uchida et al., 2007]. They can be used as a creep meter on the plate interface, assuming that the cumulative slip of repeating earthquakes corresponds to the cumulative aseismic slip in the surrounding region [e.g., Nadeau and McEvilly, 1999; Uchida et al., 2009]. In this section, we detected repeating earthquakes during the time periods of the swarm sequences and the foreshock-aftershock sequence of the 2008 Ibaraki-Oki earthquake based on waveform similarity [e.g., Igarashi et al., 2003; Igarashi et al., 2010] and estimated the amount of fault slip using the scaling relationship between seismic moment of repeating earthquakes and fault slip [Nadeau and Johnson, 1998].

We extracted *M* 2 or larger events from the catalog modified by the matched filter technique (see Section 3.3.2). The time window of the waveforms is from the P-wave arrival to 3 s after the S-wave arrival. We calculated cross-correlation coefficients of each earthquake pair using 1–4 Hz, 2–8 Hz, and 4–16 Hz band-pass filtered waveforms. Depending on the magnitude of each event, we selected a frequency band that roughly corresponds to the corner frequency of the event, i.e. 1–4 Hz for *M* 3 or larger, 2–8 Hz for *M* 2.5 or larger, and 4–16 Hz for *M* 2 or larger, assuming a 3 MPa constant stress drop. We classified earthquake pairs whose component-averaged cross-correlation coefficients are larger than 0.95 at two or more stations and whose differences in magnitude are 0.5 or less as repeating earthquakes. This criterion confirms that the earthquake pair occurred at the same location and has similar size. There are also repeating earthquakes that occurred neither in the time periods of the swarm sequences nor the foreshock-aftershock sequence of the 2008 Ibaraki-Oki earthquake. For such repeating earthquakes, we used a long-term repeating earthquake catalog in the Japan

Trench created by Uchida and Matsuzawa [2013] and Uchida et al. [2016]. We used 98 repeating earthquake sequences that occurred in the Ibaraki-Oki detection circle recorded in the repeating earthquake catalog.

We estimated the amount of fault slip using the scaling relationship between seismic moment M_o (dyn cm) of repeating earthquakes and fault slip d (cm) [Nadeau and Johnson, 1998].

$$\log(d) = -2.36 + 0.17\log(M_o) \quad (3.4)$$

This relationship was obtained in the Parkfield segment of the San Andreas Fault, and Igarashi et al. [2003] confirmed that this scaling relationship also holds true for repeating earthquakes in Kamaishi-Oki and Miyagi-Oki, the Japan Trench. The seismic moment was calculated using the relationship between seismic moment and magnitude [Hanks and Kanamori, 1979]. Then, the estimated fault slips are averaged over all repeating earthquake sequences that occurred in the Ibaraki-Oki detection circle. These are 98 repeating earthquake sequences in the long-term repeating earthquake catalog [Uchida and Matsuzawa, 2013; Uchida et al., 2016] and 17 sequences newly detected by our analysis (See Section 3.4.2).

3.4. Results

3.4.1. Earthquake swarms in the Japan Trench

We detected 94 earthquake swarm sequences from 1981 to 2008 in the Japan Trench (Figure 3.2c), using a code of the space-time ETAS model written by Zhuang et al. [2002]. During the time period 1999–2000, the estimation of ETAS parameters did not converge, probably because of a known problem of the code in case that the number of

events has an increasing trend of the seismicity rate. Among the seven ETAS parameters, A and α are the most important for our swarm detection because they determine the expected number of aftershocks of each earthquake. These two parameters have a strong trade-off (Figure 3.3). The estimated values of A and α averaged over the 14 two-year time periods are 0.15 ± 0.09 and 1.3 ± 0.2, which means that the expected numbers of aftershocks of *M* 3, *M* 5, and *M* 7 events are 0.15, 2.0, and 27 events respectively. It also should be noted that the estimation of the parameter γ, which determines how the characteristic length of the probability density of aftershock locations scales with magnitude (2.4), is rather unstable. In some of the 14 two-year time periods, the parameter γ is estimated to be zero, which means that the characteristic length of the probability density of aftershock locations does not scale with magnitude. Event location errors in the earthquake catalog and a lack of large earthquakes ($M \gtrsim 7$) in some of the 14 two-year time periods might cause the estimation of γ to be unstable. However, this unstable estimation of γ does not strongly affect our swarm detection because influences of γ on the calculation of transformed time in detection circles are small (see Appendix A2.1).

In Boso-Oki, five swarm sequences, which are thought to be related to SSEs, have been detected during the period 1981–2008 [Hirose et al., 2012]. We successfully detected the 1983, 1990, and 2002 swarms (Figure 3.2a and 3.2b). On the other hand, our analysis failed to detect the 1996 and 2007 swarm sequences. This is because the 1996 swarm have only three M3 or larger events, which is fewer than our minimum requirement (five events in a swarm sequence), and because the 2007 swarm did not satisfy the requirement that the magnitude difference between the largest (M_1) and

second largest event (M_2) is less than unity. In addition, we detected one new swarm sequence in February 1994, which was shown in the magnitude versus time diagram of Boso-Oki without identification as a swarm in Hirose et al. [2012]. These results show that our analysis could detect the known and unknown earthquake swarms in the Japan Trench and support effectiveness of the swarm detection method of Chapter 2.

Figure 3.2d shows the ratio between the number of background events in detected swarms and the number of all background events in each detection circle. We call this ratio the "swarm ratio". In addition to Boso-Oki, Ibaraki-Oki also shows very high swarm activity, which is consistent with Chapter 2 (See Figure 2.3b). At the Ibaraki-Oki detection circle, the swarm ratio is about 7 %. 19 swarm sequences occurred in the Ibaraki-Oki detection circle and are located close to the 1982 and 2008 foreshock sequences. Zoom-up figures of Ibaraki-Oki (Figure 3.4) show that hypocenters of the foreshock and swarm sequences well overlap. Both of the foreshock and swarm sequences are in the source region of the 1982 Ibaraki-Oki earthquake [Mochizuki et al., 2008]. The foreshock and swarm sequences are located to the north of a subducted seamount. Both the foreshock and swarm sequences include thrust events and are considered to have occurred on the plate interface.

In Figure 3.5, we showed the magnitude versus time diagram for the foreshock and swarm sequences. Here we use Japanese Standard Time (JST). While the average interval between the foreshock and swarm sequences is about 1.1 years, each interval varies from less than two months (e.g., March 15th to May 4th, 2008) to more than two years (e.g., May 15th, 1986 to January 6th, 1989). The occurrence time, duration, the

number of events (≥ *M* 3), and the largest event of each sequence are summarized in Table 3.1. Duration of each sequence ranges from 1 day to 30 days. The number of events (≥ *M* 3) in each sequence varies from 5 events to 37 events. The largest event in each sequence also has a large variation, i.e., the largest event in the foreshock sequence in 2008 is *M* 6.4, while that of a swarm sequence in December 1991 is *M* 3.4.

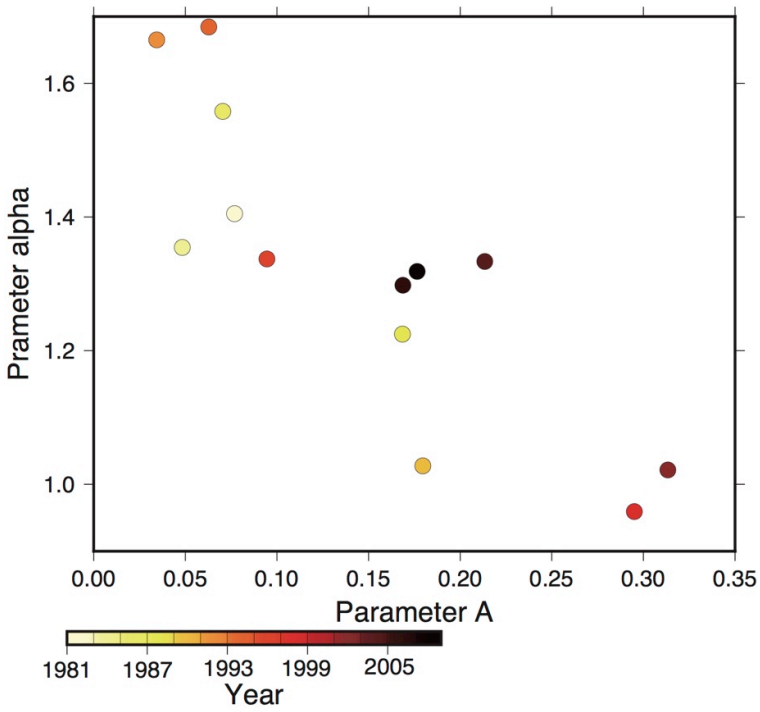

Figure 3.3 | Trade-off between the parameter *A* and *α*. The estimated parameters for each two-year period are indicated by each point, which is colored according to its year.

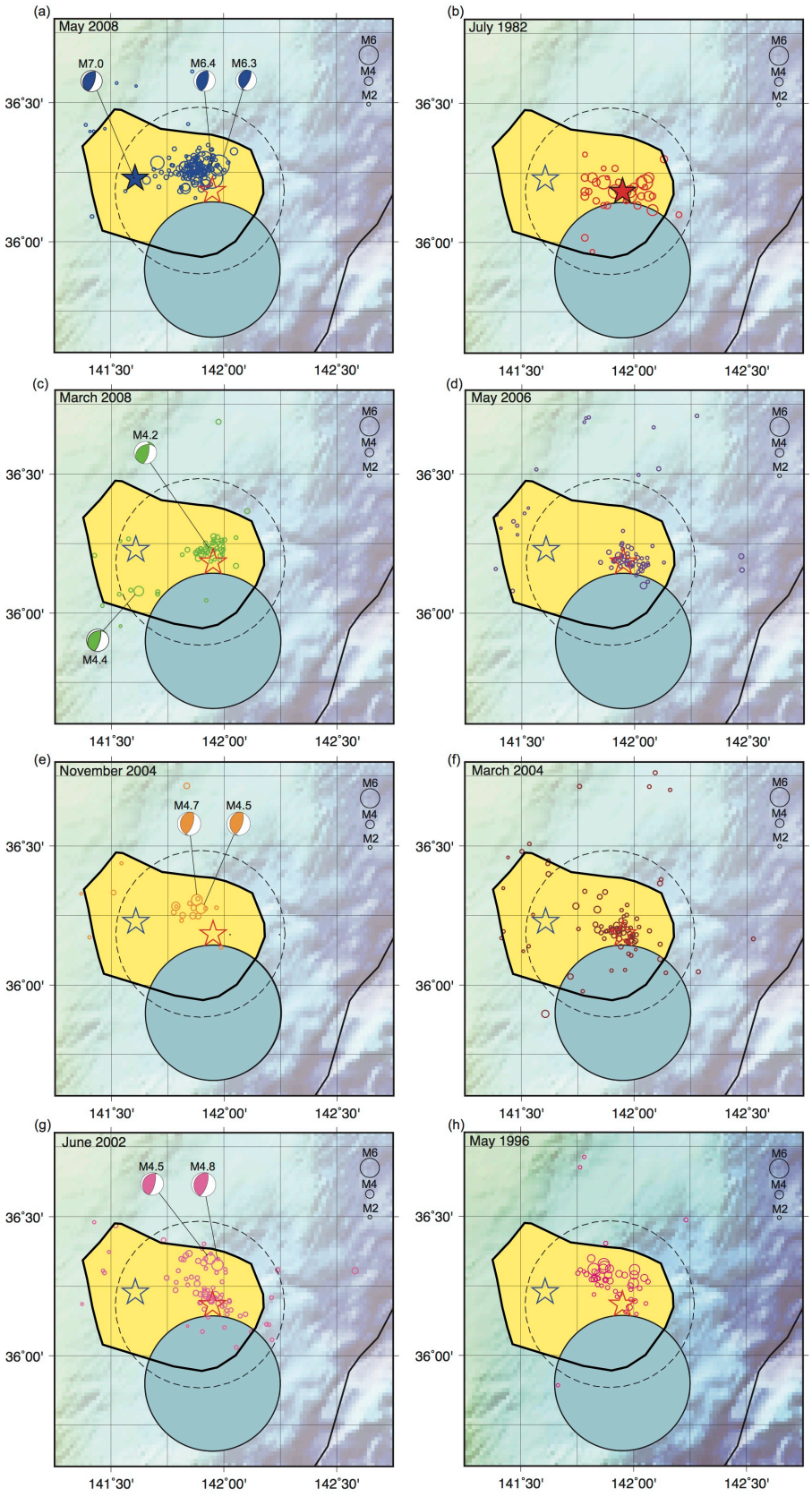

Figure 3.4 | Example hypocenters of detected swarms in Ibaraki-Oki. (a) and (b)

show the foreshock sequences in 2008 (blue circles) and 1982 (red circles) (JMA catalog). Red and blue stars indicate the hypocenters of the 1982 and 2008 *M* 7 Ibaraki-Oki earthquakes respectively. We showed the focal mechanisms of the 2008 Ibaraki-Oki earthquake and its two largest foreshocks in (a). (c)–(h) show swarm sequences in March 2008 (green), May 2006 (purple), November 2004 (orange), March 2004 (brown), June 2002 (pink), and May 1996 (magenta) respectively. The yellow shading and light blue shading denote the source area of the 1982 Ibaraki-Oki earthquake and a subducted seamount respectively. Both the source area and the location of the seamount are based on Mochizuki et al. [2008]. The dashed large circle is the Ibaraki-Oki detection circle. For earthquakes larger than *M* 4 in the swarm sequences, we showed their focal mechanisms determined by NIED. Because the focal mechanism data is available since 1997, we could not show focal mechanisms of the swarm sequence in May 1996 in (h).

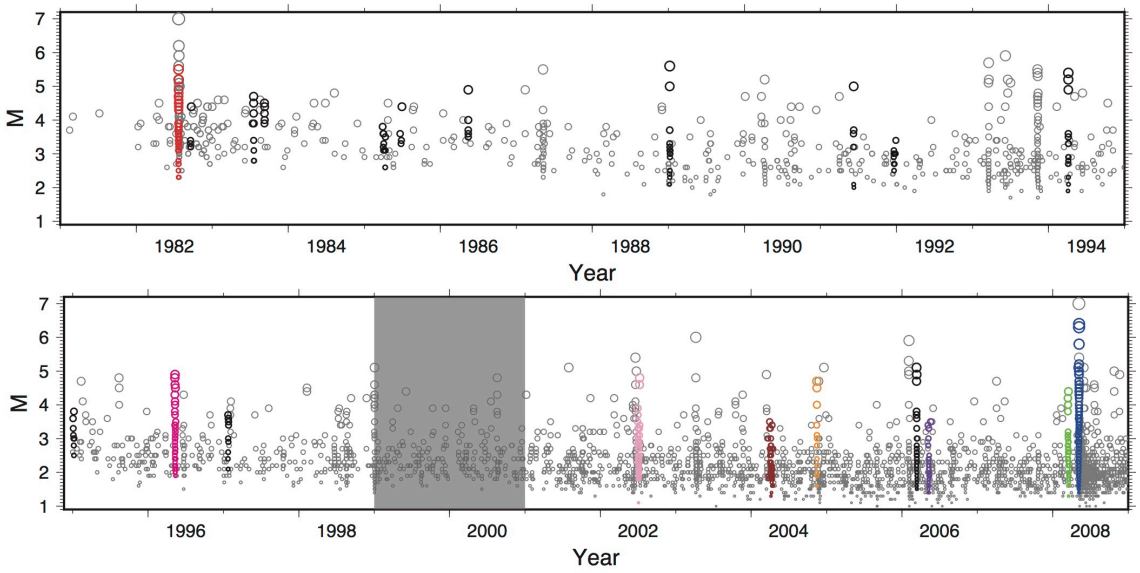

Figure 3.5 | Magnitude versus time diagram from 1981 to 2008 in the Ibaraki-Oki detection circle. Red and blue circles indicate the foreshock sequences in 1982 and

2008. Black and the other colored circles are swarm events. Grey circles denote non-swarm events. The grey shaded time period (1999–2000) is the time period when the calculation of ETAS parameters did not converge.

Table 3.1 | Characteristics of the foreshock and swarm sequences

Seismic sequence	Occurrence time	Duration (days)	Number of events (≥ *M* 3)	The largest event	Anomaly[a]	Excess events[b]	Repeater fault slip (cm)[c]
Foreshock in 2008	May 4th, 2008	4	37	*M* 6.4	6σ	23.4	1.70
Foreshock in 1982	July 23rd, 1982	3	32	*M* 5.5	9σ	24.9	N/A
Swarm in March 2008	March 15th, 2008	8	9	*M* 4.4	5σ	6.4	0.45
Swarm in May 2006	May 8th, 2006	12	5	*M* 3.5	3σ	3.2	1.38
Swarm in March 2006	March 12th, 2006	4	9	*M* 5.1	3σ	5.4	N/A
Swarm in Nov. 2004	Nov. 14th, 2004	3	8	*M* 4.7	4σ	4.7	0.21
Swarm in March 2004	March 22nd, 2004	30	9	*M* 3.7	3σ	5.0	1.04
Swarm in June 2002	June 30th, 2002	12	14	*M* 4.8	5σ	9.5	N/A
Swarm in Jan. 1997	Jan. 22nd, 1997	4	5	*M* 3.7	6σ	3.6	N/A
Swarm in May 1996	May 9th, 1996	7	20	*M* 4.9	9σ	16.0	N/A
Swarm in Jan. 1995	Jan. 2nd, 1995	13	8	*M* 4.5	5σ	4.4	N/A
Swarm in April 1994	April 5th, 1994	3	9	*M* 5.4	2σ	4.1	N/A
Swarm in Dec. 1991	Dec. 19th, 1991	11	5	*M* 3.4	5σ	3.6	N/A
Swarm in June 1991	June 9th, 1991	2	5	*M* 5.0	7σ	2.9	N/A
Swarm in Jan. 1989	Jan. 6th, 1989	4	10	*M* 5.6	4σ	6.2	N/A
Swarm in May 1986	May 15th, 1986	1	5	*M* 4.9	9σ	3.8	N/A
Swarm in June 1985	June 22nd, 1985	9	5	*M* 4.4	3σ	2.5	N/A
Swarm in March 1985	March 25th, 1985	18	12	*M* 4.5	6σ	6.9	N/A
Swarm in Sep. 1983	Sep. 9th, 1983	1	5	*M* 4.5	5σ	3.6	N/A
Swarm in July 1983	July 15th, 1983	6	7	*M* 4.7	3σ	4.6	N/A
Swarm in Sep. 1982	Sep. 18th, 1982	5	7	*M* 4.8	3σ	3.1	N/A

[a] Anomaly is degree of anomaly in the ETAS model (See Section 3.4.2).

[b] Excess events are differences between the number of observed events (≥ *M* 3) in the Ibaraki-Oki detection circle and

the number of events predicted by the ETAS model since the first *M* 3 or larger event of each sequence (See Section 3.4.2).

[c] Repeater fault slip is fault slip of repeating earthquakes estimated in Section 3.4.2.

3.4.2. Space-time distribution of the foreshock and swarm sequences in Ibaraki-Oki

We applied the matched filter technique (see Section 3.3.2) to the foreshock sequence in 2008 and four swarm sequences (March 2004, November 2004, May 2006, and March 2008), which occurred during the period 2004–2008 and whose hypocenters well overlap those of the foreshock sequences in 1982 and 2008 (see Figure 3.4). We excluded a swarm sequence in March 2006 (see Figures 3.5 and 3.6) from our analysis because its hypocenters do not overlap those of the foreshock sequences. We then detected repeating earthquakes and estimated the amount of fault slip, which was averaged over all repeating earthquake sequences that occurred in the Ibaraki-Oki detection circle, i.e., 98 repeating earthquake sequences in the long-term repeating earthquake catalog [Uchida and Matsuzawa, 2013; Uchida et al., 2016] and 17 sequences newly detected by our analysis (see Section 3.3.3).

In this section, we show space-time distribution of the foreshock sequence in 2008 and the swarm sequences in May 2006 and March 2004. Space-time distribution of the swarm sequences in March 2008 and November 2004 is shown in Appendices A2.2 and A2.3.

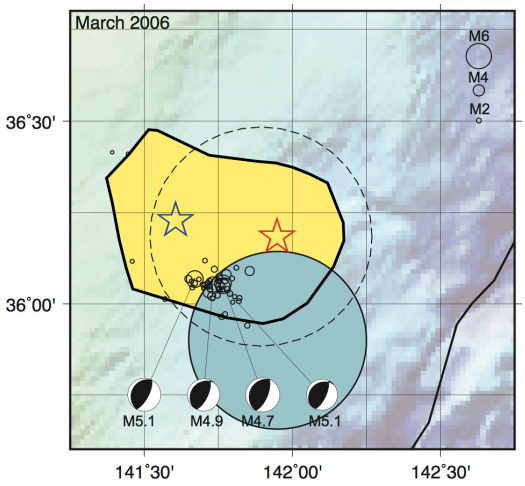

Figure 3.6 | Hypocenters of a swarm sequence in March 2006. Black circles indicate swarms (JMA catalog). Red and blue stars indicate the hypocenters of the 1982 and 2008 *M* 7 Ibaraki-Oki earthquakes respectively. The yellow shading and light blue shading denote the source area of the 1982 Ibaraki-Oki earthquake and a subducted seamount respectively. The dashed large circle is the Ibaraki-Oki detection circle. For earthquakes larger than *M* 4 in the swarm sequences, we showed their focal mechanisms determined by NIED.

3.4.2.1. Foreshock sequence of the 2008 Ibaraki-Oki earthquake

The foreshock sequence of the 2008 Ibaraki-Oki earthquake, which occurred on May 8th, 2008, started to the east of the hypocenter of the mainshock on May 4th (Figures 3.7a and 3.7b). The matched filter technique detected 1059 events from May 4th to 9th, which is 1.9 times of the JMA catalog (564 events). Repeating earthquakes were found in the foreshock sequence, suggesting occurrence of aseismic slip in their surrounding region. Quiescence of the foreshock activity can be seen about one day before the mainshock. The foreshock activity started again 12 hours before the mainshock and its hypocenters expanded in the east-west direction (Figure 3.7a). Aftershocks continued to expand in

the east direction with the speed of 20 km/day, which presumably reflects an afterslip [e.g., Peng and Zhao, 2009]. This migration also can be seen even if we see only events recorded in the JMA catalog. About one hour before the mainshock, the two largest foreshocks (M 6.4 and M 6.3) occurred to the east of the mainshock.

The comparison of the number of observed events ($\geq M$ 3) in the Ibaraki-Oki detection circle (37 events) with the number of events predicted by the ETAS model since the first M 3 or larger foreshock event (13.6 events) shows an anomaly larger than 6σ (Figure 3.7c), i.e. the probability that we observe such a high seismicity rate is less than 1.2×10^{-7}. This suggests that the foreshock sequence cannot be explained by earthquake-to-earthquake triggering.

We investigated the temporal changes in the difference between the number of observed events ($\geq M$ 3) in the Ibaraki-Oki detection circle and the number of events predicted by the ETAS model and in fault slip of repeating earthquakes (Figure 3.7d and 3.7e). Hereafter we call the difference between the number of observed events ($\geq M$ 3) and the number of events predicted by the ETAS model "the number of excess events". Both temporal changes show a large increase (21.2 events and 1.04 cm) 12 hours before the 2008 Ibaraki-Oki earthquake. Average slip rate for the 12 hours preceding the mainshock is 2.1 cm/day, which is comparable to the maximum slip rate of an SSE in Boso-Oki (1.2 cm/day) estimated by Fukuda et al. [2014].

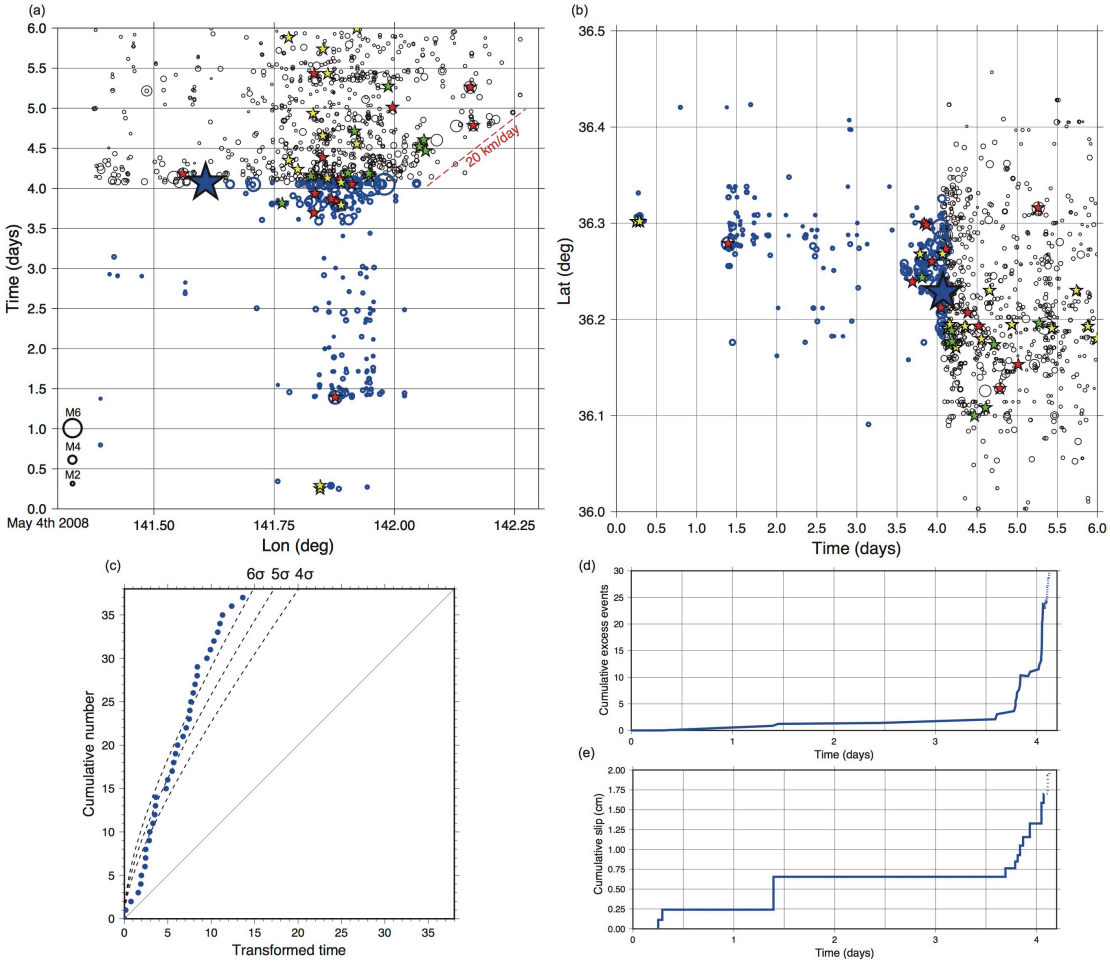

Figure 3.7 | Space-time distribution, excess events, fault slip of the foreshock sequence in 2008. (a) and (b) show time-longitude and latitude-time distributions of the foreshock sequence in 2008. Blue circles are foreshocks. Black circles are aftershocks. The large star indicates the 2008 Ibaraki-Oki earthquake. Small stars are repeating earthquakes, colored according to the manner of their repetition, i.e., yellow ones are repeating earthquakes that repeat within this foreshock-aftershock sequence, green ones are those whose similar events occurred in the other swarm sequences, and red ones are those whose similar events occurred neither in the foreshock-aftershock nor swarm sequences. (c) Transformed time of the foreshock sequence in 2008. The transformed time was calculated since the first *M* 3 or larger foreshock event. (d) and (e) show

temporal changes in the number of excess events and estimated fault slip of repeating earthquakes. Solid blue lines show the temporal changes before the mainshock.

3.4.2.2. Swarm sequence in May 2006

The swarm sequence in May 2006 started on May 8th and continued for 12 days (Figures 3.8a and 3.8b). The matched filter technique detected 149 events, which is 2.1 times of the JMA catalog (71 events). As in the foreshock sequence in 2008, repeating earthquakes were found in this swarm sequence. Furthermore, hypocenters of this swarm sequence expanded in the east and south direction from May 8th to May 10th (Figures 3.8a and 3.8b). This migration also can be seen even if we see only events recorded in the JMA catalog though events newly detected by the matched filter technique make the migration a little clearer. Its migration speed is about 10 km/day, which is comparable to migration speed of SSEs (~ 10 km/day) [Dragert et al., 2004; Fukuda et al., 2014]. Migration of hypocenters with similar speed was also observed in the swarm sequence in May 1996 (see Appendix A2.4).

The comparison of the number of observed events ($\geq M$ 3) in the Ibaraki-Oki detection circle (4 events) with the number of events predicted by the ETAS model since the first M 3 or larger swarm event (0.8 event) shows an anomaly larger than 3σ (Figure 3.8c), i.e., the probability that we observe such a high seismicity rate is less than 9.1×10^{-3}. Both the temporal changes in the number of excess events and fault slip of repeating earthquakes (Figure 3.8d and 3.8e) show a gradual increase and are similar to each other.

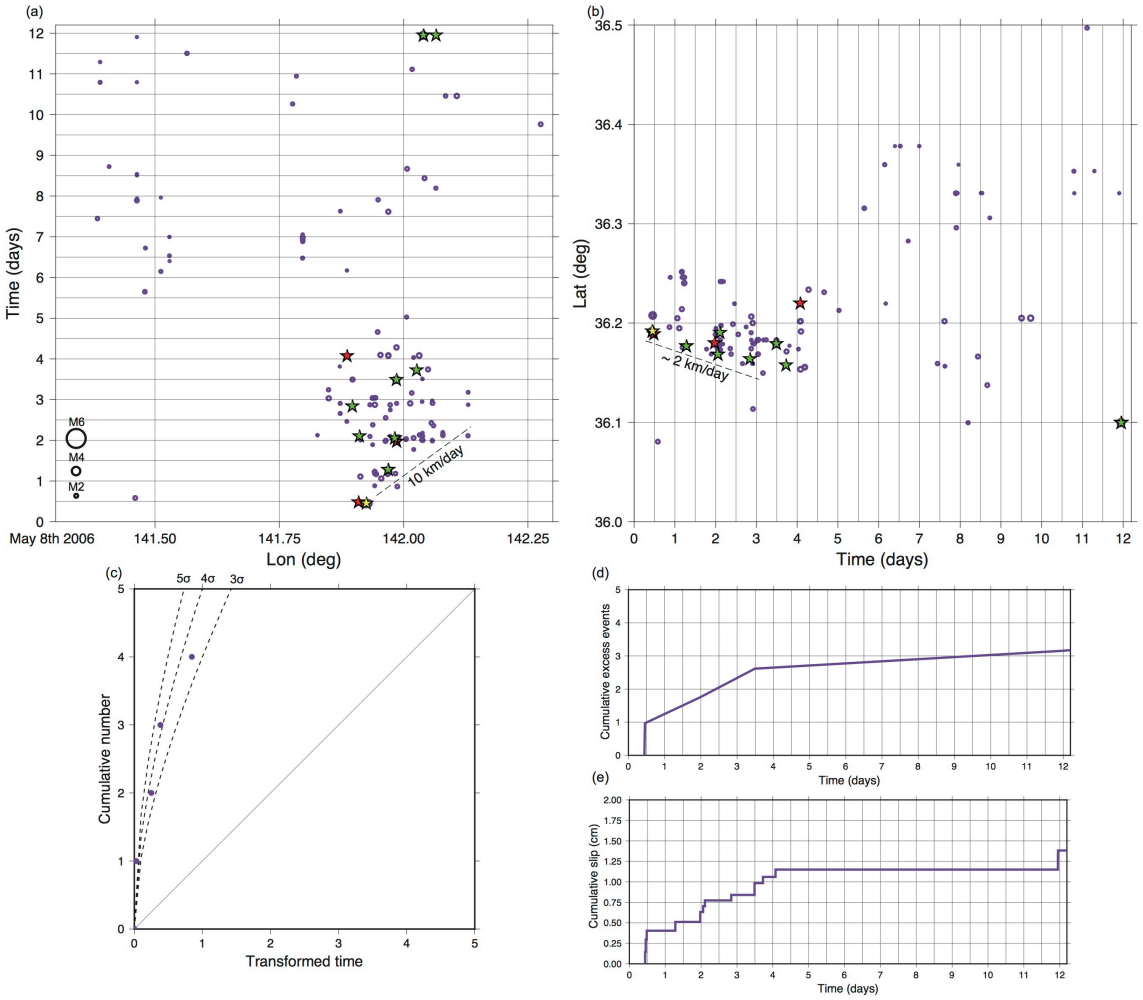

Figure 3.8 | Space-time distribution, excess events, fault slip of the swarm sequence in May 2006. (a) and (b) show time-longitude and latitude-time distributions of the swarm sequence in 2006. Purple circles are swarms. Small stars are repeating earthquakes, colored according to the same manner as Figure 3.7a (c) Transformed time of this swarm sequence. The transformed time was calculated since the first *M* 3 or larger swarm event. (d) and (e) show temporal changes in the number of excess events and estimated fault slip of repeating earthquakes.

3.4.2.3. Swarm sequence in March 2004

The swarm sequence in March 2004 started on March 22nd and continued for 30 days

(Figures 3.9a and 3.9b). The matched filter technique detected 220 events, which is 2.4 times of the JMA catalog (91 events). Repeating earthquakes were found in this swarm sequence too. On the other hand, migration of the hypocenters was not clear.

The comparison of the number of observed events ($\geq M$ 3) (7 events) in the Ibaraki-Oki detection circle with the number of events predicted by the ETAS model (2.0 event) shows an anomaly larger than 3σ (Figure 3.9c), i.e. the probability that we observe such a high seismicity rate is less than 4.4×10^{-3}. Figure 3.9d and 3.9e show the temporal changes in the number of excess events and fault slip of repeating earthquakes. The number of excess events started to increase 8 days after the initiation of this swarm sequence while the amount of fault slip of repeating earthquakes started to increase 13 days after the initiation.

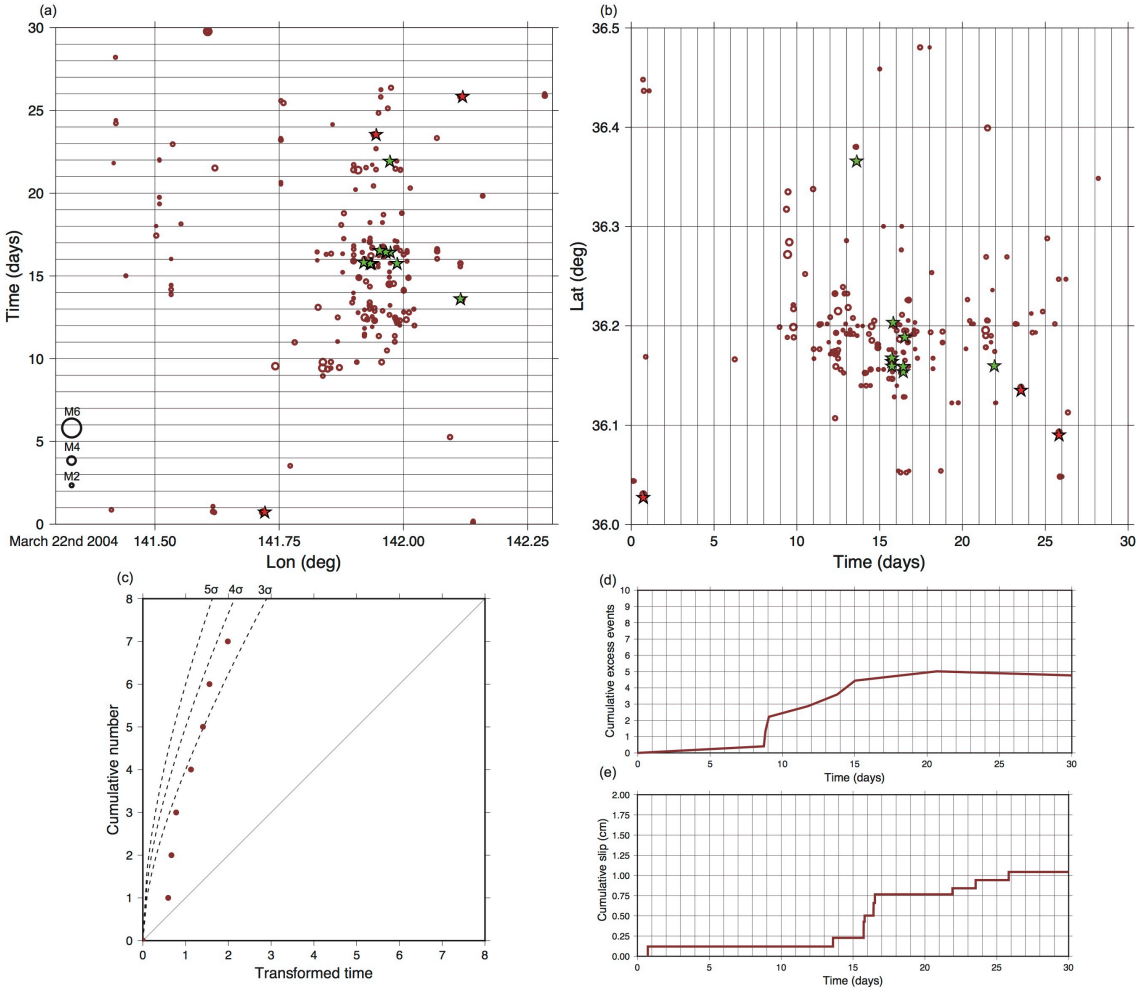

Figure 3.9 | Space-time distribution, excess events, fault slip of the swarm sequence in March 2004. (a) and (b) show time-longitude and latitude-time distributions of the swarm sequence in March 2004. Brown circles are swarms. Small stars are repeating earthquakes, colored according to the same manner as Figure 3.7a (c) Transformed time of this swarm sequence. The transformed time was calculated since the first *M* 3 or larger swarm event. (d) and (e) show temporal changes in the number of excess events and estimated fault slip of repeating earthquakes.

3.4.3. Time history of cumulative fault slip and occurrence time of swarms

In this section, we estimated cumulative fault slip of repeating earthquakes from 2000 to

2008 in the Ibaraki-Oki detection circle using the long-term repeating earthquake catalog in the Japan Trench [Uchida and Matsuzawa 2013; Uchida et al., 2016]. We used 98 repeating earthquake sequences that occurred in the Ibaraki-Oki detection circle.

In Figure 3.10, we found that average slip rate during 2000–2008 in this detection circle is 1.9 cm/year. Because the relative plate velocity here is 9.3 cm/year, this corresponds to about 80% locking, assuming that the cumulative slip of repeating earthquakes corresponds to the cumulative aseismic slip in the surrounding region [e.g., Nadeau and McEvilly, 1999; Uchida et al., 2009]. The slip deficit calculated from this locking degree during the period 1982–2008 is about 1.9 m. This is comparable to the maximum slip of the 2008 Ibaraki-Oki earthquake (1.7 m) [The Headquarters for Earthquake Research Promotion, 2008].

In Figure 3.10, we also found that the occurrence time of the swarm and foreshock sequences well correspond with large step-like increases in cumulative fault slip of repeating earthquakes. This suggests that aseismic slip in the surrounding region of the repeating earthquakes was accelerated during the periods of the swarm and foreshock sequences. On the other hand, earthquake swarms and large step-like increases in cumulative fault slip do not always corresponds with each other. For example, an increase in cumulative slip during the period of the swarm sequence in November 2004 is not large compared with other increases in non-swarm periods. Conversely, there are some large step-like increases with no corresponding swarm sequence. For example, a fault slip of 0.8 cm was observed from July 16th to August 17th, 2003. This slip was not

accompanied by swarm-like activity although 6 repeating earthquakes occurred over this time period.

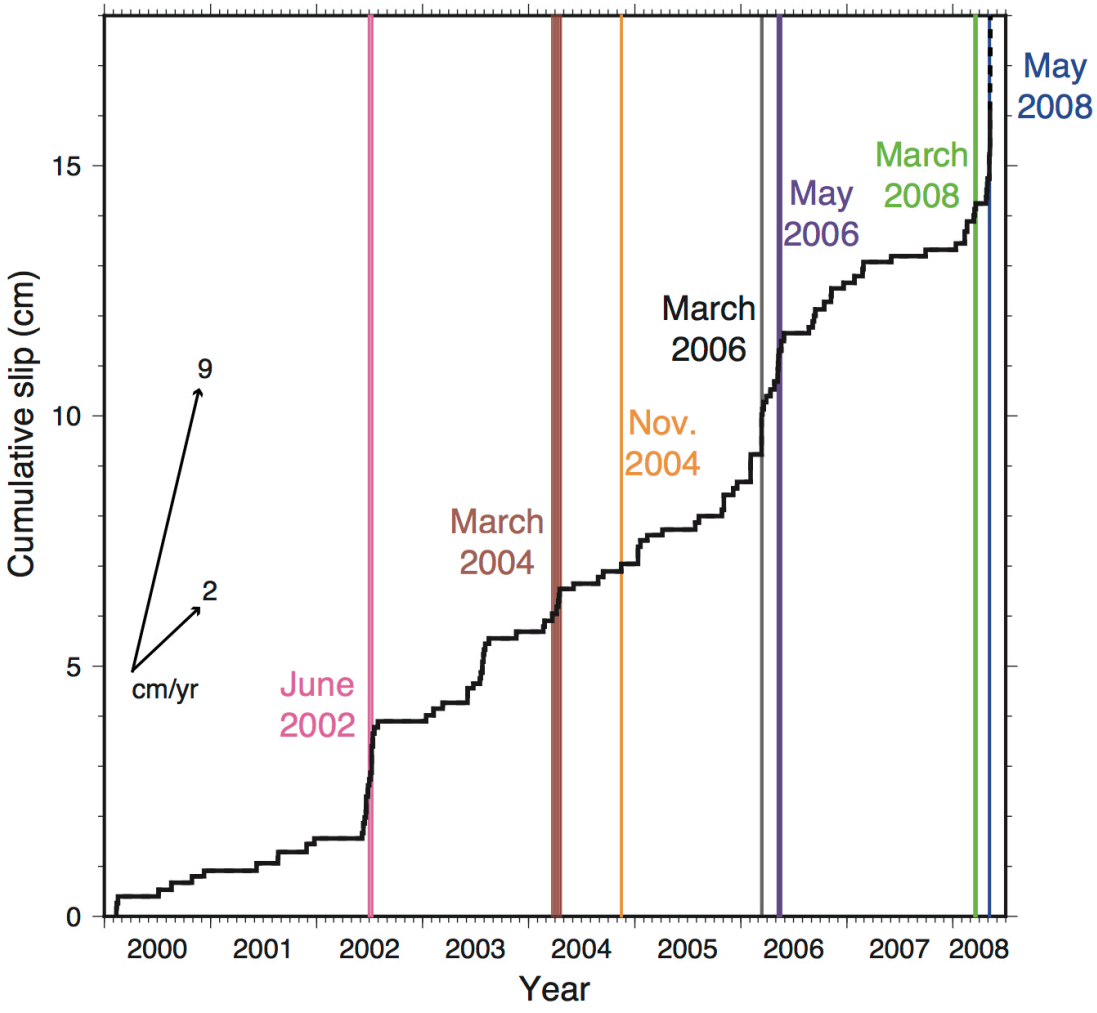

Figure 3.10 | Time history of cumulative fault slip from 2000 to 2008 in Ibaraki-Oki. A solid black line shows the time history of cumulative fault slip of repeating earthquakes before the 2008 Ibaraki-Oki earthquake (Uchida et al. 2016). A dashed black line shows the time history of cumulative fault slip after the 2008 Ibaraki-Oki earthquake. Vertical lines indicate the occurrence time of the foreshock and swarm sequences.

3.4.4. Comparison between the foreshock and swarm sequences

We then compare the foreshock and swarm sequences in terms of the degree of anomaly in the ETAS model, the number of excess events, and the amount of fault slip of repeating earthquakes (see Table 3.1 and Figure 3.11).

The foreshock sequences in 1982 and 2008 show anomalies larger than 9σ and 6σ respectively (see Table 3.1, Appendix A2.5, and Figure 3.7b). The probability that we observe as high a seismicity rate as the foreshock sequence in 1982 and 2008 is less than 6.9×10^{-12} and 1.2×10^{-7}. Swarm sequences also show comparable anomalies. For example, the swarm sequences in 1996 and 2002 showed anomalies larger than 9σ and 5σ respectively (see Table 3.1 and Appendices A2.4 and A2.6). The probability that we observe as high a seismicity rate as the swarm sequence in 1996 and 2002 is less than 6.0×10^{-10} and 1.5×10^{-5}. Thus, both the foreshock and swarm sequences show extremely large anomalies, suggesting a background phenomenon other than earthquake-to-earthquake triggering.

Figure 3.11a and 3.11b show temporal changes in the number of excess events for the foreshock sequences in 1982 and 2008 and six swarm sequences (four swarm sequences analyzed in Section 3.4.2 and two swarm sequences in 1996 and 2002). In Figure 3.11a, the foreshock sequences in 1982 and 2008 have the largest number of excess events (24.9 and 23.4 events). Among the swarm sequences, the swarm sequence in 1996 has the largest number of excess events (16.0 events) (see also Table 3.1), which is about 0.7 times of that of the foreshock sequences in 1982 and 2008. The swarm sequence in 2002 has the second largest number of excess events (9.5 events). It is also noteworthy

that an increase of the number of excess events in 12 hours preceding the 2008 Ibaraki-Oki earthquake is remarkably large (21.2 events) compared with the other increases in any 12 hours of the swarm sequences.

Figure 3.11c and 3.11d show temporal changes in estimated fault slip of repeating earthquakes during the periods of the foreshock in 2008 and four swarm sequences analyzed in Section 3.4.2. In Figure 3.11c, the foreshock sequence in 2008 has the largest fault slip (1.70 cm). Among the swarm sequences, the swarm sequence in 2006 has the largest fault slip (1.38 cm), which is 0.8 times of that of the foreshock sequence. Similar to the number of excess events, an increase of fault slip in 12 hours preceding the 2008 Ibaraki-Oki earthquake is relatively large (1.04 cm) compared with the other increases in any 12 hours of the swarm sequences.

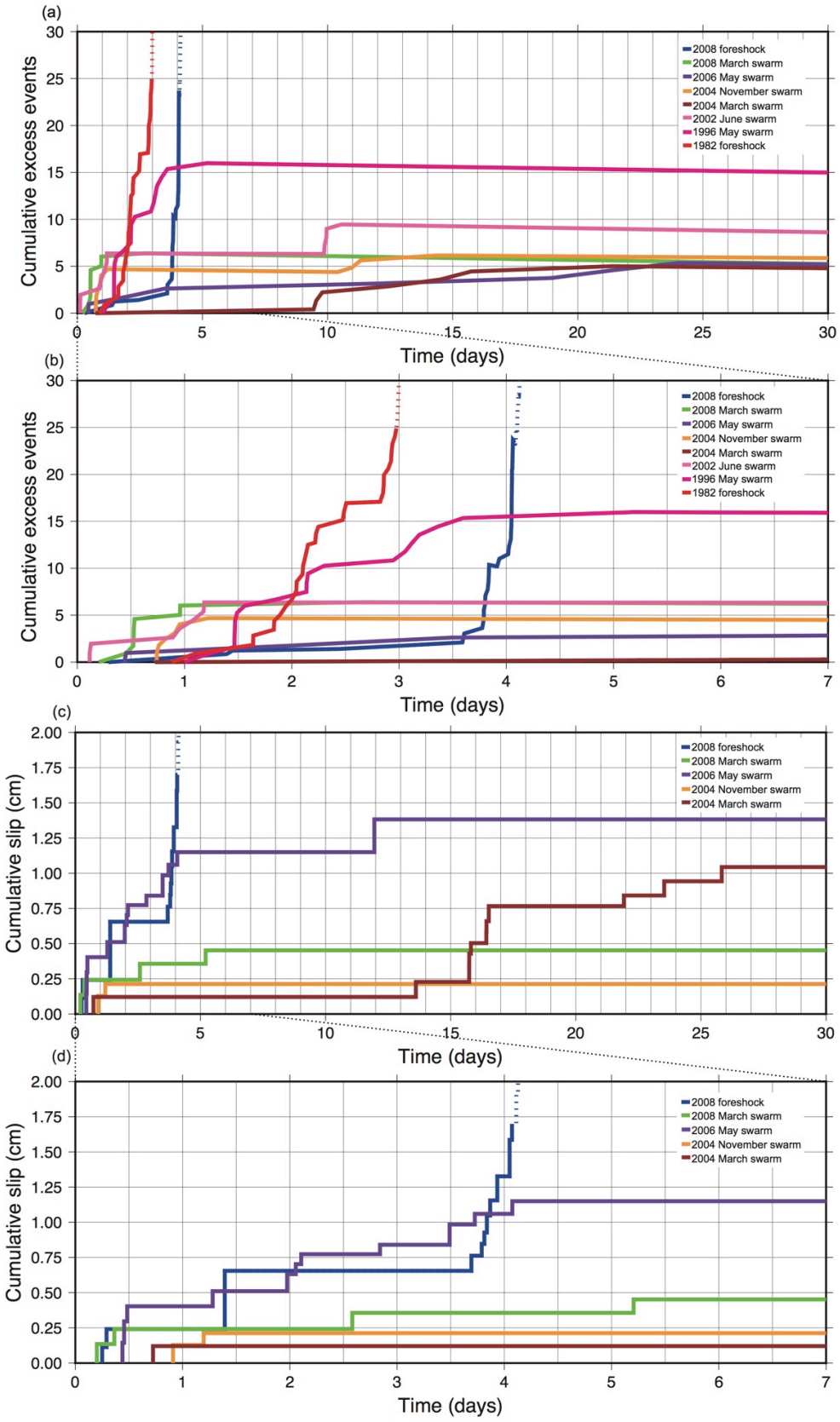

Figure 3.11 | Comparison between the foreshock and swarm sequences. (a)

Comparison of temporal changes in the number of excess events. (b) A zoom-up figure of (a). (c) Comparison of temporal changes in estimated fault slip of repeating earthquakes. (d) A zoom-up figure of (c).

3.5. Discussion

We found recurring foreshock and swarm sequences whose seismicity does not follow the ETAS model in Ibaraki-Oki (Figure 3.4 and 3.5), suggesting a background phenomenon other than earthquake-to-earthquake triggering. The swarm sequences in 2006 and 1996 showed migration of hypocenters (Figure 3.8 and Appendix A2.4), at a speed of about 10 km/day. Furthermore, repeating earthquakes were found in both the foreshock and swarm sequences, and occurrence time of the swarm sequences corresponds with large step-like increases in the time history of cumulative fault slip of repeating earthquakes (Figure 3.10), suggesting episodic aseismic slips in surrounding areas of repeating earthquakes. All these observations are consistent with the hypothesis that SSEs recurrently occur in the source region of *M* 7 Ibaraki-Oki earthquakes.

Although recurrence of SSEs is quite consistent with our observation, we cannot rule out other interpretations. Another possible mechanism that can trigger earthquake swarms is fluid migration [Waite and Smith, 2002]. Fluid reduces the strength of faults and can cause earthquake swarms. If there are recurrent fluid migrations in Ibaraki-Oki, it seems also possible that the fluid migrations recurrently reduce the strength of the same faults and trigger repeating earthquakes, although such triggering mechanism of repeating earthquakes have not been considered in previous studies.

In addition, fluid and occurrence of SSEs are closely related with each other. SSEs are also known to occur in regions where fluids are abundant [Kodaira et al., 2004; Saffer and Tobin, 2011; Saffer and Wallace, 2015]. Mochizuki et al. [2008] proposed the existence of fluid-rich sediment along the plate interface over the subducted seamount in Ibaraki-Oki, which is located just south to the foreshock and swarm sequences (Figure 3.4). Such fluid might facilitate occurrence of SSEs and earthquake swarms. Further research is needed to clarify the relationship among fluid, SSEs, and earthquake swarms in Ibaraki-Oki.

Uchida et al. [2016] found 3-year periodic coincidences of clusters of medium earthquakes ($\geq M$ 5) and increases in slip rate estimated from repeating earthquakes in Sanriku-Oki, which is the northernmost part of the Japan Trench. Their observation is similar to the coincidences of earthquake swarms ($\geq M$ 3) and large step-like increases in fault slip of repeating earthquakes in Figure 3.10 although periodicity is not clear in our study. In addition, the time scales of the clusters of medium earthquakes ($\geq M$ 5) in Sanriku-Oki (from months to years) and the earthquake swarms ($\geq M$ 3) in Ibaraki-Oki (from a day to a month) are different. This implies that SSEs in the Japan Trench can have various time scales (from a day to years), which is similar to long-term (months or years) and short-term (days) SSEs in the Nankai subduction zone [Obara and Kato, 2016].

In Figure 3.11, the foreshock sequences in 1982 and 2008 showed the largest number of excess events (24.9 and 23.4 events, which is about 1.5 times of that of the swarm sequence in 1996). Similarly, the foreshock sequence in 2008 showed the largest fault

slip of repeating earthquakes (1.75 cm, which is 1.2 times of that of the swarm sequence in 2006). Given that background seismicity rates during time periods of SSEs are known to be roughly proportional to moment rates of the SSEs [Reverso et al., 2016], these results imply that SSEs that triggered the foreshock sequences in 1982 and 2008 have larger seismic moments than the other SSEs that triggered the swarm sequences. In addition, the large increases in the number of excess events and the amount of fault slip 12 hours before the 2008 Ibaraki-Oki earthquake imply a large moment rate of the SSE preceding the mainshock. Matsumura [2010] examined background micro-seismicity changes preceding the 1982 and 2008 Ibaraki-Oki earthquakes and found a similarity between them. They suggested the existence and repetition of a typical preparatory stage leading to the 1982 and 2008 Ibaraki-Oki earthquakes, which lasts several months. This idea is consistent with our interpretation that relatively large SSEs preceded both the 1982 and 2008 Ibaraki-Oki earthquakes although these SSEs are considered to have started not several months before but only a few days before the mainshocks (see Figures 3.7, 3.11, and Appendix A2.5).

Our observations are similar to what was observed in earthquake cycle simulations [e.g., Lapusta and Liu, 2009; Noda et al., 2013]. In earthquake cycle simulations, many SSEs spontaneously occur in a seismogenic patch as its locked region shrink due to plate loading, and one of the spontaneous SSEs grows and accelerates, leading to nucleation of a large earthquake that ruptures the entire seismogenic patch. In our observations, the seismogenic patch corresponds to the source region of the 1982 and 2008 Ibaraki-Oki earthquakes, and the spontaneous SSEs in the earthquake cycle simulations correspond to SSEs that triggered the swarm sequences. Furthermore, large increases in the number

of excess events and the amount of fault slip 12 hours before the 2008 Ibaraki-Oki earthquake might reflect the final acceleration of the slip rate in the nucleation phase of the 2008 Ibaraki-Oki earthquake.

Our results suggest that large SSEs preceded the 1982 and 2008 Ibaraki-Oki earthquakes and that these two SSEs can be differentiated from the other SSEs in terms of the number of excess events and the amount of fault slip of repeating earthquakes (Figure 3.11). However, this may not always hold true for large earthquakes in other regions. This is because how large earthquakes nucleate strongly depends on frictional properties in each region. In the above discussion, we only considered one large seismogenic patch and neglected small seismogenic patches inside it. If we have a small patch whose size is comparable to the critical nucleation size [e.g., Rubin and Ampuero, 2005] of the large seismogenic patch, nucleation of the large event becomes much more complicated [Noda et al., 2013]. A large SSE preceding the large event, which is the nucleation phase of the large patch, sometimes can be skipped due to cascade-up process from the small patch to the large patch [Ellsworth and Beroza, 1995; Ide and Aochi, 2005; Ide and Aochi, 2013; Noda et al., 2013]. In this case, what we can observe just before the large event is small nucleation in the small patch, and it seems difficult to differentiate it from the other small SSEs.

3.6. Conclusion

We found recurring swarm and foreshock sequences in the source region of the 1982 and 2008 *M* 7 Ibaraki-Oki earthquakes. These foreshock and swarm sequences have anomalously high seismicity rates inexplicable by the ETAS model [e.g., Ogata, 1988]

and contain repeating earthquakes [e.g., Ellsworth, 1995], strongly suggesting recurrence of SSEs in Ibaraki-Oki. Furthermore, the number of excess events and the amount of fault slip of repeating earthquakes suggest that SSEs preceding the 1982 and 2008 Ibaraki-Oki have larger seismic moments than the other SSEs which triggered the swarm sequences, and that the moment rate of the SSE preceding the 2008 Ibaraki-Oki earthquake increased 12 hours before the mainshock, which can be interpreted as the nucleation phase of the 2008 Ibaraki-Oki earthquake. Our results imply that we can differentiate SSEs preceding large earthquakes from the other SSEs in Ibaraki-Oki in terms of the number of excess events and the amount of fault slip of repeating earthquakes, which probably reflect the seismic moments and moment rates of the SSEs. Therefore, monitoring excess events and fault slip of repeating earthquakes might be useful for assessing the imminence of future large earthquakes in Ibaraki-Oki. Furthermore, by finding regions similar to Ibaraki-Oki, where characteristic large earthquakes and SSEs recurrently occur, in other subduction zones, we can further test the hypothesis that there are differences between SSEs preceding large earthquakes and the other SSEs. This is crucially important for studies on earthquake predictability and seismic risk assessment.

4. Overall Discussion

4.1. Structure of the seismogenic zone implied by our study

In Chapter 2, we made a global earthquake swarm catalog and found that curvature of incoming plate before subduction positively correlates with swarm activity in subduction zones. This implies that earthquake swarms are more likely to occur in subduction zones with abundant fluids and marked heterogeneity on the plate interface [e.g., Uyeda, 1983; Ranero et al., 2003]. Given that earthquake swarms in subduction zones are often triggered by SSEs [e.g., Ozawa et al., 2003], SSE activity at seismogenic depths may also be high in such subduction zones. In Chapter 3, we reveled recurrence of SSEs in the source region of the 1982 and 2008 *M* 7 Ibaraki-Oki earthquakes. The SSEs preceding the *M* 7 events might have large seismic moments than the other SSEs. Furthermore, the moment rate of the SSE preceding the 2008 Ibaraki-Oki earthquake might have increased 12 hours before the mainshock, which can be interpreted as the nucleation phase of the 2008 Ibaraki-Oki earthquake.

Then, what kind of structure of the seismogenic zone do Chapter 2 and Chapter 3 imply? Figure 4.1 summarize schematic illustration of a typical subduction zone, i.e., geometry of plate interface, seismicity distribution, and slow slip activity. In subduction zones with large incoming plate curvature, fractures related to slab bending (horst and graben) are well developed. These fractures facilitate hydration of the incoming plate and make locking on the plate interface heterogeneous [e.g., Uyeda, 1983; Tanioka et al., 1997; Ranero et al., 2003]. In such subduction zones, SSEs accompanied by earthquake swarms occur at various locations of the seismogenic zone. This is consistent with previous studies that suggest the relation of SSEs to fluids and

heterogeneity on the plate interface [e.g., Kodaira et al., 2004; Saffer and Wallace, 2015] (see also Section 4.3). Furthermore, results and insights in Chapter 3 suggest that SSEs can occur even inside locked regions of large earthquakes. This idea is also supported by recent observations of SSEs in the Japan Trench and northern Chile [e.g., Ito et al., 2013; Ruiz et al., 2014] (see also Section 4.4).

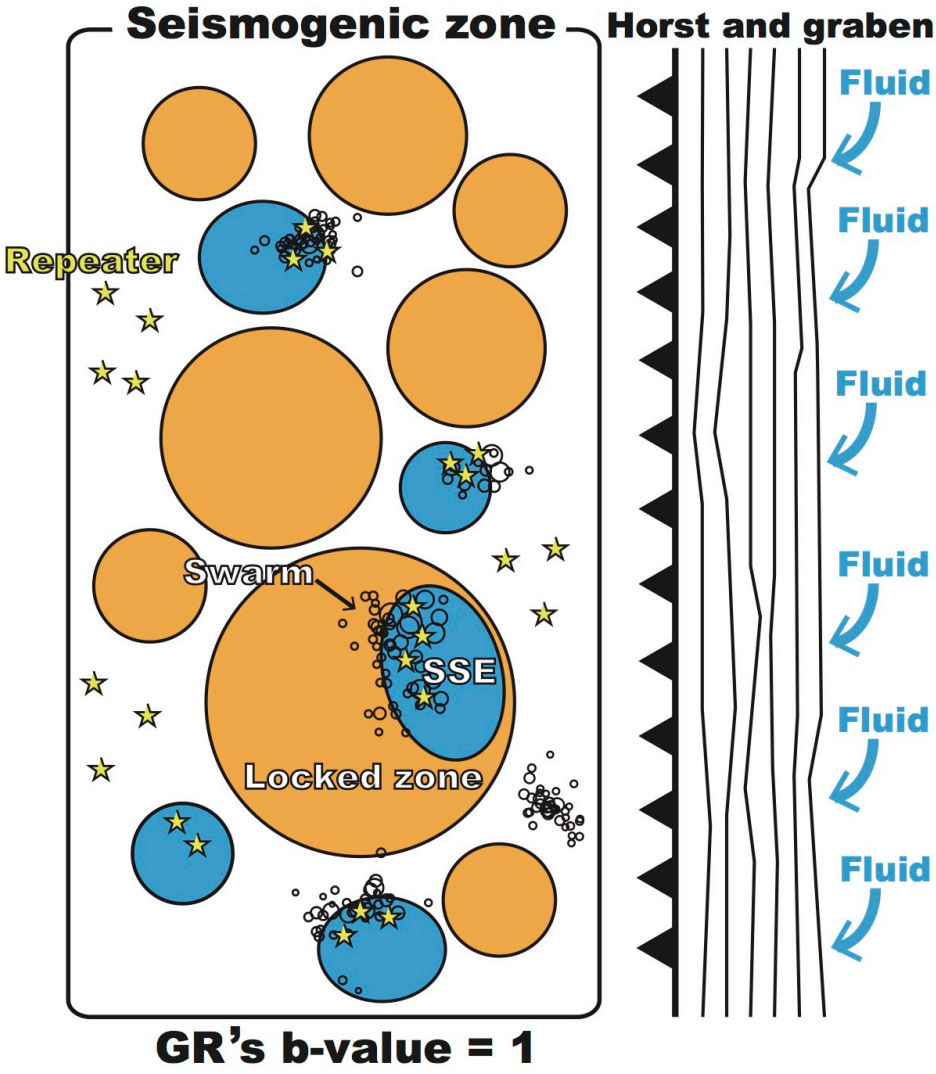

Figure 4.1 | Schematic picture of the seismogenic zone. Crooked lines indicate fractures related to slab bending (horst and graben). These fractures facilitate hydration of the incoming plate and make locking on the plate interface heterogeneous. Orange

patches are locked zones, which are distributed according to the Gutenberg–Richter relationship (b = 1.0) [Gutenberg and Richter, 1944]. Blue patches are SSE zones. Small black circles indicate earthquake swarms. Small yellow stars are repeating earthquakes.

4.2. Tectonic controls on seismicity in subduction zones

On the other hand, seismicity in subduction zones is also influenced by factors not considered in Figure 4.1. Seismicity rates in subduction zones are basically proportional to relative plate velocity because plate velocity represents the strain rate on the plate interface, and thus determines the recurrence intervals of repeating events in subduction zones [Ide, 2013]. For example, the Tonga trench is known to have the highest background seismicity rate among subduction zones worldwide due to the highest relative plate velocity there (larger than 200 mm/yr) [Ide, 2013]. The b-value of earthquake magnitude–frequency distributions [Gutenberg and Richter, 1944], which is fixed in Figure 4.1 (b = 1.0), positively correlates with plate age of the incoming plate probably because plate age determines slab buoyancy and the tectonic stress state in subduction zones [Nishikawa and Ide, 2014]. For instance, Vanuatu and Mexico are known to be characterized by subducting plates younger than 30 Ma and low b-value ($\lesssim$ 0.9) [Nishikawa and Ide, 2014]. In contrast to Figure 4.1, some subduction zones, such as Cascadia, Nankai, and southern Chile, have little fracturing related to slab bending because of small curvature of the incoming plate [e.g., Nishikawa and Ide, 2015]. These subduction zones are characterized by smooth plate interface and dry slab [e.g., Uyeda 1983; Canales et al., 2017] and associated with anomalously low background seismicity rate and characteristic megathrust earthquakes [Ide, 2013; Nishikawa and Ide, 2015].

Summarizing these studies, seismicity in subduction zones, including earthquake swarm activity, is basically controlled by relative plate velocity, plate age, and plate curvature since these tectonic properties control the strain rate on the plate interface, tectonic stress state, roughness of the plate interface, and hydration of the incoming plate. Combinations of these tectonic properties seem to well explain variations in seismicity among subduction zones worldwide.

In contrast, tectonic controls on variations in slow earthquake activity (i.e., SSEs, tectonic tremors, and VLFEs) among subduction zones are still unclear. This is an important problem that should be addressed in future studies. This study proposes that SSE activity at seismogenic depths might be high in subduction zones with large curvature of the incoming plate (see Figure 4.1). This hypothesis should be further tested by geodetic and seismic observations in the future.

4.3. Relationship among SSEs, earthquake swarms, fluid, and heterogeneity on the plate interface

SSEs, earthquake swarms, fluid, and heterogeneity on the plate interface are closely related with each other. Previous studies have suggested that both SSEs and earthquake swarms occur in fluid-rich regions with a compositionally and geometrically heterogeneous plate interface [e.g., Kodaira et al., 2004; Ando et al., 2012; Skarbek et al., 2012; Holtkamp and Brudzinski, 2014; Saffer and Wallace, 2015; Poli et al., 2017; Yabe and Ide, 2017]. For instance, Saffer and Wallace [2015] pointed out that shallow SSEs and earthquake swarms at the northern Hikurangi margin occur on the plate

interface characterized by elevated pore-fluid pressure and geometric complexity such as a subducted seamount. In Chapter 2, we also found that earthquake swarm activity is especially active in subduction zones with large curvature of the incoming plate, i.e., fluid-rich subduction zones with a rough (i.e., heterogeneous) plate interface (see Figure 4.1). In Chapter 3, we found that earthquake swarms containing repeating earthquakes had recurrently occurred in the vicinity of a fluid-rich region associated with sediment entrained with a subducted seamount in Ibaraki-Oki (see Figure 3.4), and we suggested that recurrent SSEs had triggered the earthquake swarms there. Ibaraki-Oki is similar to the northern Hikurangi margin in terms of abundance of fluid and geometric complexity. Given these studies, fluid and heterogeneity on the plate interface can be proposed as necessary conditions for occurrence of both SSEs and earthquake swarms.

Nevertheless, there is still one unclear point regarding what causes earthquake swarms. Considering previous studies [e.g., Waite and Smith, 2002], not only SSEs but also fluid migration seems to be able to trigger earthquake swarms in subduction zones because fluid reduces the strength of interplate faults. Additionally, not only fluid migration itself but also propagation of a pulse of high pore-fluid pressure along the plate interface [e.g., Rice, 1992; Frank et al., 2015] might be able to trigger earthquake swarms. Then, what percentage of earthquake swarms in subduction zones are directly triggered by SSEs? The close relationship between SSEs and fluid, which was mentioned above, makes it further difficult to differentiate swarms directly triggered by SSEs from those triggered by fluid migration. Furthermore, these two mechanisms may not be independent. In rock experiments, it is known that a fluid injection also can trigger an aseismic slip on a fault [Guglielmi et al., 2015]. Therefore, it is also possible that fluid

migration on the plate interface primarily triggers SSEs and then indirectly trigger earthquake swarms mediated by the SSEs. In addition, a complex interaction between fault slips and pore-fluid via dilatant strengthening and thermal pressurization also has been proposed as a candidate of the mechanism for SSEs [e.g., Suzuki and Yamashita, 2009; Segall et al., 2010]. In order to answer the question above, it is important to further investigate the cause of each earthquake swarm through geodetic and seismic observations.

4.4. SSEs and earthquake predictability

Previous studies [e.g., Kato et al., 2012; Ito et al., 2013; Ruiz et al., 2014] and results in Chapter 3 suggested that SSEs can occur even inside locked regions of large earthquakes (see Figure 4.1). Furthermore, behaviors of SSEs preceding the large earthquakes may be different from the other SSEs as suggested by numerical simulations [e.g., Lapusta and Liu, 2009; Matsuzawa et al., 2010; Noda et al., 2013] and results in Chapter 3. It is crucial to accumulate such case studies for discussing earthquake predictability. It seems useful to detect and monitor aseismic slips inside locked regions on the plate interface through geodetic measurements and repeating earthquake analyses for assessing the imminence of future large earthquakes.

On the other hand, Chapter 2 shows that only 6% of large earthquakes ($M \geq 6.5$) in subduction zones were preceded by swarm-like foreshocks ($M \geq 4.5$), which are potentially related to SSEs, and that 75% of large earthquakes were not preceded by any foreshocks ($M \geq 4.5$). A global investigation of foreshock activity ($M \geq 4.0$) by Marsan et al. [2014] also suggests that accelerating seismicity rates, possibly related to SSEs,

preceded only 18% of large earthquakes ($M \geq 6.5$) during the period 1981–2013 in the ANSS catalog. Given these results, it is clear that there are many large earthquakes not preceded by detectable SSEs, and it seems impossible to predict such large earthquakes. These large earthquakes probably result from a cascade-up process from a small seismogenic patch to a large seismogenic patch [Ellsworth and Beroza, 1995; Ide and Aochi, 2005; Ide and Aochi, 2013; Noda et al., 2013]. In order to elucidate the mechanism of such large earthquakes, it is important to reveal the hierarchical structure of the seismogenic zone. In Kamaishi-Oki, the Japan Trench, the hierarchical structure inside a medium seismogenic patch (≈ M5) was actually revealed by Uchida et al. [2007] and Uchida et al. [2012]. Uchida et al. [2012] found that small patches ($\lesssim$ M3) on the edge of the medium seismogenic patch are more frequently ruptured than small patches near the center of the medium patch and that ruptures of the small patches near the center of the medium patch is limited to the latter half of the earthquake cycles of the medium patch. Likewise, by revealing the hierarchical structure inside a large patch ($M \gtrsim 6.5$) in the future, we may be able to obtain some constraints on the patterns of large earthquake occurrence.

In addition, it is also important to improve the accuracy of probabilistic forecasts of earthquakes by modifying statistical models such as the ETAS model [e.g., Ogata, 1988]. Even though many SSEs occur without following large earthquakes, it is quite possible that the SSEs induce stress perturbation in the seismogenic zone and modulate background seismicity rate there [Liu et al., 2007; Uchida et al., 2016]. In Guerrero, Mexico, an SSE in the deeper extension of the seismogenic zone actually caused a long-term increase in the background seismicity rate, which lasted 6 months [Liu et al.,

2007; Chapter 2]. Such influences of SSEs on the background seismicity rate should be taken into account in statistical models in order to improve the probabilistic forecasts.

5. Overall Conclusion

In this study, we aimed to obtain implications for global SSE activity and the mechanism of large earthquake occurrence through detection of earthquake swarms at subduction zones globally and repeating earthquake analyses.

In Chapter 2, we presented a method for detecting earthquake swarms using the space-time epidemic-type aftershock-sequence (ETAS) model [e.g., Zhuang et al., 2002] and revealed swarm activity in subduction zones worldwide. In subduction zones, such as Ibaraki-Oki, Japan, we also detected foreshock sequences of large earthquakes as earthquake swarms. In these regions, the large earthquakes may have been preceded by SSEs. Furthermore, we found that the swarm activity in subduction zones is positively correlated with curvature of the incoming plate before subduction. This correlation implies that swarm activity is controlled by hydration of incoming plate and/or by heterogeneity on the plate interface due to fracturing related to slab bending. The global earthquake swarm catalog created by this study may be useful for future global investigations of SSE activity. The observed correlation between curvature of the incoming plate and swarm activity will be important for elucidating tectonic controls on SSE activity in the future.

In Chapter 3, we revealed recurrence of SSEs in the source region of the 1982 and 2008 M 7 Ibaraki-Oki earthquakes through detection of earthquake swarms and repeating earthquake analyses. The SSEs preceding the M 7 events might have larger seismic moments than the other SSEs that triggered the swarm sequences. Furthermore, the moment rate of the SSE preceding the 2008 Ibaraki-Oki earthquake might have

increased 12 hours before the mainshock, which can be interpreted as the nucleation phase of the 2008 Ibaraki-Oki earthquake. This study elucidated the relationship between the *M* 7 Ibaraki-Oki earthquakes and recurring SSEs in their source region. These results and insights will be important for studies on the mechanism of large earthquake occurrence and earthquake predictability.

This study proposed a complex structure of the seismogenic zone in subduction zones. In subduction zones with large incoming plate curvature, fracturing related to slab bending facilitates hydration of the incoming plate and makes the plate interface rough (i.e., heterogeneous) [e.g., Uyeda, 1983; Ranero et al., 2003]. In such subduction zones, SSEs accompanied by earthquake swarms can occur at various locations of the seismogenic zone. Furthermore, SSEs can occur even inside locked regions of large earthquakes. Behaviors of these SSEs may change in the later stages of interseismic periods of the large earthquakes. It is necessary to further test these hypotheses proposed by this study through geodetic and seismic observations in the future.

Appendices

A1. Appendices for Chapter 2

A1.1. Estimated ETAS parameters for the 100 study regions

We listed the estimated ETAS parameters for the 100 study regions in Table A1.1. Each region has three 5-year time periods, i.e., 1995–1999, 2000–2004, and 2005–2009. For time periods when the ETAS model did not converge, we noted "N/A".

Table A1.1 | Estimated ETAS parameters for the 100 study regions

Region	Lon. (deg)	Lat. (deg)	Period	A	c	α	p	D	q	γ
CENTRAL CHILE1	286.559	-34.4336	1995	1.45E-01	3.21E-02	1.70E+00	1.25E+00	1.48E-03	1.48E+00	1.06E+00
			2000	1.16E-01	4.22E-01	1.59E+00	2.62E+00	2.61E-02	5.15E+00	0.00E+00
			2005	8.19E-02	3.50E-02	2.46E+00	1.46E+00	2.11E-03	2.35E+00	1.43E+00
CENTRAL CHILE2	287.176	-32.4042	1995	2.37E-01	4.25E-02	1.67E+00	1.15E+00	1.99E-02	2.55E+00	3.75E-01
			2000	N/A	N/A	N/A	N/A	N/A	N/A	N/A
			2005	1.54E-01	2.84E-02	1.63E+00	1.35E+00	6.60E-03	2.83E+00	1.15E+00
CENTRAL CHILE3	287.528	-29.9344	1995	1.57E-01	4.80E-02	1.89E+00	1.14E+00	3.29E-02	2.98E+00	3.16E-01
			2000	N/A	N/A	N/A	N/A	N/A	N/A	N/A
			2005	6.54E-02	4.90E-02	1.87E+00	1.40E+00	4.24E-02	7.60E+00	1.19E+00
CENTRAL CHILE4	287.882	-28.0499	1995	7.81E-03	6.49E-02	3.20E+00	1.30E+00	2.01E-02	2.05E+00	2.76E-01
			2000	2.61E-02	1.90E-01	2.30E+00	1.62E+00	1.48E-02	1.49E+00	0.00E+00
			2005	8.48E-02	1.20E-02	2.27E+00	1.24E+00	3.64E-03	1.99E+00	7.25E-01
NORTH CHILE	288.42	-25.0107	1995	4.52E-01	6.03E-02	7.42E-01	1.47E+00	1.63E-02	1.90E+00	7.08E-01
			2000	1.48E-01	6.68E-03	1.83E+00	1.16E+00	6.10E-03	1.75E+00	3.53E-01
			2005	3.11E-01	1.36E-02	1.29E+00	1.22E+00	5.24E-03	2.06E+00	9.10E-01
PERU1	287.115	-18.2901	1995	N/A	N/A	N/A	N/A	N/A	N/A	N/A
			2000	4.51E-01	3.27E-02	1.25E+00	1.36E+00	2.82E-02	2.04E+00	4.45E-01
			2005	N/A	N/A	N/A	N/A	N/A	N/A	N/A
PERU2	285.683	-17.0443	1995	N/A	N/A	N/A	N/A	N/A	N/A	N/A
			2000	3.43E-01	3.80E-02	1.40E+00	1.31E+00	8.00E-02	7.29E+00	1.40E+00
			2005	5.88E-02	4.14E-03	3.17E+00	1.12E+00	1.68E-02	6.16E+00	2.23E+00
PERU3	282.421	-13.9013	1995	1.59E-01	1.26E-01	1.58E+00	1.50E+00	6.05E-03	1.92E+00	8.22E-01
			2000	N/A	N/A	N/A	N/A	N/A	N/A	N/A
			2005	1.72E-01	5.98E-02	1.61E+00	1.30E+00	9.88E-03	2.11E+00	8.91E-01

COSTA RICA	275.382	8.68547	1995	N/A	N/A	N/A	N/A	N/A	N/A	N/A
			2000	4.05E-02	9.02E-02	2.33E+00	1.47E+00	2.61E-02	3.31E+00	4.88E-01
			2005	N/A	N/A	N/A	N/A	N/A	N/A	N/A
NICARAGUA	271.442	11.5991	1995	2.68E-01	1.71E-02	1.14E+00	1.14E+00	2.48E-02	1.48E+00	0.00E+00
			2000	2.66E-01	1.56E-02	1.58E+00	1.06E+00	2.26E-02	1.80E+00	1.71E-01
			2005	1.13E-01	4.53E-03	1.43E+00	1.10E+00	7.37E-02	3.52E+00	0.00E+00
GUATEMALA	267.145	13.6184	1995	1.46E-01	4.94E-02	1.33E+00	1.29E+00	2.92E-02	2.48E+00	0.00E+00
			2000	9.25E-02	8.83E-02	1.70E+00	1.36E+00	1.38E-02	1.33E+00	0.00E+00
			2005	9.81E-02	1.83E-02	8.80E-01	1.38E+00	2.84E-02	1.98E+00	5.51E-01
MEXICO1	265.005	14.6887	1995	1.57E-01	5.47E-02	1.75E+00	1.32E+00	4.72E-02	2.84E+00	0.00E+00
			2000	4.47E-01	6.27E-03	8.90E-01	1.05E+00	1.58E-02	1.23E+00	0.00E+00
			2005	N/A	N/A	N/A	N/A	N/A	N/A	N/A
MEXICO2	263.192	15.3519	1995	3.72E-01	6.26E-03	8.33E-01	1.15E+00	1.91E-01	6.38E+00	1.43E-01
			2000	1.13E-01	1.60E-02	9.19E-01	1.55E+00	5.89E-02	4.99E+00	0.00E+00
			2005	N/A	N/A	N/A	N/A	N/A	N/A	N/A
MEXICO3	260.716	16.0733	1995	2.55E-01	7.98E-03	9.74E-01	1.20E+00	7.66E-02	4.36E+00	4.26E-01
			2000	2.67E-01	3.00E-03	1.66E+00	1.04E+00	7.04E-02	3.88E+00	4.24E-01
			2005	N/A	N/A	N/A	N/A	N/A	N/A	N/A
MEXICO4	258.822	16.8079	1995	N/A	N/A	N/A	N/A	N/A	N/A	N/A
			2000	2.11E-01	3.72E-03	2.00E+00	1.03E+00	9.05E-02	6.61E+00	9.96E-01
			2005	3.50E-02	7.18E-02	2.54E+00	1.42E+00	4.93E-04	1.86E+00	2.44E+00
ALEUTIAN1	197.227	53.2164	1995	N/A	N/A	N/A	N/A	N/A	N/A	N/A
			2000	1.64E-01	1.05E-02	2.13E+00	1.03E+00	1.37E-02	4.18E+00	6.28E-01
			2005	8.86E-02	7.96E-03	2.32E+00	1.15E+00	5.69E-04	1.73E+00	1.16E+00
ALEUTIAN2	194.115	52.508	1995	2.51E-01	4.72E-02	1.10E+00	1.46E+00	3.70E-02	6.01E+00	3.33E-01
			2000	1.95E-01	8.66E-04	1.63E+00	1.06E+00	5.13E-03	2.13E+00	2.71E-02
			2005	1.69E-01	1.26E-02	1.79E+00	1.23E+00	8.59E-02	1.58E+01	7.59E-01
ALEUTIAN3	190.618	51.6742	1995	1.77E-01	2.54E-02	1.35E+00	1.33E+00	7.95E-03	2.64E+00	3.92E-01
			2000	N/A	N/A	N/A	N/A	N/A	N/A	N/A
			2005	N/A	N/A	N/A	N/A	N/A	N/A	N/A
ALEUTIAN4	187.124	51.0636	1995	2.33E-01	3.11E-02	1.42E+00	1.36E+00	3.82E-03	1.78E+00	5.16E-01
			2000	2.40E-01	4.76E-04	1.42E+00	1.12E+00	1.12E-03	1.76E+00	5.43E-01
			2005	N/A	N/A	N/A	N/A	N/A	N/A	N/A
ALEUTIAN5	184.078	50.7055	1995	1.22E-01	4.43E-02	1.74E+00	1.32E+00	6.23E-02	1.80E+01	1.15E+00
			2000	1.54E-01	9.78E-04	1.34E+00	1.15E+00	3.87E-03	3.46E+00	8.60E-01
			2005	2.50E-01	7.10E-03	1.23E+00	1.27E+00	8.31E-03	3.04E+00	8.30E-01
ALEUTIAN6	180.426	50.5859	1995	2.56E-01	1.44E-02	1.35E+00	1.25E+00	8.12E-03	1.92E+00	8.75E-02
			2000	N/A	N/A	N/A	N/A	N/A	N/A	N/A

			2005	2.27E-01	9.14E-03	1.28E+00	1.35E+00	6.19E-03	2.92E+00	1.01E+00
ALEUTIAN7	177.017	50.9262	1995	2.14E-01	1.51E-02	1.54E+00	1.34E+00	1.25E-02	3.17E+00	2.84E-01
			2000	4.07E-01	9.67E-03	1.21E+00	1.23E+00	1.28E-03	1.55E+00	1.06E+00
			2005	2.76E-01	7.95E-03	1.02E+00	1.27E+00	9.09E-03	3.18E+00	7.48E-01
KAMCHATKA1	162.424	53.4079	1995	4.70E-01	3.10E-02	1.01E+00	1.46E+00	6.03E-03	1.91E+00	8.07E-01
			2000	1.72E-01	8.34E-02	1.87E+00	1.55E+00	3.93E-03	2.15E+00	1.01E+00
			2005	N/A	N/A	N/A	N/A	N/A	N/A	N/A
KAMCHATKA2	160.759	51.7241	1995	5.23E-01	2.47E-02	6.59E-01	1.41E+00	7.10E-03	2.06E+00	4.57E-01
			2000	1.23E-01	8.02E-02	2.16E+00	1.52E+00	9.72E-03	2.78E+00	8.16E-01
			2005	1.89E-01	5.34E-03	1.09E+00	1.11E+00	1.41E-02	4.56E+00	3.90E+00
KAMCHATKA3	158.42	49.7317	1995	1.29E-01	5.02E-01	1.56E+00	1.95E+00	1.43E-02	4.91E+00	1.26E+00
			2000	5.32E-02	6.93E-03	2.07E+00	1.28E+00	2.94E-02	4.22E+00	0.00E+00
			2005	1.16E-01	2.37E-01	1.85E-01	2.16E+00	1.98E-02	2.20E+00	0.00E+00
KAMCHATKA4	156.384	48.1819	1995	3.70E-01	2.28E-03	9.78E-01	1.02E+00	2.10E-02	1.99E+00	0.00E+00
			2000	7.47E-02	2.35E-01	2.19E+00	1.66E+00	6.07E-03	2.57E+00	8.24E-01
			2005	4.23E-01	3.72E-02	1.71E+00	1.20E+00	4.39E-03	1.30E+00	5.17E-01
KURILE1	154.018	46.4168	1995	2.82E-01	3.20E-03	1.39E+00	1.07E+00	1.53E-02	2.01E+00	0.00E+00
			2000	9.12E-03	7.53E-01	4.59E+00	2.03E+00	4.83E-03	3.25E+00	1.76E+00
			2005	3.39E-01	5.91E-02	1.68E+00	1.15E+00	4.24E-03	1.73E+00	9.74E-01
KURILE2	151.849	45.0104	1995	2.63E-01	1.23E-02	1.39E+00	1.25E+00	5.04E-03	2.17E+00	9.33E-01
			2000	4.44E-02	8.46E-02	2.59E+00	1.39E+00	2.69E-03	2.01E+00	1.41E+00
			2005	5.03E-01	2.69E-02	1.62E+00	1.06E+00	1.54E-02	3.20E+00	7.90E-01
KURILE3	149.189	43.6163	1995	1.93E-01	1.19E-02	1.64E+00	1.20E+00	3.13E-03	1.88E+00	9.60E-01
			2000	9.68E-02	9.06E-03	1.78E+00	1.12E+00	2.11E-03	1.61E+00	1.00E+00
			2005	1.88E-01	5.92E-03	8.07E-01	1.24E+00	4.97E-03	1.41E+00	0.00E+00
HOKKAIDO	146.641	42.2508	1995	5.98E-02	8.49E-03	2.51E+00	1.17E+00	2.04E-03	1.23E+00	4.72E-01
			2000	5.41E-01	1.34E-02	1.52E+00	1.03E+00	2.48E-03	1.70E+00	1.04E+00
			2005	3.40E-02	1.49E-02	1.95E+00	1.32E+00	5.73E-03	1.82E+00	9.61E-01
JAPAN TRENCH1	143.943	38.5956	1995	1.09E-01	1.44E-02	1.89E+00	1.13E+00	2.54E-03	1.58E+00	8.47E-01
			2000	1.82E-01	2.90E-02	1.53E+00	1.16E+00	8.59E-02	1.53E+01	1.36E+00
			2005	N/A	N/A	N/A	N/A	N/A	N/A	N/A
JAPAN TRENCH2	143.004	36.4893	1995	1.04E-01	8.32E-03	8.44E-01	1.14E+00	2.59E-02	7.18E+00	1.74E+00
			2000	2.16E-01	1.85E-02	1.01E+00	1.18E+00	2.73E-02	2.96E+00	7.54E-01
			2005	2.20E-01	7.92E-03	1.24E+00	1.23E+00	1.05E-02	2.80E+00	9.18E-01
IZU BONIN1	142.196	31.646	1995	6.14E-02	1.08E-02	2.88E+00	1.07E+00	2.07E-03	2.57E+00	1.21E+00
			2000	4.01E-01	4.38E-03	1.86E+00	1.03E+00	3.68E-03	1.75E+00	9.85E-01
			2005	N/A	N/A	N/A	N/A	N/A	N/A	N/A
IZU BONIN2	142.754	29.0456	1995	6.08E-02	8.10E-01	2.12E+00	1.87E+00	4.08E-02	5.45E+00	0.00E+00

			2000	N/A	N/A	N/A	N/A	N/A	N/A	N/A
			2005	N/A	N/A	N/A	N/A	N/A	N/A	N/A
IZU BONIN3	143.145	26.5794	1995	N/A	N/A	N/A	N/A	N/A	N/A	N/A
			2000	5.08E-01	1.18E-01	0.00E+00	1.09E+00	4.75E-03	1.95E+00	2.00E-02
			2005	N/A	N/A	N/A	N/A	N/A	N/A	N/A
IZU BONIN4	145.282	22.7685	1995	N/A	N/A	N/A	N/A	N/A	N/A	N/A
			2000	N/A	N/A	N/A	N/A	N/A	N/A	N/A
			2005	3.45E-01	7.28E-03	1.18E+00	1.14E+00	1.29E-02	2.43E+00	3.06E-01
MARIANA1	146.872	20.7385	1995	N/A	N/A	N/A	N/A	N/A	N/A	N/A
			2000	5.62E-01	1.11E-02	9.08E-02	1.36E+00	8.97E-03	2.68E+00	0.00E+00
			2005	2.38E-01	4.72E-02	4.48E-01	1.54E+00	2.30E-02	3.43E+00	2.51E-01
MARIANA2	147.489	19.0967	1995	3.84E-01	1.98E-01	1.42E-02	1.23E+00	4.54E-02	4.85E+00	0.00E+00
			2000	4.37E-01	1.69E-02	4.70E-01	1.34E+00	9.46E-03	3.64E+00	1.03E+00
			2005	2.32E-01	7.68E-02	3.26E-02	1.47E+00	2.26E-02	3.48E+00	0.00E+00
MARIANA3	147.66	16.4783	1995	N/A	N/A	N/A	N/A	N/A	N/A	N/A
			2000	5.05E-01	2.58E-02	1.01E+00	1.24E+00	5.08E-02	6.74E+00	4.94E-01
			2005	N/A	N/A	N/A	N/A	N/A	N/A	N/A
MARIANA4	146.768	14.0855	1995	N/A	N/A	N/A	N/A	N/A	N/A	N/A
			2000	5.16E-01	3.05E-02	3.48E-01	1.30E+00	3.97E-02	4.33E+00	5.48E-01
			2005	N/A	N/A	N/A	N/A	N/A	N/A	N/A
MARIANA5	145.161	12.4625	1995	1.27E-01	4.67E-02	1.39E+00	1.41E+00	6.43E-03	1.48E+00	0.00E+00
			2000	2.01E-01	1.04E-02	6.73E-01	1.27E+00	3.26E-02	3.62E+00	5.36E-01
			2005	N/A	N/A	N/A	N/A	N/A	N/A	N/A
MARIANA6	141.449	11.1457	1995	N/A	N/A	N/A	N/A	N/A	N/A	N/A
			2000	3.58E-01	3.96E-03	2.62E-01	1.19E+00	2.84E-02	3.89E+00	5.64E-01
			2005	1.77E-01	7.74E-02	2.20E+00	1.33E+00	5.42E-03	2.25E+00	1.03E+00
TONANKAI	136.977	33.3418	1995	N/A	N/A	N/A	N/A	N/A	N/A	N/A
			2000	1.18E-02	1.30E-01	2.59E+00	1.88E+00	7.58E-03	8.86E+00	1.46E+00
			2005	N/A	N/A	N/A	N/A	N/A	N/A	N/A
KYUSHU RYUKYU1	131.546	29.0074	1995	1.70E-01	3.50E-02	1.62E+00	1.22E+00	3.85E-02	8.46E+00	5.77E-01
			2000	3.35E-01	1.33E-02	1.24E+00	1.08E+00	1.46E-02	3.22E+00	0.00E+00
			2005	N/A	N/A	N/A	N/A	N/A	N/A	N/A
KYUSHU RYUKYU2	130.306	27.4196	1995	1.94E-01	3.80E-02	1.65E+00	1.31E+00	1.89E-02	4.94E+00	4.87E-01
			2000	2.03E-01	3.58E-02	1.05E+00	1.32E+00	1.01E-02	3.47E+00	8.12E-01
			2005	N/A	N/A	N/A	N/A	N/A	N/A	N/A
KYUSHU RYUKYU3	128.872	25.8377	1995	2.08E-01	6.98E-03	1.28E+00	1.18E+00	1.39E-02	3.63E+00	9.79E-01
			2000	1.50E-01	3.46E-02	1.28E+00	1.28E+00	1.76E-02	7.04E+00	1.36E+00
			2005	N/A	N/A	N/A	N/A	N/A	N/A	N/A

KYUSHU RYUKYU4	127.197	24.441	1995	N/A	N/A	N/A	N/A	N/A	N/A	N/A
			2000	N/A	N/A	N/A	N/A	N/A	N/A	N/A
			2005	1.96E-01	7.81E-03	1.17E+00	1.22E+00	7.82E-03	3.49E+00	0.00E+00
LUZON	119.898	19.2044	1995	N/A	N/A	N/A	N/A	N/A	N/A	N/A
			2000	N/A	N/A	N/A	N/A	N/A	N/A	N/A
			2005	2.04E-01	7.95E-02	1.10E+00	1.35E+00	2.27E-03	1.39E+00	6.39E-02
PHILIPPINES1	125.798	12.5265	1995	3.88E-01	2.33E-02	1.50E+00	1.21E+00	1.56E-02	3.07E+00	6.15E-01
			2000	1.20E-01	1.04E-02	1.79E+00	1.11E+00	1.31E-01	8.13E+00	1.03E-01
			2005	1.30E-01	3.12E-02	2.03E+00	1.33E+00	1.67E-02	4.84E+00	1.90E+00
PHILIPPINES2	126.609	10.2269	1995	4.58E-01	2.48E-02	1.34E+00	1.27E+00	1.13E-02	2.56E+00	6.37E-01
			2000	1.42E-01	3.85E-02	1.65E+00	1.17E+00	2.47E-02	2.96E+00	2.80E-02
			2005	1.53E-01	2.31E-02	2.16E+00	1.37E+00	3.56E-03	1.46E+00	8.25E-01
PHILIPPINES3	127.139	7.71769	1995	3.95E-01	2.52E-02	1.13E+00	1.33E+00	1.16E-02	2.44E+00	3.02E-01
			2000	8.62E-02	1.76E-01	1.66E+00	1.40E+00	6.38E-02	7.87E+00	8.09E-01
			2005	1.21E-01	2.68E-02	1.73E+00	1.36E+00	5.61E-03	1.49E+00	0.00E+00
PHILIPPINES4	127.746	5.69643	1995	1.26E-01	1.08E-02	1.90E+00	1.06E+00	8.39E-02	4.54E+00	0.00E+00
			2000	N/A	N/A	N/A	N/A	N/A	N/A	N/A
			2005	N/A	N/A	N/A	N/A	N/A	N/A	N/A
PHILIPPINES5	128.579	3.58538	1995	1.45E-01	3.48E-02	1.51E+00	1.11E+00	8.55E-03	1.54E+00	3.20E-02
			2000	9.23E-02	6.58E-02	2.02E+00	1.32E+00	2.55E-02	2.84E+00	5.46E-01
			2005	N/A	N/A	N/A	N/A	N/A	N/A	N/A
PAPUA1	134.558	-0.0120035	1995	6.83E-01	2.35E-02	1.00E+00	1.27E+00	4.32E-02	2.33E+00	0.00E+00
			2000	1.18E-01	2.44E-02	2.04E+00	1.29E+00	2.26E-03	1.68E+00	1.14E+00
			2005	N/A	N/A	N/A	N/A	N/A	N/A	N/A
PAPUA2	136.824	-0.367443	1995	3.97E-01	5.15E-02	1.33E+00	1.33E+00	3.29E-02	2.45E+00	4.76E-01
			2000	1.65E-01	5.89E-02	1.15E+00	1.61E+00	2.87E-03	1.21E+00	0.00E+00
			2005	N/A	N/A	N/A	N/A	N/A	N/A	N/A
NEW GUINEA1	140.647	-1.92197	1995	1.29E-02	1.39E+00	2.84E+00	7.20E+00	1.01E-03	1.64E+00	5.36E-01
			2000	N/A	N/A	N/A	N/A	N/A	N/A	N/A
			2005	1.63E-01	2.72E-02	2.11E+00	1.30E+00	1.84E-02	5.35E+00	9.77E-01
NEW GUINEA2	142.955	-3.01809	1995	4.42E-01	5.22E-02	9.94E-01	1.31E+00	8.68E-02	7.16E+00	7.34E-01
			2000	4.51E-01	3.44E-02	9.88E-01	1.40E+00	1.17E-01	1.02E+01	7.81E-01
			2005	N/A	N/A	N/A	N/A	N/A	N/A	N/A
TONGA1	187.36	-16.46	1995	2.92E-02	6.50E-02	1.85E+00	1.29E+00	3.07E-02	3.15E+00	2.34E-01
			2000	1.63E-01	2.02E-02	1.14E+00	1.16E+00	1.23E-02	2.08E+00	7.36E-01
			2005	4.00E-01	1.80E-02	1.17E+00	1.21E+00	3.24E-02	1.68E+00	1.22E-01
TONGA2	187.043	-19.2016	1995	6.72E-02	1.48E+00	1.54E+00	1.82E+00	4.21E-03	1.64E+00	1.07E+00
			2000	N/A	N/A	N/A	N/A	N/A	N/A	N/A

			2005	1.50E-01	1.52E-01	1.84E+00	1.26E+00	2.84E-02	2.91E+00	7.09E-01
TONGA3	186.134	-21.5319	1995	2.14E-01	6.50E-01	5.94E-01	1.52E+00	2.58E-02	1.97E+00	1.50E-01
			2000	5.16E-01	9.74E-03	1.64E+00	1.03E+00	2.39E-01	9.84E+00	5.55E-02
			2005	2.07E-01	9.59E-02	1.73E+00	1.23E+00	3.66E-02	2.97E+00	6.57E-01
TONGA4	184.622	-25.8547	1995	1.37E-01	7.50E-01	1.31E+00	2.31E+00	8.15E-02	4.17E+00	0.00E+00
			2000	N/A	N/A	N/A	N/A	N/A	N/A	N/A
			2005	3.07E-01	6.88E-02	1.06E+00	1.42E+00	2.28E-02	1.88E+00	0.00E+00
KERMADEC1	184.062	-28.3997	1995	1.53E-01	1.25E-01	1.17E+00	1.37E+00	3.82E-01	1.03E+01	3.73E-02
			2000	9.81E-02	1.29E-01	2.12E+00	1.47E+00	5.08E-02	2.79E+00	4.62E-02
			2005	4.00E-01	3.40E-02	1.09E+00	1.25E+00	3.63E-02	2.28E+00	3.50E-01
KERMADEC2	183.241	-30.578	1995	1.63E-01	6.01E-02	1.26E+00	1.20E+00	2.32E-01	4.08E+00	0.00E+00
			2000	2.43E-01	3.21E-02	1.81E+00	1.14E+00	2.87E-02	1.90E+00	2.30E-01
			2005	2.78E-01	1.91E-02	1.43E+00	1.16E+00	1.81E-01	5.43E+00	8.01E-01
KERMADEC3	182.299	-32.7588	1995	1.98E-01	9.94E-02	1.61E+00	1.28E+00	2.29E-01	4.61E+00	6.89E-01
			2000	4.57E-01	1.22E-02	1.69E+00	1.08E+00	1.31E-02	1.60E+00	7.95E-01
			2005	2.21E-01	1.03E-02	1.30E+00	1.15E+00	1.05E-01	4.06E+00	1.14E+00
KERMADEC4	181.475	-34.571	1995	2.40E-01	4.91E-02	1.85E+00	1.26E+00	2.51E-02	1.54E+00	1.06E+00
			2000	4.62E-01	1.62E-02	9.47E-01	1.15E+00	2.17E-02	1.94E+00	6.65E-01
			2005	2.54E-01	1.53E-02	1.36E+00	1.20E+00	1.09E-01	3.77E+00	5.26E-01
KERMADEC5	180.287	-36.8165	1995	N/A	N/A	N/A	N/A	N/A	N/A	N/A
			2000	6.06E-01	3.54E-02	5.75E-01	1.26E+00	1.17E-02	1.49E+00	1.32E+00
			2005	3.88E-01	4.01E+00	9.50E-01	3.45E+00	4.63E-03	1.11E+00	0.00E+00
HIKURANGI	179.189	-39.0132	1995	8.42E-02	4.05E+00	1.99E+00	3.22E+00	4.06E-02	1.98E+00	0.00E+00
			2000	5.70E-01	2.81E-02	1.95E-01	1.20E+00	1.69E-02	1.71E+00	0.00E+00
			2005	N/A	N/A	N/A	N/A	N/A	N/A	N/A
NEW ZEALAND1	164.231	-48.3333	1995	N/A	N/A	N/A	N/A	N/A	N/A	N/A
			2000	N/A	N/A	N/A	N/A	N/A	N/A	N/A
			2005	5.23E-01	4.59E-02	1.21E+00	1.19E+00	6.35E-03	1.55E+00	6.40E-01
NEW ZEALAND2	165.125	-46.9573	1995	N/A	N/A	N/A	N/A	N/A	N/A	N/A
			2000	5.55E-01	3.74E-02	1.30E+00	1.18E+00	2.29E-02	5.97E+00	1.23E+00
			2005	3.40E-01	5.79E-02	1.58E+00	1.20E+00	8.56E-03	3.14E+00	1.10E+00
NEW ZEALAND3	166.68	-45.3155	1995	N/A	N/A	N/A	N/A	N/A	N/A	N/A
			2000	N/A	N/A	N/A	N/A	N/A	N/A	N/A
			2005	3.43E-01	4.56E-02	1.57E+00	1.20E+00	4.22E-03	2.57E+00	1.21E+00
VANUATU1	170.352	-22.3907	1995	1.56E-01	1.16E-02	9.76E-01	1.16E+00	1.36E-01	4.23E+00	0.00E+00
			2000	1.45E-01	3.02E-02	1.95E+00	1.25E+00	1.50E-02	1.98E+00	5.20E-01
			2005	2.10E-01	2.09E-02	1.41E+00	1.37E+00	3.13E-02	2.89E+00	2.44E-01
VANUATU2	168.704	-20.7816	1995	1.32E-01	1.87E-02	9.45E-01	1.17E+00	3.37E-02	2.23E+00	1.23E-02

			2000	1.19E-01	2.39E-02	2.01E+00	1.20E+00	1.06E-02	1.91E+00	5.92E-01
			2005	1.90E-01	2.11E-02	1.52E+00	1.35E+00	1.65E-02	2.08E+00	3.11E-01
VANUATU3	167.441	-18.3293	1995	6.11E-02	1.52E-01	1.41E+00	1.71E+00	5.73E-03	2.11E+00	8.03E-01
			2000	1.27E-01	5.08E-03	1.70E+00	1.18E+00	5.61E-02	6.30E+00	5.07E-01
			2005	1.63E-01	1.16E-02	1.65E+00	1.23E+00	2.46E-02	2.40E+00	2.77E-01
VANUATU4	166.647	-16.1856	1995	7.41E-02	6.73E-02	1.42E+00	1.59E+00	6.49E-03	2.03E+00	7.67E-01
			2000	1.25E-01	6.29E-03	1.59E+00	1.22E+00	2.46E-02	2.67E+00	1.62E-01
			2005	1.60E-01	4.62E-03	1.33E+00	1.14E+00	9.29E-02	5.13E+00	5.47E-02
VANUATU5	164.847	-11.854	1995	3.99E-01	2.21E-02	8.66E-01	1.21E+00	1.55E-02	2.37E+00	7.68E-01
			2000	1.43E-01	3.96E-02	1.39E+00	1.18E+00	8.21E-03	1.54E+00	0.00E+00
			2005	1.96E-01	2.31E-02	1.64E+00	1.20E+00	1.27E-02	2.41E+00	9.49E-01
VANUATU6	162.701	-11.2078	1995	3.45E-01	9.21E-02	5.78E-01	1.57E+00	1.26E-01	1.88E+01	1.08E+00
			2000	4.09E-01	2.57E-02	8.87E-01	1.22E+00	7.53E-01	2.69E+01	0.00E+00
			2005	1.68E-01	4.45E-02	1.53E+00	1.43E+00	6.28E-02	3.18E+00	0.00E+00
SOLOMON1	160.425	-10.545	1995	N/A	N/A	N/A	N/A	N/A	N/A	N/A
			2000	3.26E-01	8.39E-03	1.20E+00	1.10E+00	3.74E-02	2.46E+00	1.65E-02
			2005	N/A	N/A	N/A	N/A	N/A	N/A	N/A
SOLOMON2	158.675	-9.57663	1995	N/A	N/A	N/A	N/A	N/A	N/A	N/A
			2000	1.19E-01	2.02E-02	1.32E+00	1.32E+00	5.98E-03	1.74E+00	3.27E-01
			2005	1.89E-01	3.17E-02	1.44E+00	1.25E+00	1.43E-02	3.76E+00	1.00E+00
SOLOMON3	155.902	-7.81313	1995	N/A	N/A	N/A	N/A	N/A	N/A	N/A
			2000	1.94E-01	9.76E-02	1.64E+00	1.55E+00	3.22E-02	3.28E+00	4.20E-01
			2005	1.25E-01	1.09E-01	2.68E+00	1.42E+00	1.03E-02	1.96E+00	1.09E+00
NEW BRITAIN1	154.405	-6.72063	1995	1.26E-01	8.49E-01	1.58E+00	1.92E+00	1.33E-03	1.47E+00	1.09E+00
			2000	N/A	N/A	N/A	N/A	N/A	N/A	N/A
			2005	7.32E-01	1.32E-02	4.76E-01	1.11E+00	5.88E-03	1.50E+00	0.00E+00
NEW BRITAIN2	151.429	-6.37437	1995	3.08E-01	3.93E-02	1.09E+00	1.19E+00	1.00E-02	1.76E+00	7.52E-01
			2000	2.42E-01	5.84E-02	1.45E+00	1.31E+00	2.23E-02	2.21E+00	4.09E-01
			2005	1.86E-01	4.50E-02	1.48E+00	1.28E+00	6.77E-03	1.80E+00	6.80E-01
SERAM	130.87	-3.08191	1995	9.98E-02	1.71E-02	2.03E+00	1.17E+00	1.48E-02	1.40E+00	0.00E+00
			2000	N/A	N/A	N/A	N/A	N/A	N/A	N/A
			2005	4.79E-02	1.54E-01	3.04E+00	1.33E+00	4.14E-01	3.64E+01	9.52E-01
CELEBES	120.954	1.74771	1995	2.81E-01	2.23E-01	1.23E+00	1.25E+00	1.34E-03	1.34E+00	5.50E-01
			2000	N/A	N/A	N/A	N/A	N/A	N/A	N/A
			2005	N/A	N/A	N/A	N/A	N/A	N/A	N/A
MALUKU	126.353	1.31086	1995	7.52E-02	1.19E-02	1.95E+00	1.13E+00	1.27E-02	3.41E+00	1.84E+00
			2000	1.19E-01	9.56E-03	1.67E+00	1.21E+00	9.59E-02	8.59E+00	2.26E-01
			2005	1.09E-01	5.71E-02	2.33E+00	1.12E+00	4.22E-03	1.70E+00	5.70E-01

JAVA1	116.882	-11.2945	1995	N/A	N/A	N/A	N/A	N/A	N/A	N/A
			2000	N/A	N/A	N/A	N/A	N/A	N/A	N/A
			2005	2.72E-01	9.20E-03	7.32E-01	1.27E+00	9.54E-04	1.68E+00	3.01E+00
JAVA2	114.693	-11.0819	1995	1.70E-01	2.91E-01	2.17E+00	1.55E+00	5.60E-04	1.33E+00	2.19E+00
			2000	N/A	N/A	N/A	N/A	N/A	N/A	N/A
			2005	1.78E-01	1.39E-02	1.09E+00	1.30E+00	8.48E-04	2.98E+00	5.17E+00
JAVA3	110.567	-10.4731	1995	N/A	N/A	N/A	N/A	N/A	N/A	N/A
			2000	N/A	N/A	N/A	N/A	N/A	N/A	N/A
			2005	7.32E-01	2.38E-02	8.43E-01	1.17E+00	2.91E-03	1.54E+00	1.02E+00
JAVA4	108.469	-10.0859	1995	N/A	N/A	N/A	N/A	N/A	N/A	N/A
			2000	N/A	N/A	N/A	N/A	N/A	N/A	N/A
			2005	4.15E-01	7.14E-02	1.49E+00	1.36E+00	4.59E-03	1.72E+00	1.06E+00
JAVA5	106.447	-9.3398	1995	N/A	N/A	N/A	N/A	N/A	N/A	N/A
			2000	N/A	N/A	N/A	N/A	N/A	N/A	N/A
			2005	2.08E-01	7.41E-02	2.77E+00	1.34E+00	3.52E-03	3.07E+00	3.65E+00
JAVA6	104.937	-8.53664	1995	N/A	N/A	N/A	N/A	N/A	N/A	N/A
			2000	3.83E-01	1.60E-02	6.29E-01	1.20E+00	1.86E-03	1.43E+00	9.52E-01
			2005	N/A	N/A	N/A	N/A	N/A	N/A	N/A
SUMATRA1	102.863	-7.23155	1995	N/A	N/A	N/A	N/A	N/A	N/A	N/A
			2000	2.52E-01	7.37E-02	1.77E+00	1.25E+00	7.71E-03	2.28E+00	1.03E+00
			2005	N/A	N/A	N/A	N/A	N/A	N/A	N/A
SUMATRA2	101.424	-5.92375	1995	N/A	N/A	N/A	N/A	N/A	N/A	N/A
			2000	2.81E-01	8.13E-02	1.64E+00	1.28E+00	1.45E-02	2.76E+00	7.38E-01
			2005	4.44E+00	8.72E-03	1.07E+00	1.01E+00	7.64E-03	1.53E+00	4.08E-01
SUMATRA3	99.8371	-3.97694	1995	N/A	N/A	N/A	N/A	N/A	N/A	N/A
			2000	N/A	N/A	N/A	N/A	N/A	N/A	N/A
			2005	8.16E-01	1.39E-02	9.79E-01	1.11E+00	4.53E-03	1.71E+00	5.99E-01
SUMATRA4	98.6722	-2.41254	1995	N/A	N/A	N/A	N/A	N/A	N/A	N/A
			2000	N/A	N/A	N/A	N/A	N/A	N/A	N/A
			2005	8.53E-01	1.82E-02	8.43E-01	1.17E+00	6.35E-03	1.69E+00	0.00E+00
SUMATRA5	93.2361	4.41069	1995	N/A	N/A	N/A	N/A	N/A	N/A	N/A
			2000	1.74E-01	2.13E-01	3.26E+00	1.79E+00	1.14E-03	1.37E+00	4.39E+00
			2005	6.71E-01	1.49E+00	6.12E-01	1.46E+00	8.02E-03	1.29E+00	0.00E+00
ANDAMAN1	91.7187	9.11452	1995	N/A	N/A	N/A	N/A	N/A	N/A	N/A
			2000	2.85E+00	4.56E-02	2.14E+00	1.27E+00	1.51E-03	1.02E+00	1.93E+00
			2005	5.17E-01	2.68E-02	1.30E+00	1.16E+00	5.98E-03	1.48E+00	6.18E-01
ANDAMAN2	91.6839	11.2831	1995	N/A	N/A	N/A	N/A	N/A	N/A	N/A
			2000	N/A	N/A	N/A	N/A	N/A	N/A	N/A

			2005	1.36E+00	1.74E-02	1.27E+00	1.06E+00	2.45E-03	1.16E+00	0.00E+00
SOUTH SANDWICH1	333.161	-55.5818	1995	5.17E-02	1.18E-02	1.86E+00	1.30E+00	1.02E-03	1.72E+00	1.89E+00
			2000	1.50E-01	1.05E-01	2.37E+00	1.23E+00	2.33E-03	1.15E+00	6.33E-01
			2005	1.26E-01	6.60E-01	7.30E-01	1.78E+00	7.98E-03	2.31E+00	6.84E-01
SOUTH SANDWICH2	334.984	-56.804	1995	3.36E-02	1.07E-02	2.07E+00	1.23E+00	1.05E-03	2.04E+00	2.19E+00
			2000	N/A	N/A	N/A	N/A	N/A	N/A	N/A
			2005	1.81E-01	1.46E-02	1.08E+00	1.08E+00	1.17E-01	1.06E+01	0.00E+00
SOUTH SANDWICH3	335.442	-58.5248	1995	N/A	N/A	N/A	N/A	N/A	N/A	N/A
			2000	N/A	N/A	N/A	N/A	N/A	N/A	N/A
			2005	7.10E-02	1.47E-02	1.84E+00	1.34E+00	7.57E-02	7.57E+00	0.00E+00

A1.2. Examples of detection failures due to the requirement of Pb ≥ 0.5.

In the southern Japan Trench (Ibaraki-Boso-Oki), we reversed the requirement (Pb < 0.5) to look at aftershock sequences and detected seismic sequences with anomalously high seismicity rates during 1995–2009. Two of the three detected seismic sequences were aftershock sequences of *M* 7 class events (see Figure A1.1). On the other hand, one of the sequences seemed not to be related with any large event or any detected swarm. It occurred in the foreshock region of the 2011 M9 Tohoku-Oki earthquake. We could not detect this sequence as a swarm sequence because this sequence had a foreshock sequence following the ETAS model.

We also repeated the same analysis in the Kurile Trench. We detected six seismic sequences (see Figure A1.2). Two of the six sequences are aftershock sequences of large events (a M8.3 event in 2006 and a M6.9 event in 2009). Other three sequences are succeeding parts of the 1995 Itrup swarm (Figure 2.6a), a swarm offshore of Simushir Island in 1997, and a swarm offshore of Simushir Island in 2006 (Figure 2.6c), whose beginning parts were detected in our analysis (see Figure 2.5a, 2.6a, and 2.6c). In

contrast, the remaining one sequence offshore of Itrup Island seemed not to be related with any large event or any detected swarm sequence. We could not detect this sequence as a swarm sequence because this sequence had a foreshock sequence following the ETAS model.

These results show that the requirement (Pb $\geq$ 0.5) prevents us from detecting aftershock sequences with anomalously high seismicity rates, but there are also missed earthquake swarms due to this requirement. We may underestimate the number of events in each swarm sequence because we sometimes miss a succeeding part of each swarm sequence as in the first scenario in Section 2.5.3. However, the number of swarm sequences is not strongly affected by the requirement of Pb $\geq$ 0.5 because detection failures as in the second scenario in Section 2.5.3 are relatively rare. In both the southern Japan Trench and the Kurile Trench, we miss only one sequence while we wholly or partially detected nine and ten swarm sequences there (Section 2.4.1.1 and Section 2.4.1.2). Therefore, the number of missed swarm sequences is small compared with the number of detected swarm sequences.

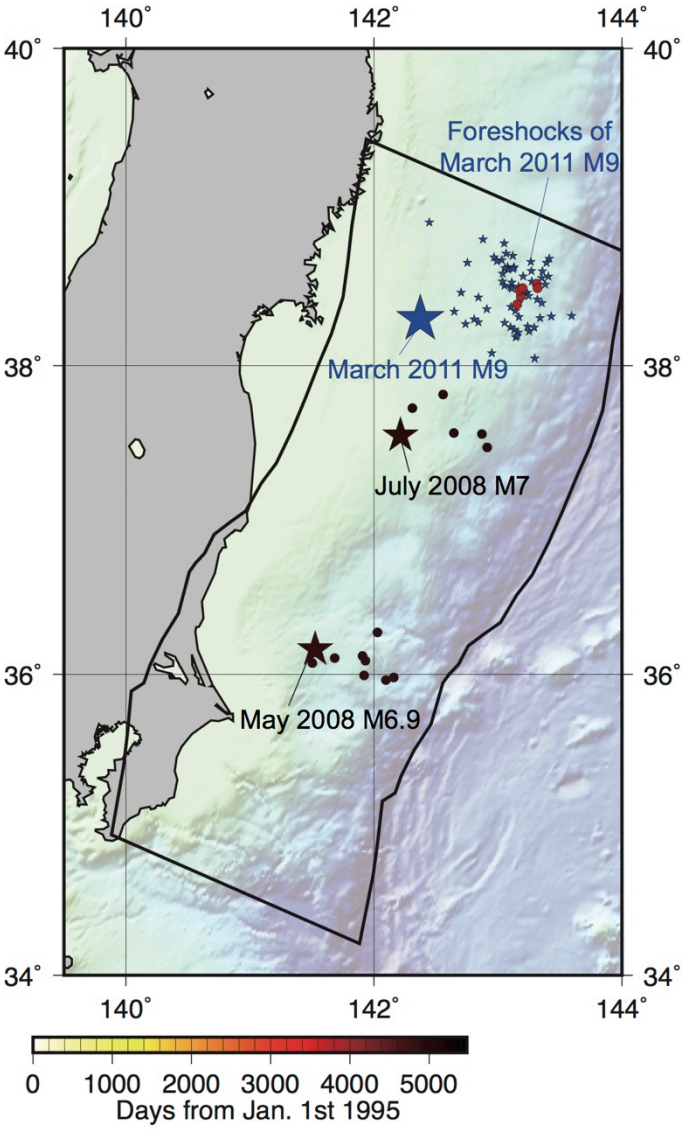

Figure A1.1 | Hypocenters of potential earthquake swarms whose Pb of the first event is less than 0.5 in the southern Japan Trench. Small circles are the potential earthquake swarms. They are colored according to their occurrence time. Large stars are hypocenters of large earthquakes. Small stars are foreshocks of the 2011 M9 Tohoku-Oki earthquake.

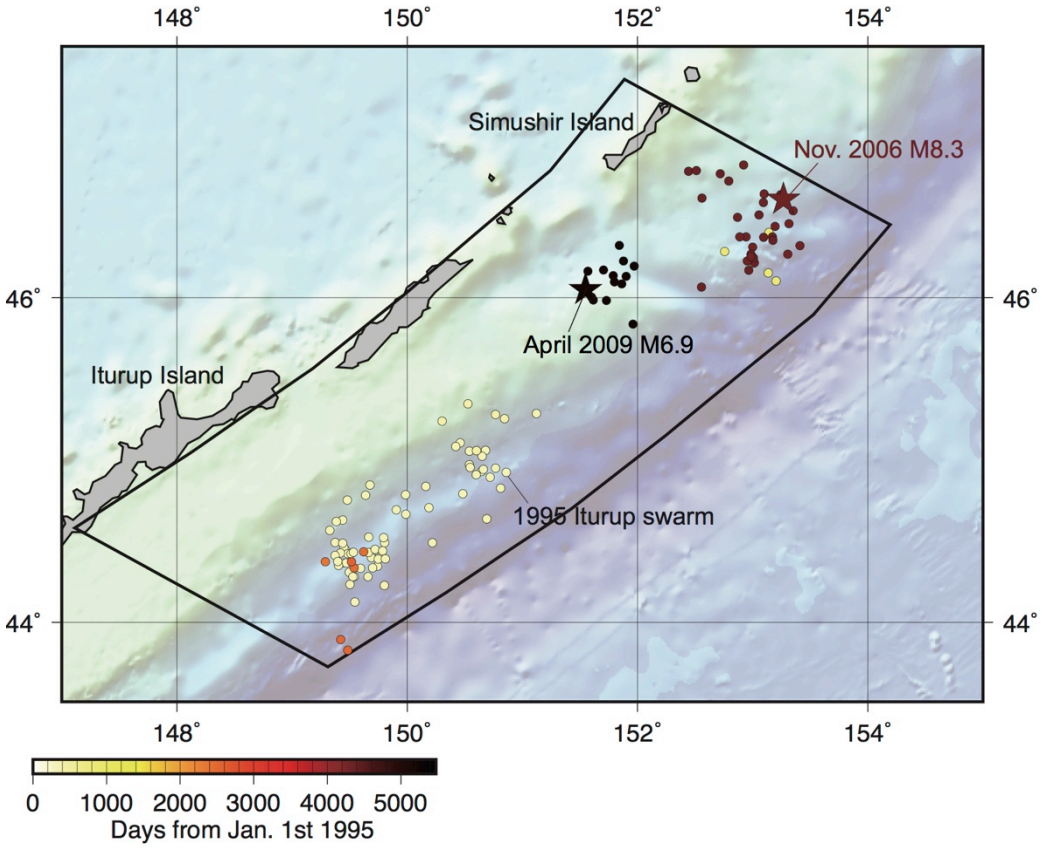

Figure A1.2 | Hypocenters of potential earthquake swarms whose Pb of the first event is less than 0.5 in the Kurile region. Small circles are hypocenters of the potential earthquake swarms. They are colored according to their occurrence time. Large stars are hypocenters of large earthquakes.

A 1.2. Calculation of curvature of the incoming plate before subduction

For each trench section, we made several bathymetric cross-sections extending 100-km-seaward from the trench (see Figure A1.3). We fitted cubic functions to these cross-sections (see Figure A1.3b) and calculated the curvature of each profile. The curvature of the incoming plate was then defined as the median curvature taken over all the cross-sections. Cross-sections located close to seamounts and ridges were excluded because we could not reliably calculate the plate curvature in these cases. Calculated

plate curvatures are shown in Figure A1.4.

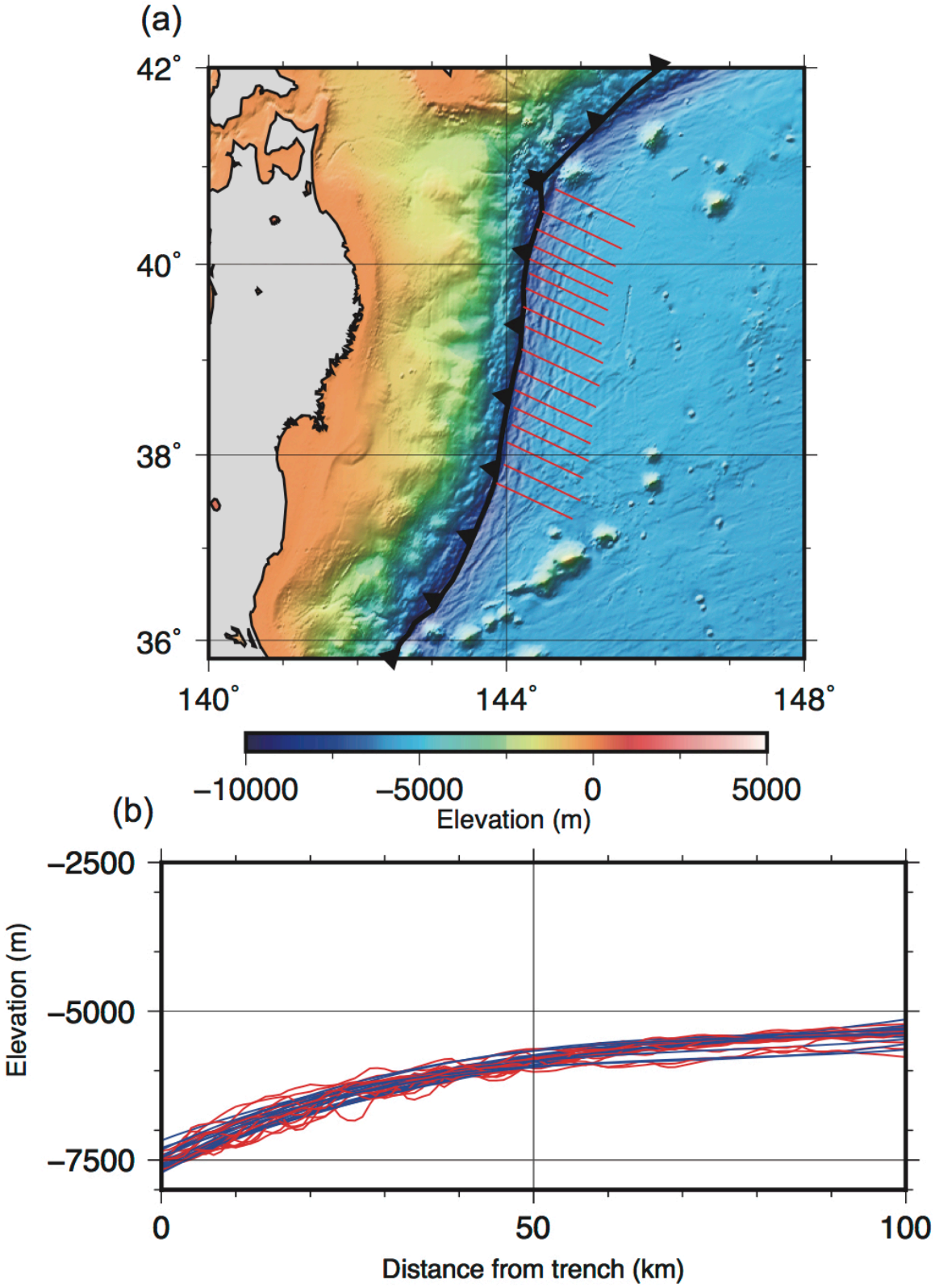

Figure A1.3 | Calculation of curvature of the incoming plate before subduction. (a)

Bathymetry of Tohoku-Oki, Japan; locations of the cross-sections shown in (b) are indicated by red lines. (b) Bathymetric cross-sections of the Japan Trench (red lines) and cubic functions fitted to the bathymetry (blue lines).

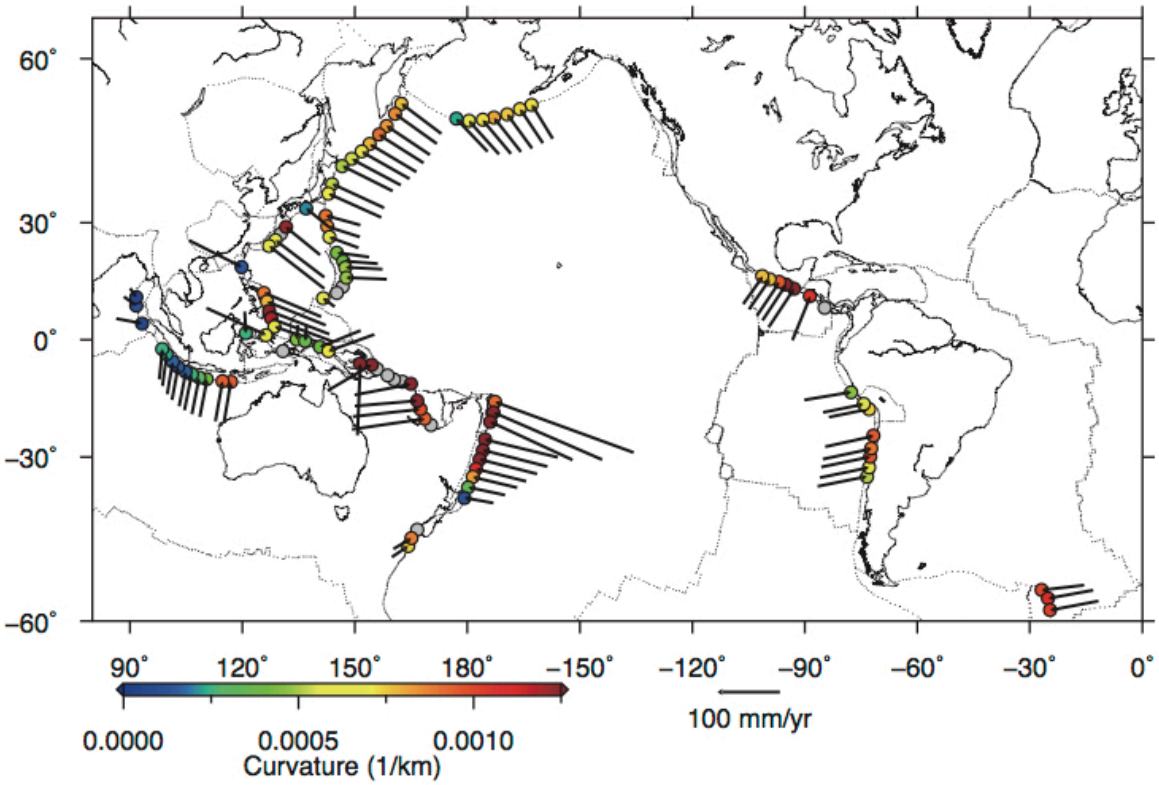

Figure A1.4 | Calculated curvature of the incoming plate before subduction for the 100 regions used in this study. The color of each circle indicates the curvature of the incoming plate before subduction. The orientation and length of each arrow indicate the plate velocity. We were unable to calculate plate curvature for 11 regions due to the presence of seamounts and ridges; these regions are shown as grey circles.

A2. Appendices for Chapter 3

A2.1. Influences of the parameter γ on detection of earthquake swarms

For the period 1991–1993, for which the parameter γ was estimated to be zero, we repeated our swarm detection using a typical value of $\gamma\,(=\,1.0)$ instead. We detected 12 swarm sequences using $\gamma\,=\,1.0$ (Figure A2.1). 11 of the 12 swarm sequences are the same as swarm sequences detected using $\gamma\,=\,0$. This suggests that the parameter γ does not strongly affect our swarm detection.

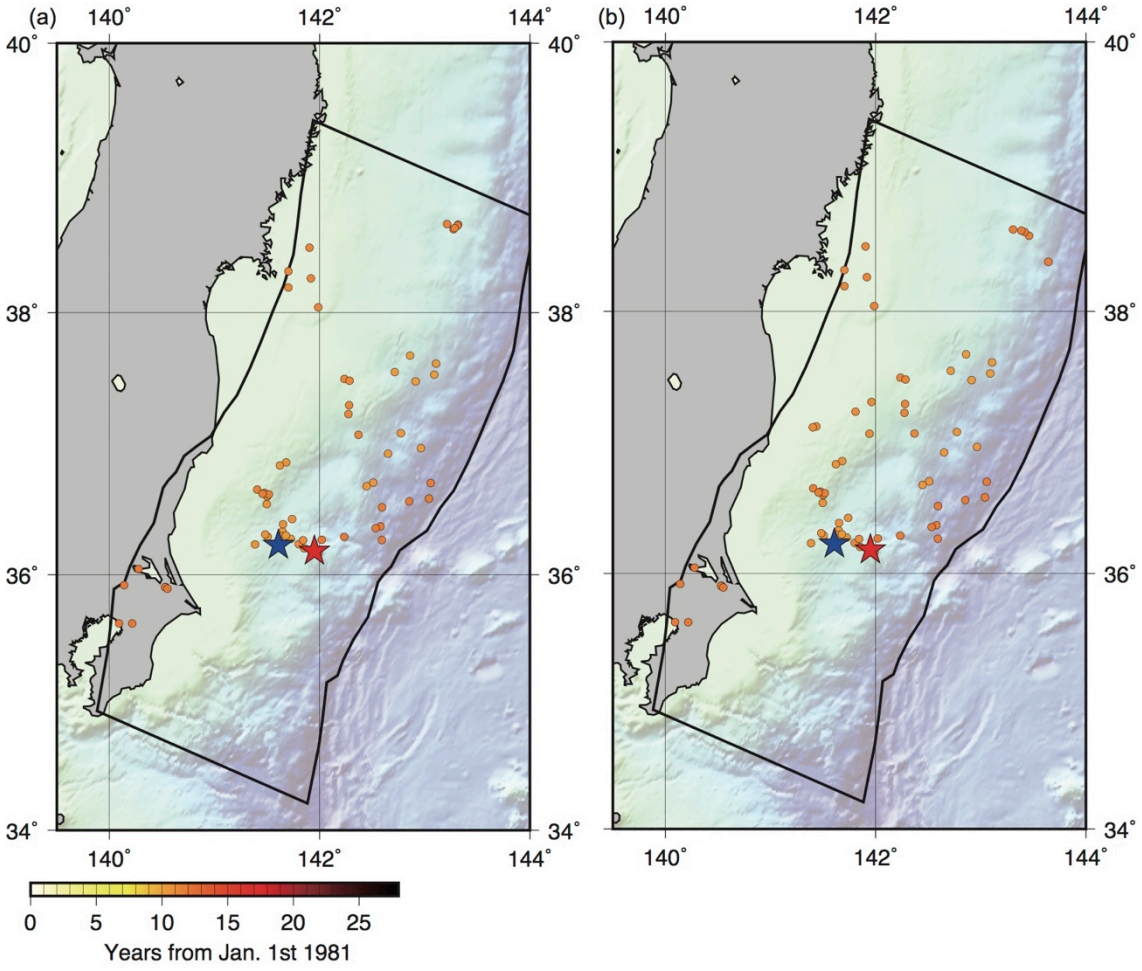

Figure A2.1 | Hypocenters of detected swarms during the period 1991–1993. (a) Swarms detected using $\gamma\,=\,0$. (b) Swarms detected using $\gamma\,=\,1.0$. Small circles indicate the hypocenters of the detected swarms. Red and blue stars indicate the

hypocenters of the 1982 and 2008 M 7 Ibaraki-Oki earthquakes respectively.

A2.2. Swarm sequence in March 2008

The swarm sequence in March 2008 started on March 15th and continued for 8 days (Figure A2.2). The matched filter technique detected 91 events, which is 1.7 times of the JMA catalog (55 events). Repeating earthquakes were found in this swarm sequence. The comparison of the number of observed events ($\geq M$ 3) in the Ibaraki-Oki detection circle (8 events) with the number of events predicted by the ETAS model (1.6 event) shows an anomaly larger than 5σ (Figure A2.2c), i.e. the probability that we observe such a high seismicity rate is less than 2.7×10^{-4}.

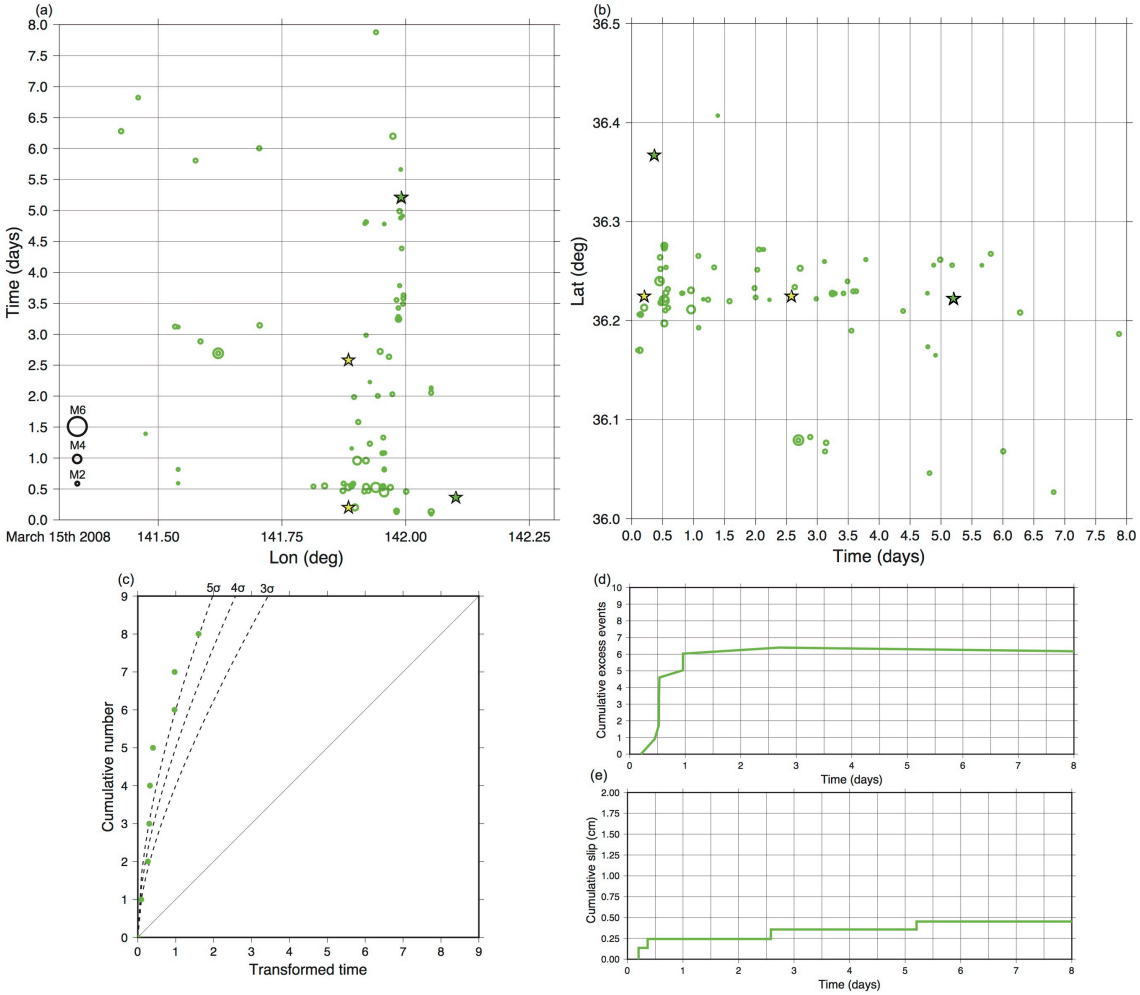

Figure A2.2 | Space-time distribution, excess events, fault slip of the swarm sequence in March 2008. (a) and (b) show time-longitude and latitude-time distributions of the swarm sequence in March 2008. Green circles are swarms. Small stars are repeating earthquakes, colored according to the same manner as Figure 3.7a. (c) Transformed time of this swarm sequence. The transformed time was calculated since the first *M* 3 or larger swarm event. (d) and (e) show temporal changes in the number of excess events and estimated fault slip of repeating earthquakes.

A2.3. Swarm sequence in November 2004

The swarm sequence in November 2004 started on November 14th and continued for 3

days (Figure A2.3). The matched filter technique detected 37 events, which is 1.9 times of the JMA catalog (20 events). Repeating earthquakes were found in this swarm sequence. The comparison of the number of observed events ($\geq M$ 3) in the Ibaraki-Oki detection circle (6 events) with the number of events predicted by the ETAS model (1.3 event) shows an anomaly larger than 4σ (Figure A2.3c), i.e. the probability that we observe such a high seismicity rate is less than 2.2×10^{-3}.

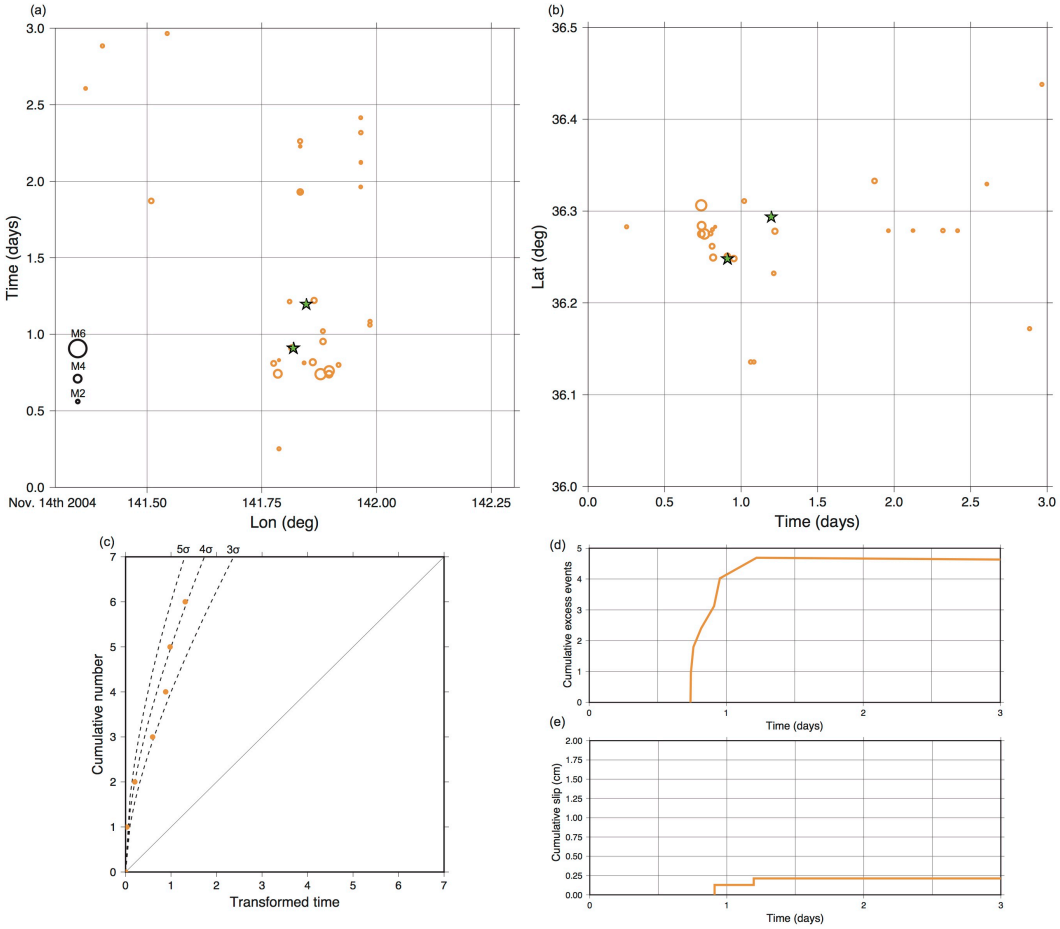

Figure A2.3 | Space-time distribution, excess events, fault slip of the swarm sequence in November 2004. (a) and (b) show time-longitude and latitude-time distributions of the swarm sequence in November 2004. Orange circles are swarms. Small stars are repeating earthquakes, colored according to the same manner as Figure

3.7a. (c) Transformed time of this swarm sequence. The transformed time was calculated since the first *M* 3 or larger swarm event. (d) and (e) show temporal changes in the number of excess events and estimated fault slip of repeating earthquakes.

A2.4. Swarm sequence in May 1996

The swarm sequence in May 1996 started on May 9th and continued for 7 days (Figure A2.4). Repeating earthquakes were found in this swarm sequence. Hypocenters of this swarm sequence migrated in the southeast direction from May 9th to May 12^{h}. Its migration speed is about 10 km/day. The comparison of the number of observed events ($\geq$ *M* 3) (19 events) in the Ibaraki-Oki detection circle with the number of events predicted by the ETAS model (3.0 event) shows an anomaly larger than 9σ (Figure A2.4b), i.e. the probability that we observe such a high seismicity rate is less than 5.6 $\times$ 10^{-10}.

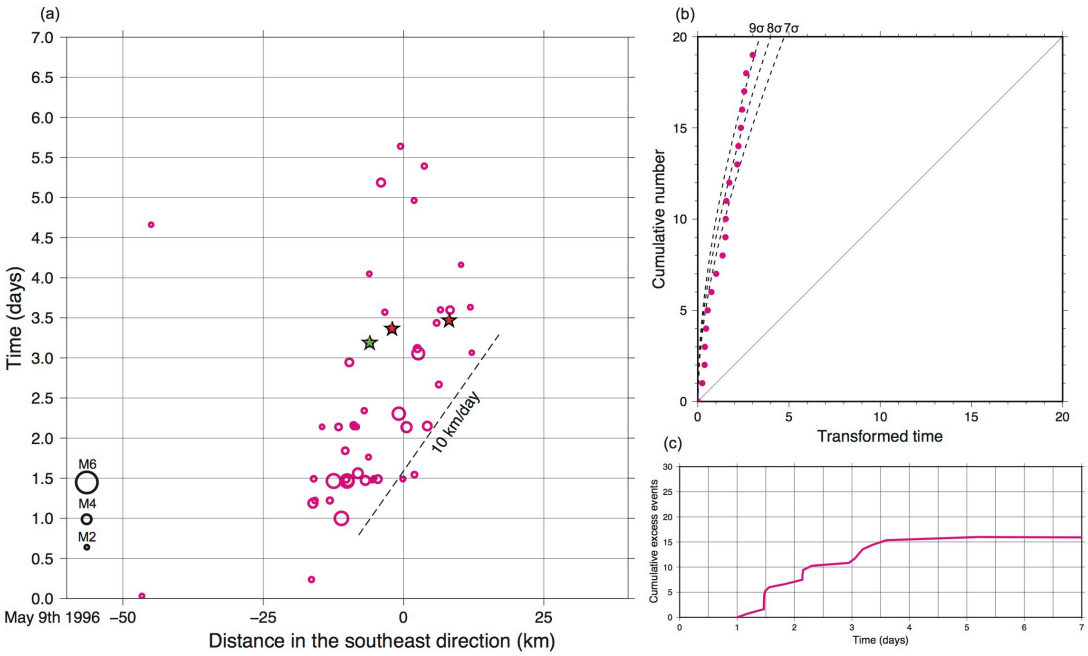

Figure A2.4 | Space-time distribution and excess events of the swarm sequence in

1996. (a) Space-time distribution of the swarm sequence in 1996 (JMA catalog). The horizontal axis is distance in the southeast direction from (36.2ºN, 141.9ºE). Magenta circles are swarms. Small stars are repeating earthquakes, colored according to the same manner as Figure 3.7a. (b) Transformed time of this swarm sequence. The transformed time was calculated since the first M 3 or larger swarm event. (c) Temporal changes in the number of excess events.

A2.5. Foreshock sequence in July 1982

The foreshock sequence of the 1982 Ibaraki-Oki earthquake, which occurred on July 23rd, 1982, started around the hypocenter of the mainshock on July 21st (Figure A2.5). The comparison of the number of observed events ($\geq$ M 3) (32 events) in the Ibaraki-Oki detection circle with the number of events predicted by the ETAS model (7.1 event) shows an anomaly larger than 9σ (Figure A2.5c), i.e. the probability that we observe such a high seismicity rate is less than 6.9×10^{-12}.

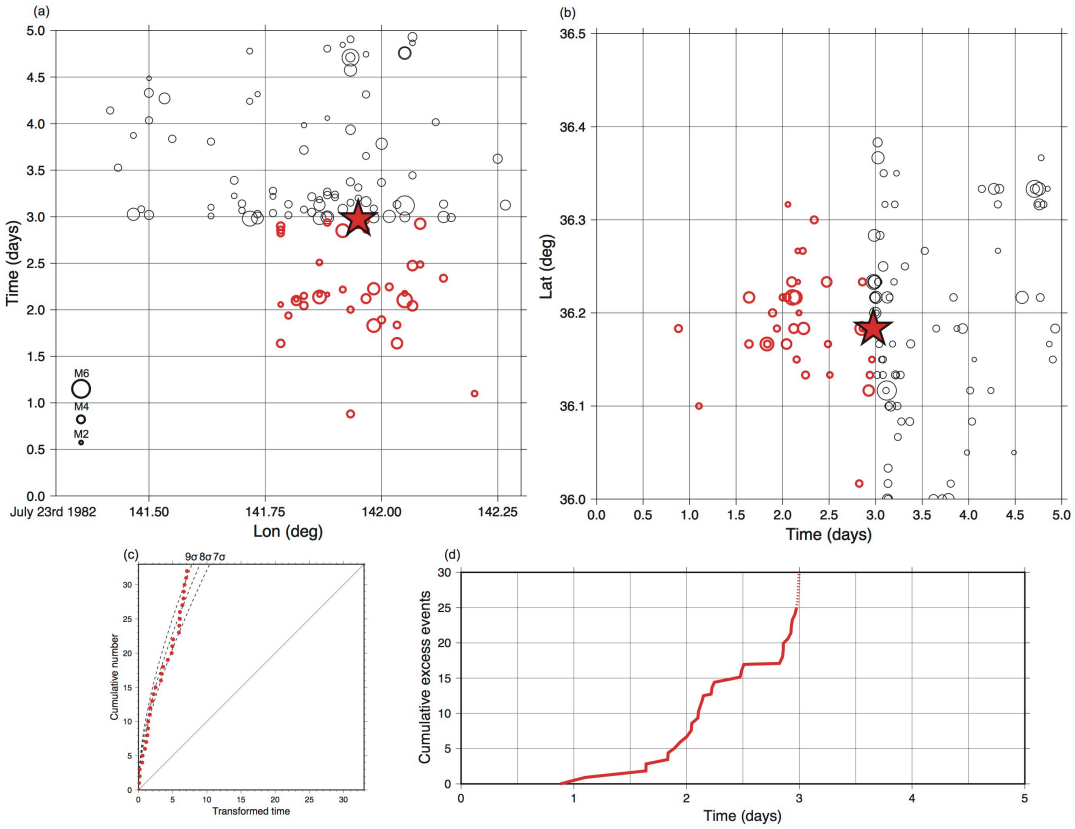

Figure A2.5 | Space-time distribution and excess events of the foreshock sequence in 1982. (a) and (b) show time-longitude and latitude-time distributions of the foreshock sequence in 1982 (JMA catalog). Red circles are swarms. Black circles are aftershocks. The large star indicates the 1982 Ibaraki-Oki earthquake. (c) Transformed time of the foreshock sequence in 1982. The transformed time was calculated since the first M 3 or larger foreshock event. (d) Temporal changes in the number of excess events.

A2.6. Swarm sequence in June 2002

The swarm sequence in June 2002 started on June 30th and continued for 12 days (Figure A2.6). Repeating earthquakes were found in this swarm sequence. The comparison of the number of observed events ($\geq M$ 3) (12 events) in the Ibaraki-Oki detection circle with the number of events predicted by the ETAS model (2.5 event)

shows an anomaly larger than 5σ (Figure A2.6c), i.e. the probability that we observe such a high seismicity rate is less than 1.5×10^{-5}.

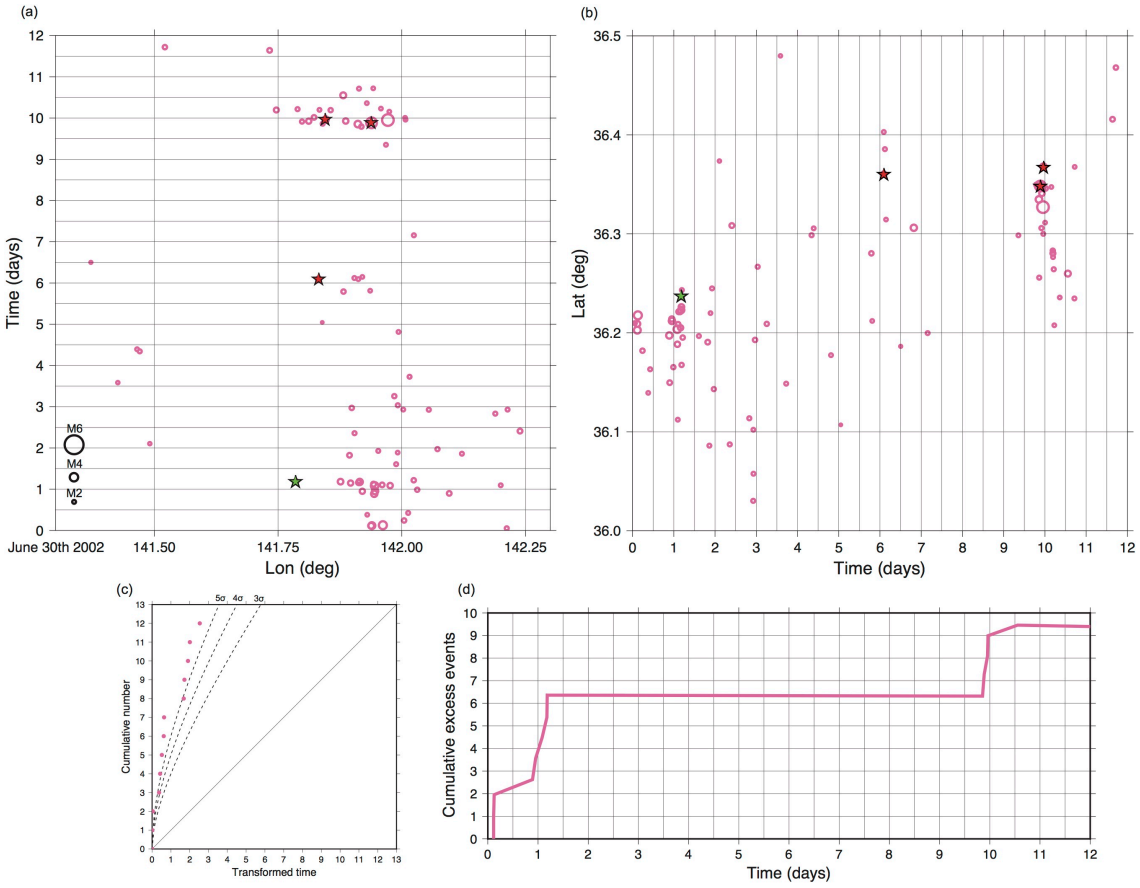

Figure A2.6 | Space-time distribution and excess events of the swarm sequence in 2002. (a) and (b) show time-longitude and latitude-time distributions of the swarm sequence in 2002 (JMA catalog). Pink circles are swarms. Small stars are repeating earthquakes, colored according to the same manner as Figure 3.7a. (c) Transformed time of this swarm sequence. The transformed time was calculated since the first *M* 3 or larger swarm event. (d) Temporal changes in the number of excess events.

Acknowledgements

I am deeply grateful to my advisor, Prof. S. Ide for helpful discussions and supports. I also would like to deeply thank the thesis committee (Assoc. Prof. Aitaro Kato, Prof. Kazushige Obara, Prof. Takaya Iwasaki, Assoc. Prof. Jiancang Zhuang, and Assoc. Prof. Ryosuke Ando) for reviewing this thesis.

I am also grateful to members of Ide laboratory, Ando laboratory, Solid Earth Science Group, Seismogenesis Seminar, and Seismology Seminar at Earthquake Research Institute for constructive discussions.

This study was supported by JSPS KAKENHI (15J08193 and 16H02219), MEXT KAKENHI (16H06477), and the MEXT Earthquake and Volcano Hazards Observation and Research Program. Figures were prepared using Generic Mapping Tool [Wessel and Smith, 1998].

Finally, I'm deeply indebted to my family including my two cats and one lizard, Charco, Cha-Cha, and Tokage-kun for support and encouragement throughout my study, and to my friends, especially Lyu Weida, Tēnn Uî-tsùn, and Lîm Khái-īn.

References

Ammon, C. J., H. Kanamori, and T. Lay (2008), A great earthquake doublet and seismic stress transfer cycle in the central Kuril islands, *Nature*, **451**(7178), 561–565, doi:10.1038/nature06521.

Ando, R., N. Takeda, and T. Yamashita (2012), Propagation dynamics of seismic and aseismic slip governed by fault heterogeneity and Newtonian rheology, *J. Geophys. Res.*, **117**(B11), B11308, doi:10.1029/2012JB009532.

Ando, R., and K. Imanishi (2011), Possibility of Mw 9.0 mainshock triggered by diffusional propagation of after-slip from Mw 7.3 foreshock, *Earth Planets Space*, **63**(7), 767–771, doi:10.5047/eps.2011.05.016.

Aoyama, H., M. Takeo, and S. Ide (2002), Evolution mechanisms of an earthquake swarm under the Hida Mountains, central Japan, in 1998, *J. Geophys. Res.*, 107(B8), doi:10.1029/2001JB000540.

Araki, E., et al. (2017), Recurring and triggered slow-slip events near the trench at the Nankai Trough subduction megathrust, *Science*, **356**(6343), 1157–1160, doi:10.1126/science.aan3120.

Beroza, G. C., and S. Ide (2011), Slow earthquakes and nonvolcanic tremor, *Annu. Rev. Earth and Planet. Sci.*, **39**, 271–296, doi:10.1146/annurev-earth-040809-152531.

Bird, P. (2003), An updated digital model of plate boundaries, *Geochem. Geophys. Geosyst.* **4,** 1027, doi:10.1029/2001GC000252.

Bird, P., Y. Y. Kagan, D. D. Jackson, F. P. Schoenberg, and M. J. Werner (2009), Linear and nonlinear relations between relative plate velocity and seismicity, *Bull. Seismol. Soc. Am.*, **99**(6), 3097–3113, doi:10.1785/0120090082.

Bletery, Q., A. M. Thomas, A. W. Rempel, L. Karlstrom, A. Sladen, and L. De Barros

(2016), Mega-earthquakes rupture flat megathrusts, *Science*, **354**(6315), 1027–1031, doi:10.1126/science.aag0482.

Bouchon, M., V. Durand, D. Marsan, H. Karabulut, and J. Schmittbuhl (2013), The long precursory phase of most large interplate earthquakes, *Nat. Geosci.*, **6**(4), 299–302, doi:10.1038/ngeo1770.

Båth, M. (1965), Lateral inhomogeneities of the upper mantle, *Tectonophysics*, **2**, 483–514, doi:10.1016/0040-1951(65)90003-X.

Canales, J. P., S. M. Carbotte, M. R. Nedimović, and H. Carton (2017), Dry Juan de Fuca slab revealed by quantification of water entering Cascadia subduction zone, *Nat. Geosci.*, **10**(11), 864–870, doi:10.1038/ngeo3050.

Delahaye, E. J., J. Townend, M. E. Reyners, and G. Rogers (2009), Microseismicity but no tremor accompanying slow slip in the Hikurangi subduction zone, New Zealand, *Earth Planet. Sci. Lett.*, **277**(1), 21–28, doi:10.1016/j.epsl.2008.09.038.

Dieterich, J. H. (1979), Modeling of rock friction: 1. Experimental results and constitutive equations, *J. Geophys. Res.*, **84**(B5), 2161–2168, doi: 10.1029/JB084iB05p02161.

Dieterich, J. H. (1992), Earthquake nucleation on faults with rate-and state-dependent strength, *Tectonophysics*, **211**(1-4), 115–134, doi:10.1016/0040-1951(92)90055-B.

Dixon, T. H., Y. Jiang, R. Malservisi, R. McCaffrey, N. Voss, M. Protti, and V. Gonzalez (2014), Earthquake and tsunami forecasts: Relation of slow slip events to subsequent earthquake rupture, *Proc. Natl. Acad. Sci. USA*, **111**(48), 17039–

17044, doi:10.1073/pnas.1412299111.

Dragert, H., K. Wang, and G. Rogers, (2004), Geodetic and seismic signatures of episodic tremor and slip in the northern Cascadia subduction zone, *Earth planet. space*, **56**(12), 1143–1150, doi:10.1186/BF03352578.

Earthquake Prediction Information Division, JMA (2008), The Earthquake of M7.0 off Ibaraki Prefecture on May 8, 2008, *Report of CCEP*, **80**, 4-10.

Ellsworth, W. L. (2013), Injection-induced earthquakes, *Science,* **341,** 1225942, doi:10.1126/science.1225942.

Ellsworth, W. L., and G. C. Beroza (1995), Seismic evidence for an earthquake nucleation phase, *Science*, **268**(5212), 851–855, doi:10.1126/science.268.5212.851.

Ellsworth, W.L., (1995), Characteristic earthquake and long-term earthquake forecasts: implications of central California seismicity, in *Urban Disaster Mitigation: The Role of Science and Technology,* edited by F. Y. Cheng and M. S. Sheu, pp1–14, Elsevier Sci., New York.

Faccenda, M., T. V. Gerya, and L. Burlini (2009), Deep slab hydration induced by bending-related variations in tectonic pressure, *Nat. Geosci.,* **2**, 790–793, doi:10.1038/ngeo656.

Forsyth, D. W., Y. Yang, M. D. Mangriotis, and Y. Shen, (2003), Coupled seismic slip on adjacent oceanic transform faults, *Geophys. Res. Lett.*, **30**(12), doi:10.1029/2002GL016454.

Frank, W. B., N. M. Shapiro, A. L. Husker, V. Kostoglodov, H. S. Bhat, and M. Campillo (2015), Along-fault pore-pressure evolution during a slow-slip event in Guerrero, Mexico, *Earth Planet. Sci. Lett.*, **413**, 135–143,

doi:10.1016/j.epsl.2014.12.051.

Fukuda, J. I., A. Kato, K. Obara, S. Miura, and T. Kato (2014), Imaging of the early acceleration phase of the 2013–2014 Boso slow slip event. *Geophys. Res. Lett.*, **41**(21), 7493–7500, doi:10.1002/2014GL061550.

Guglielmi, Y., F. Cappa, J. P. Avouac, P. Henry, and D. Elsworth (2015), Seismicity triggered by fluid injection–induced aseismic slip, *Science*, **348**(6240), 1224–1226, doi:10.1126/science.aab0476.

Gutenberg, B., and C. F. Richter (1944), Frequency of earthquakes in California, *Bull. Seismol. Soc. Am*. **34,** 185–188.

Hanks, T. C., and H. Kanamori (1979), Moment magnitude scale, *J. Geophys. Res.,* **84**, 2348–2350, doi:10.1029/JB084iB05p02348.

Hess, H. H. (1962), History of Oceanic Basins, *Petrologic studies; a volume in honor of A. F. Buddington* edited by A. E. J. Engel, Harold L. James, and B. F. Leonard, Geological Society of America, Boulder, 599–620 (1962).

Hirose, H., H. Kimura, B. Enescu, and S. Aoi, (2012), Recurrent slow slip event likely hastened by the 2011 Tohoku earthquake, *Proc. Natl. Acad. Sci. USA*, **109**(38), 15157–15161, doi:10.1073/pnas.1202709109.

Hirose, H., K. Hirahara, F. Kimata, N. Fujii, and S. I. Miyazaki, (1999), A slow thrust slip event following the two 1996 Hyuganada earthquakes beneath the Bungo Channel, southwest Japan, *Geophys. Res. Lett.*, **26**(21), 3237–3240, doi: 10.1029/1999GL010999.

Holtkamp, S. G., and M. R. Brudzinski (2011), Earthquake swarms in circum-Pacific subduction zones, *Earth Planet. Sci. Lett.*, **305**(1), 215–225, doi:10.1016/j.epsl.2011.03.004.

Holtkamp, S., and M. R. Brudzinski (2014), Megathrust earthquake swarms indicate frictional changes which delimit large earthquake ruptures, *Earth Planet. Sci. Lett.*, **390**, 234–243, doi: 10.1016/j.epsl.2013.10.033.

Ide, S. (2013), The proportionality between relative plate velocity and seismicity in subduction zones, *Nat. Geosci.* **6,** 780–784, doi:10.1038/ngeo1901.

Ide, S., and H. Aochi (2005), Earthquakes as multiscale dynamic ruptures with heterogeneous fracture surface energy, *J. Geophys. Res.,* **110**(B11), B11303, doi:10.1029/2004JB003591.

Ide, S., and H. Aochi (2013), Historical seismicity and dynamic rupture process of the 2011 Tohoku-Oki earthquake, *Tectonophysics*, **600**, 1–13, doi:10.1016/j.tecto.2012.10.018.

Ide, S., A. Baltay, and G. C. Beroza (2011), Shallow dynamic overshoot and energetic deep rupture in the 2011 Mw 9.0 Tohoku-Oki earthquake. *Science*, **332**(6036), 1426–1429, doi:10.1126/science.1207020.

Ide, S., G. C. Beroza, D. R. Shelly, and T. Uchide (2007), A scaling law for slow earthquakes. *Nature*, **447**(7140), 76–79, doi:10.1038/nature05780.

Igarashi, T. (2010), Spatial changes of inter‐plate coupling inferred from sequences of small repeating earthquakes in Japan, *Geophys. Res. Lett.*, **37**(20), L20304, doi:10.1029/2010GL044609.

Igarashi, T., T. Matsuzawa, and A. Hasegawa (2003), Repeating earthquakes and interplate aseismic slip in the northeastern Japan subduction zone, *J. Geophys. Res.*, **108**(B5), ESE 8, doi:10.1029/2002JB001920.

Ito, Y., K. Obara, K. Shiomi, S. Sekine, and H. Hirose (2007), Slow earthquakes coincident with episodic tremors and slow slip events, *Science*, **315**(5811), 503–

506, doi:10.1126/science.1134454.

Ito, Y., R. Hino, M. Kido, H. Fujimoto, Y. Osada, D. Inazu, Y. Ohta, T. Iinuma, M. Ohzono, S. Miura, M. Mishina, K. Suzuki, T. Tsuji, and J. Ashi (2013), Episodic slow slip events in the Japan subduction zone before the 2011 Tohoku-Oki earthquake, *Tectonophysics*, **600**, 14–26, doi: 10.1016/j.tecto.2012.08.022.

Kanamori, H. (1986), Rupture process of subduction-zone earthquakes, *Annu. Rev. Earth and Planet. Sci.*, **14**(1), 293–322.

Kato, A., J. I. Fukuda, T. Kumazawa, and S. Nakagawa (2016), Accelerated nucleation of the 2014 Iquique, Chile Mw 8.2 Earthquake, *Sci. Rep.*, **6**, 24792, doi:10.1038/srep24792.

Kato, A., J. I. Fukuda, and K. Obara (2013), Response of seismicity to static and dynamic stress changes induced by the 2011 M9. 0 Tohoku‐Oki earthquake, *Geophys. Res. Lett.*, **40**(14), 3572–3578, doi:10.1002/grl.50699.

Kato, A., K. Obara, T. Igarashi, H. Tsuruoka, S. Nakagawa, and N. Hirata (2012), Propagation of slow slip leading up to the 2011 Mw 9.0 Tohoku-Oki earthquake, *Science*, **335**(6069), 705–708, doi:10.1126/science.1215141.

Kato, A., T. Igarashi, and K. Obara (2014), Detection of a hidden Boso slow slip event immediately after the 2011 Mw 9.0 Tohoku - Oki earthquake, Japan, *Geophys. Res. Lett.*, **41**(16), 5868–5874, doi:10.1002/2014GL061053.

Kodaira, S., T. Iidaka, A. Kato, J. O. Park, T. Iwasaki, and Y. Kaneda, (2004), High pore fluid pressure may cause silent slip in the Nankai Trough, *Science*, **304**(5675), 1295–1298, doi:10.1126/science.1096535.

Lapusta, N., and Y. Liu (2009), Three-dimensional boundary integral modeling of spontaneous earthquake sequences and aseismic slip, *J. Geophys. Res*, **114**(B9),

doi:10.1029/2008JB005934.

Lay, T., et al. (2005), The great Sumatra-Andaman earthquake of 26 December 2004, *Science*, **308**(5725), 1127–1133, doi:10.1126/science.1112250.

Liu, Y., J. R. Rice, and K. M. Larson (2007), Seismicity variations associated with aseismic transients in Guerrero, Mexico, 1995–2006, *Earth Planet. Sci. Lett.*, **262**(3), 493–504, doi:10.1016/j.epsl.2007.08.018.

Llenos, A. L., J. J. McGuire, and Y. Ogata (2009), Modeling seismic swarms triggered by aseismic transients, *Earth Planet. Sci. Lett.*, **281**(1), 59–69, doi:10.1016/j.epsl.2009.02.011.

Maeda, K. (1996), The use of foreshocks in probabilistic prediction along the Japan and Kuril trenches, *Bull. Seismol. Soc. Am.*, **86**(1A), 242–254.

Marsan, D., A. Helmstetter, M. Bouchon, and P. Dublanchet, (2014), Foreshock activity related to enhanced aftershock production, *Geophys. Res. Lett.*, **41**(19), 6652–6658, doi:10.1002/2014GL061219.

Matsumura, S. (2010), Discrimination of a preparatory stage leading to M7 characteristic earthquakes off Ibaraki Prefecture, Japan, *J. Geophys. Res.,* **115**(B1), doi:10.1029/2009JB006584.

Matsuzawa, T., H. Hirose, B. Shibazaki, and K. Obara (2010), Modeling short - and long-term slow slip events in the seismic cycles of large subduction earthquakes, *J. Geophys. Res.,* **115**(B12), 1–14, doi:10.1029/2010JB007566.

Matsuzawa, T., N. Uchida, T. Igarashi, T. Okada, and A. Hasegawa (2004), Repeating earthquakes and quasi-static slip on the plate boundary east off northern Honshu, Japan, *Earth Plantes Space*, **56**(8), 803–811, doi:10.1186/BF03353087.

Mochizuki, K., T. Yamada, M. Shinohara, Y. Yamanaka, and T. Kanazawa (2008),

Weak interplate coupling by seamounts and repeating M~ 7 earthquakes, *Science*, **321**(5893), 1194–1197, doi:10.1126/science.1160250.

Moreno, M., C. Haberland, O. Oncken, A. Rietbrock, S. Angiboust, and O. Heidbach (2014), Locking of the Chile subduction zone controlled by fluid pressure before the 2010 earthquake, *Nat. Geosci.*, **7**(4), 292–296, doi:10.1038/ngeo2102.

Müller, R. D., M. Sdrolias, C. Gaina, and W. R. Roest (2008), Age, spreading rates, and spreading asymmetry of the world's ocean crust, *Geochem. Geophys. Geosyst*. **9,** Q04006, doi:10.1029/2007GC001743.

Nadeau, R. M., and L. R. Johnson (1998), Seismological studies at Parkfield VI: Moment release rates and estimates of source parameters for small repeating earthquakes, *Bull. Seismol. Soc. Am.*, **88**(3), 790–814.

Nadeau, R. M., and T. V. McEvilly (1999), Fault slip rates at depth from recurrence intervals of repeating microearthquakes. *Science*, **285**(5428), 718–721, doi:10.1126/science.285.5428.718.

Nishide N., et al. (2000), Nationwide activity of low-frequency earthquakes in the lower crust in Japan, *Proc. Jpn. Earth Planet. Sci. Jt. Meet.*, Abstr. Sk-P002, Tokyo: Geod. Soc. Jpn.

Nishikawa, T., and S. Ide (2014), Earthquake size distribution in subduction zones linked to slab buoyancy, *Nat. Geosci,* **7**, 904–908, doi:10.1038/ngeo2279.

Nishikawa, T., and S. Ide (2015), Background seismicity rate at subduction zones linked to slab-bending-related hydration, *Geophys. Res. Lett.*, **42**(17), 7081–7089, doi:10.1002/2015GL064578.

Nishikawa, T., and S. Ide (2017), Detection of earthquake swarms at subduction zones globally: insights into tectonic controls on swarm activity, *J. Geophys. Res*.,

122(7), 5325–5343, doi:10.1002/2017JB014188.

Noda, H., M. Nakatani, and T. Hori (2013), Large nucleation before large earthquakes is sometimes skipped due to cascade‐up—Implications from a rate and state simulation of faults with hierarchical asperities, *J. Geophys. Res.*, **118**(6), 2924–2952, doi:10.1002/grl.50962.

Obara, K. (2002), Nonvolcanic deep tremor associated with subduction in southwest Japan, *Science*, 296(5573), 1679–1681, doi:10.1126/science.1070378.

Obara, K., and A. Kato (2016), Connecting slow earthquakes to huge earthquakes. *Science*, **353**(6296), 253-257, doi:10.1126/science.aaf1512.

Obara, K., and Y. Ito (2005), Very low frequency earthquakes excited by the 2004 off the Kii peninsula earthquakes: A dynamic deformation process in the large accretionary prism, *Earth Planets Space*, **57**(4), 321–326, doi:10.1186/BF03352570.

Ogata, Y. (1988), Statistical models for earthquake occurrences and residual analysis for point processes, *J. Am. Stat. Assoc*. **83,** 9–27, doi:10.1080/01621459.1988.10478560

Ogata, Y. (2005), Detection of anomalous seismicity as a stress change sensor, *J. Geophys. Res.*, **110**(B5), B05S06, doi:10.1029/2004JB003245.

Ohnaka, M. (1992), Earthquake source nucleation: a physical model for short-term precursors, *Tectonophysics*, **211**(1-4), 149–178, doi:10.1016/0040-1951(92)90057-D.

Okutani, T., and S. Ide (2011), Statistic analysis of swarm activities around the Boso Peninsula, Japan: Slow slip events beneath Tokyo Bay?, *Earth Planets Space,* **63,** 419–426.

Ozawa, S., S. Miyazaki, Y. Hatanaka, T. Imakiire, M. Kaidzu, and M. Murakami (2003), Characteristic silent earthquakes in the eastern part of the Boso peninsula, Central Japan, *Geophys. Res. Lett.*, **30**(6), 16, doi:10.1029/2002GL016665.

Peacock, S. M. (1996), Thermal and Petrologic Structure of Subduction Zones, in Subduction Top to Bottom (eds G. E. Bebout, D. W. Scholl, S. H. Kirby and J. P. Platt), American Geophysical Union, Washington, D. C., doi:10.1029/GM096p0119.

Peng, Z., and P. Zhao (2009), Migration of early aftershocks following the 2004 Parkfield earthquake, *Nat. Geosci.*, **2**(12), 877–881, doi:10.1038/NGEO697.

Poli, P., A. M. Jeria, and S. Ruiz (2017), The Mw 8.3 Illapel earthquake (Chile): Preseismic and postseismic activity associated with hydrated slab structures, *Geology*, G38522-1, doi:10.1130/G38522.1.

Radiguet, M., et al. (2012), Slow slip events and strain accumulation in the Guerrero gap, Mexico, *J. Geophys. Res.*, **117**(B4), B04305, doi: 10.1029/2011JB008801.

Radiguet, M., et al. (2016), Triggering of the 2014 Mw7. 3 Papanoa earthquake by a slow slip event in Guerrero, Mexico, *Nat. Geosci*, **9**(11), 829–833, doi:10.1038/NGEO2817.

Ranero, C. R., J. P. Morgan, K. McIntosh, and C. Reichert (2003), Bending-related faulting and mantle serpentinization at the Middle America trench, *Nature,* **425**, 367–373, doi:10.1038/nature01961.

Reverso, T., D. Marsan, A. Helmstetter, and B. Enescu (2016), Background seismicity in Boso Peninsula, Japan: Long - term acceleration, and relationship with slow slip events, *Geophys. Res. Lett.*, **43**(11), 5671–5679, doi:10.1002/2016GL068524.

Reverso, T., D. Marsan, and A. Helmstetter (2015), Detection and characterization of

transient forcing episodes affecting earthquake activity in the Aleutian Arc system, *Earth Planet. Sci. Lett.*, **412**, 25–34, doi:10.1016/j.epsl.2014.12.012.

Rice, J. R. (1992), Fault Stress States, Pore Pressure Distributions, and the Weakness of the San Andreas Fault, in *Fault Mechanics and Transport Properties of Rocks*, edited by B. Evans and T. Wong, pp. 475–503, Chapter 20, Elsevier Sci., New York.

Richter, C. F. (1958), Elementary Seismology, pp. 66–79, W.H. Freeman, San Francisco, Calif.

Roland, E., and J. J. McGuire (2009), Earthquake swarms on transform faults, *Geophys. J. Int.*, **178**(3), 1677–1690, doi:10.1111/j.1365-246X.2009.04214.x.

Rubin, A. M., and J. P. Ampuero (2005), Earthquake nucleation on (aging) rate and state faults, *J. Geophys. Res.*, **110**(B11), doi:10.1029/2005JB003686.

Ruiz, S., M. Metois, A. Fuenzalida, J. Ruiz, F. Leyton, R. Grandin, C. Vigny, R. Madariaga, and J. Campos (2014), Intense foreshocks and a slow slip event preceded the 2014 Iquique Mw 8.1 earthquake, *Science*, **345**(6201), 1165–1169, doi:10.1126/science.1256074.

Saffer, D. M., and H. J. Tobin (2011), Hydrogeology and mechanics of subduction zone forearcs: fluid flow and pore pressure, *Annu. Rev. Earth and Planet. Sci.,* **39,** 157–186, doi:10.1146/annurev-earth-040610-133408.

Saffer, D. M., and L. M. Wallace (2015), The frictional, hydrologic, metamorphic and thermal habitat of shallow slow earthquakes, *Nat. Geosci.,* **8**(8), 594–600, doi:10.1038/ngeo2490.

Sagiya, T. (2004), Interplate coupling in the Kanto district, central Japan, and the Boso Peninsula silent earthquake in May 1996, Pure and Applied Geophys, **161**(11),

2327–2342, doi:10.1007/s00024-004-2566-6.

Scholz, C. H., and J. Campos (2012), The seismic coupling of subduction zones revisited, *J. Geophys. Res.*, **117**(B5), B05310, doi:10.1029/2011JB009003.

Segall, P., A. M. Rubin, A. M. Bradley, and J. R. Rice (2010). Dilatant strengthening as a mechanism for slow slip events, *J. Geophys. Res.*, **115**(B12), B12305, doi: 10.1029/2010JB007449.

Shelly, D. R., G. C. Beroza, and S. Ide (2007), Non-volcanic tremor and low-frequency earthquake swarms, *Nature*, **446**(7133), 305–307, doi:10.1038/nature05666.

Shibazaki, B., and M. Matsu'ura (1992), Spontaneous processes for nucleation, dynamic propagation, and stop of earthquake rupture, *Geophys. Res. Lett.*, **19**(12), 1189–1192, doi:10.1029/92GL01072.

Shillington, D. J., A. Bécel, M. R. Nedimović, H. Kuehn, S. C. Webb, G. A. Abers, K. M. Keranen, J. Li, M. Delescluse, and G. A. Mattei-Salicrup (2015), Link between plate fabric, hydration and subduction zone seismicity in Alaska, *Nat. Geosci.*, **8**(12), 961–964, doi:10.1038/ngeo2586.

Skarbek, R. M., A. W. Rempel, and D. A. Schmidt (2012), Geologic heterogeneity can produce aseismic slip transients, *Geophys. Res. Lett.*, 39(21), L21306, doi:10.1029/2012GL053762

Smith, W. H. F., and D. T. Sandwell (1997), Global Sea Floor Topography from Satellite Altimetry and Ship Depth Soundings, *Science* **277,** 1956–1962, doi: 10.1126/science.277.5334.1956.

Suzuki, T., and T. Yamashita (2009), Dynamic modeling of slow earthquakes based on thermoporoelastic effects and inelastic generation of pores, *J. Geophys. Res.*, **114**(B6), B00A04, doi:10.1029/2008JB006042.

Tanioka, Y., L. Ruff, and K. Satake (1997), What controls the lateral variation of large earthquake occurrence along the Japan Trench?, *Isl. Arc*, **6**(3), 261–266, doi:10.1111/j.1440-1738.1997.tb00176.x.

The Headquarters for Earthquake Research Promotion (1995), Evaluation of seismic activities for November 1995 (December 13, 1995). [Available at http://www.jishin.go.jp/main/chousa/95nov/.]

The Headquarters for Earthquake Research Promotion (2008), Evaluation of seismic activities for April 2008 (May 12, 2008). [Available at http://www.jishin.go.jp/main/chousa/08may/.]

Toda, S., R. S. Stein, and T. Sagiya, (2002), Evidence from the AD 2000 Izu islands earthquake swarm that stressing rate governs seismicity, *Nature*, **419**(6902), 58–61, doi:10.1038/nature00997.

Tse, S. T., and J. R. Rice (1986), Crustal earthquake instability in relation to the depth variation of frictional slip properties, *J. Geophys. Res.*, **91**(B9), 9452–9472, doi:10.1029/JB091iB09p09452.

Uchida, N., S. Yui, S. Miura, T. Matsuzawa, A. Hasegawa, Y. Motoya, and M. Kasahara (2009), Quasi-static slip on the plate boundary associated with the 2003 M8. 0 Tokachi-oki and 2004 M7. 1 off-Kushiro earthquakes, Japan, *Gondwana Res.*, **16**(3), 527–533, doi:10.1016/j.gr.2009.04.002.

Uchida, N., T. Iinuma, R. M. Nadeau, R. Bürgmann, and R. Hino (2016), Periodic slow slip triggers megathrust zone earthquakes in northeastern Japan, *Science*, **351**(6272), 488–492, doi:10.1126/science.aad3108.

Uchida, N., T. Matsuzawa, W. L. Ellsworth, K. Imanishi, K. Shimamura, and A. Hasegawa (2012), Source parameters of microearthquakes on an interplate

asperity off Kamaishi, NE Japan over two earthquake cycles, *Geophys. J. Int.*, **189**(2), 999–1014, doi:10.1111/j.1365-246X.2012.05377.x.

Uchida, N., and T. Matsuzawa (2013), Pre-and postseismic slow slip surrounding the 2011 Tohoku-oki earthquake rupture, *Earth Planet. Sci. Lett.*, **374**, 81–91, doi:10.1016/j.epsl.2013.05.021.

Uchida, N., et al. (2007), Source parameters of a M4. 8 and its accompanying repeating earthquakes off Kamaishi, NE Japan: Implications for the hierarchical structure of asperities and earthquake cycle, *Geophys. Res. Lett.*, **34**(20), L20313, doi:10.1029/2007GL031263.

Ueno, H., et al. (2002), Improvement of hypocenter determination procedures in the Japan Meteorological Agency, *Quarterly Journal of Seismology*, **65**, 123–134.

Utsu, T. (1961), A statistical study on the occurrence of aftershocks, *Geophysical Magazine*, **30**(4), 521–605.

Uyeda, S. (1983), Comparative subductology. *Episodes*, **2**, 19–24.

Uyeda, S., and H. Kanamori (1979), Back - arc opening and the mode of subduction. *J. Geophys. Res.*, **84**(B3), 1049–1061, doi:10.1029/JB084iB03p01049.

Vallée, M., et al. (2013), Intense interface seismicity triggered by a shallow slow slip event in the Central Ecuador subduction zone, *J. Geophys. Res.*, **118**(6), 2965–2981, doi:10.1002/jgrb.50216.

Vidale, J. E., and P. M. Shearer (2006), A survey of 71 earthquake bursts across southern California: Exploring the role of pore fluid pressure fluctuations and aseismic slip as drivers, *J. Geophys. Res.*, **111**(B5), B05312, doi:10.1029/2005JB004034.

Waite, G. P., and R. B. Smith (2002), Seismic evidence for fluid migration

accompanying subsidence of the Yellowstone caldera, *J. Geophys. Res.,* **107**(B9), 2177, doi:10.1029/2001JB000586.

Wallace, L. M., and J. Beavan (2010), Diverse slow slip behavior at the Hikurangi subduction margin, New Zealand, *J. Geophys. Res.*, **115**(B12), B12402, doi: 10.1029/2010JB007717.

Wessel, P., and W. H. F. Smith (1998), New, improved version of the Generic Mapping Tools Released, Eos Trans. AGU, **79**(47), 579–579, doi:10.1029/98EO00426.

Wiemer, S., and M. Wyss (2000), Minimum magnitude of completeness in earthquake catalogs: Examples from Alaska, the western United States, and Japan, *Bull. Seismol. Soc. Am.*, **90**(4), 859–869, doi:10.1785/0119990114.

Woessner, J., and S. Wiemer (2005), Assessing the quality of earthquake catalogues: Estimating the magnitude of completeness and its uncertainty, *Bull. Seismol. Soc. Am.*, **95**(2), 684–698, doi:10.1785/0120040007.

Yabe, S., and S. Ide (2017), Slip‐behavior transitions of a heterogeneous linear fault, *J. Geophys. Res.*, **122**(1), 387–410, doi:10.1002/2016JB013132.

Yoshioka, S., Y. Matsuoka, and S. Ide (2015), Spatiotemporal slip distributions of three long-term slow slip events beneath the Bungo Channel, southwest Japan, inferred from inversion analyses of GPS data, *Geophys. J. Int.*, **201**(3), 1437–1455, doi:10.1093/gji/ggv022.

Zaliapin, I., and Y. Ben-Zion (2016), A global classification and characterization of earthquake clusters, *Geophys. J. Int.*, **207**(1), 608–634, doi:10.1093/gji/ggw300.

Zhuang, J., Y. Ogata, and D. Vere-Jones (2002), Stochastic declustering of space–time earthquake occurrences, *J. Am. Stat. Assoc.*, **97,** 369–380, doi:10.1198/016214502760046925.